ACTIVE PHOTONIC DEVICES BASED ON TWO-DIMENSIONAL ELECTRON GAS IN ENGINEERED SEMICONDUCTOR HETEROJUNCTION

Ph.D. Thesis

By

VISHAL KAUSHIK

Under the Supervision of

Dr. Mukesh Kumar

DEPARTMENT OF ELECTRICAL ENGINEERING

INDIAN INSTITUTE OF TECHNOLOGY INDORE

January 2022

ACTIVE PHOTONIC DEVICES BASED ON TWO-DIMENSIONAL ELECTRON GAS IN ENGINEERED SEMICONDUCTOR HETEROJUNCTION

A THESIS

Submitted in partial fulfillment of the

requirements for the award of the degree

of

DOCTOR OF PHILOSOPHY

By

VISHAL KAUSHIK

Under the Supervision of
Dr. Mukesh Kumar

DEPARTMENT OF ELECTRICAL ENGINEERING

INDIAN INSTITUTE OF TECHNOLOGY INDORE

January 2022

INDIAN INSTITUTE OF TECHNOLOGY INDORE

CANDIDATE'S DECLARATION

I hereby certify that the work which is being presented in the thesis entitled **"Active Photonic Devices based on Two-Dimensional Electron Gas in Engineered Semiconductor Heterojunction,"** in the partial fulfillment of the requirements for the award of the degree of **Doctor of Philosophy** and submitted in the **Department of Electrical Engineering, Indian Institute of Technology Indore**, is an authentic record of my own work carried out during the time period from **July, 2016** to **January, 2022** under the supervisions of **Dr. Mukesh Kumar**, Associate Professor, Electrical Engineering, IIT Indore and **Dr. Suchandan Pal**, Chief Scientist, CSIR-CEERI Pilani.

The matter presented in this thesis has not been submitted by me for the award of any other degree of this or any other institute.

10/01/2022
Signature of the student with date

(VISHAL KAUSHIK)

This is to certify that the above statement made by the candidate is correct to the best of our knowledge.

10-01-2022
Signature of Thesis Supervisor with date

(Dr. MUKESH KUMAR)

10-01-2022
Signature of Thesis Supervisor #2 with date

(Dr. SUCHANDAN PAL)

Vishal Kaushik has successfully given his Ph.D. Oral Examination held on 08/08/2022

10-08-2022
Signature of Thesis Supervisor #1 with date

(Dr. MUKESH KUMAR)

10-08-2022
Signature of Thesis Supervisor #2 with date

(Dr. SUCHANDAN PAL)

ACKNOWLEDGEMENTS

Time flies. It has been six years since I joined Ph.D. research. Looking back at past years I feel lucky that I have entered a field which I have been passionately interested in. This journey has been one with plenty of challenges, opportunities, and knowledge sharing. Many individuals have made important contributions in this journey both scientific and non-scientific from my mentors, co-workers, friends, and family.

It is genuine pleasure to express my deep sense of thanks and gratitude to my guide and mentor **Dr. Mukesh Kumar** for his continuous support, encouragement, and advice throughout the whole stage of my Ph.D. research. Though his specific contributions to this thesis are too numerous to list, some particularly admirable quality is that he was always accessible and open to fresh ideas for new research directions which gave me a lot of freedom to explore my interests. Through his valuable advice and technical expertise, he constantly pushed the thesis work in the right direction.

I am thankful to my co-supervisor **Dr. Suchandan pal** for his scientific inputs and facilities for my research work. I would also like to thank **Dr. Santosh Kumar Vishvakarma** and **Dr. Kazi Sabiruddin** for serving as my PSPC members, willing to share their precious time and valuable suggestions during various stages of my research.

Furthermore, I would like to acknowledge the support from Sophisticated Instrumentation Centre at IIT Indore, Hybrid Nanodevice Research Group, Department of Electrical Engineering, Department of Material Engineering & Material Science, IIT Indore for providing partial characterization facilities.

I gratefully acknowledge the fellowship received towards my Ph.D. from Ministry of Human Resource Development **(MHRD)** and Council of Scientific and Industrial Research **(CSIR)**, Government of India.

A special thanks goes to all my fellow members of Optoelectronic Nanodevice Device Research Laboratory including Dr. Swati Rajput, Dr. Lalit Singh, Dr. Sulabh, Dr. Sourabh Jain, Prem Babu, Suresh Kumar Pandey, Rahul Dev Mishra, Santosh Kumar, and Ashutosh Kumar who all made this journey memorable with fruitful experiences.

I would certainly be remiss to not mention and sincerely thank **Dr. Swati Rajput** for playing the role that she had throughout this long journey. Her timely suggestions, enthusiasm and dynamism has constantly motivated me, and her cheerful attitude has made the journey much easier for me.

I profoundly thank all my friends Shashwat Bhandari, Shivkeerat Singh, Tushar Goel, Sajjan Rajpoot, Abhinav Singh Parihar, Pawan Katewa, Dr. Mayoorika Shukla, Nikita Guha, Vipul Jain, and Vishesh Manjunath. It has been a pleasure and honor to have known and learned from all of them.

Last, but definitely not the least I am profoundly indebted to my family. It is my parents' (**Dr. Ajay Kaushik, Dr. Sunita Kaushik**) unconditional love, care, and support from the first very step that a mediocre child like me has reached up to here. It is their endless sacrifices for my studies which have provided a solid foundation for my future. It is my privilege to thank my brother and sister-in-law **Abhinav Kaushik** and **Varnika Kaushik** for their friendship, empathy, and great sense of humor.

Dedicated to My Beloved Mummy & Papa, my brother and sister-in-law

List of Publication

A. Publications from PhD thesis work

A1. In referred journals (03):

1. **V Kaushik**, S. Rajput, S. Srivastav, L. Singh, P. Babu, E. Heidari, M. Ahmed, Y.A. Hadeethi, H. Dalir, V.J. Sorger, and M. Kumar, “On-chip Nanophotonic Broadband Wavelength Detector with 2D-Electron Gas”, **Nanophotonics**, Accepted November 2021. **(Impact Factor-8.449).**
2. **V. Kaushik,** S. Rajput, S. Srivastava, S. Jain, L. Singh and M. Kumar, "Efficient Sub-bandgap Photodetection via Two-Dimensional Electron Gas in ZnO Based Heterojunction”, Journal of Lightwave Technology, 2020, Doi: 10.1109/JLT.2020.3003371 **(I.F. = 4.288).**
3. **V. Kaushik**, S. Rajput, and M. Kumar, “Broadband Optical Modulation in Zinc Oxide based Heterojunction via Optical Lifting”, **Optics Letters**, vol. 45, no. 2, pp. 363-366, January 2020. **(Impact Factor-3.714).**

A2. In refereed conferences (02):

1. **V. Kaushik**, S. Rajput and M. Kumar, “Voltage Dependence of Lattice Period in Anodized Alumina based Photonic Crystal” ICOL-2019 (IRDE Dehradun).
2. **V. Kaushik,** S. Rajput, and M. Kumar, “Temperature dependence of grain size in highly porous Anodic Alumina”, Photonics-2018, IIT Delhi.

B. Other publications during PhD:

B1. In referred journals (11):

1. S. Rajput, **V. Kaushik**, L. Singh, S. Srivastava, S.K. Pandey, R.D. Mishra, and M. Kumar, "Efficient Photodetector based on Sub-bandgap Transition in Silicon-ITO Distributed Heterojunctions", **Journal of Lightwave Technology**, vol. 39, no. 21, pp. 6886-6892. **(Impact Factor-4.288)**
2. S. Rajput, **V. Kaushik**, L. Singh, S. Srivastava, and M. Kumar, "Optical Modulator based on Silicon-ITO Grating Embedded Rib Structure with Tunable Group Delay", **Optics Letters**, vol. 46, no. 14, pp. 3468-3471, June 2021. **(Impact Factor-3.776)**
3. L. Singh, S. Srivastava, S. Rajput, **V. Kaushik**, R. D. Mishra, and M. Kumar, "Optical Switch with Ultra High Extinction Ratio Using Electrically Controlled Metal Diffusion", **Optics Letters**, vol. 46, no. 11, pp. 2626-2629, May 2021. **(Impact Factor-3.714)**
4. S. Rajput**, V. Kaushik,** P. Babu, P. Tiwari, A.K. Srivastava, and M. Kumar, "Optical Modulation via Coupling of Distributed Heterojunctions in Si-ITO based Subwavelength Grating", **Physical Review Applied**, Accepted on 1st April 2021. **(Impact Factor-4.985)**
5. R.D. Mishra, L. Singh, S. Rajput, **V. Kaushik,** S. Srivastava, and M. Kumar, "Engineered Nanophotonic Waveguide with Ultra-low Dispersion", **Applied Optics**, vol. 60, no. 16, May 2021. **(Impact Factor-1.961)**
6. S. Srivastava, L. Singh, **V. Kaushik**, S. Rajput, and M. Kumar, "Nanophotonic Waveguide based on Engineered Horizontal-vertical Slots for Polarization Independent Bio-chemical Sensing", **Journal of Optical Society of America B,** vol. 38, no. 3, pp. 749-757, February 2021. **(Impact Factor-2.3)**
7. S. Rajput**, V. Kaushik**, S. Jain, P. Tiwari, A.K. Srivastava, and M. Kumar, "Optical Modulation in Hybrid Waveguide based on Si-ITO

Heterojunction", **Journal of Lightwave Technology**, vol. 38, no. 6, pp.1365-1371, March 2020. **(Impact Factor-4.288)**

8. S. Rajput**, V. Kaushik,** S. Jain, and M. Kumar, "Slow Light Enhanced Phase Shifter based on Low-Loss Silicon-ITO Hollow Waveguide", IEEE Photonics Journal, vol. 11, no. 1, pp.1-8, February 2019. **(Impact Factor-2.833)**
9. S. Rajput, **V. Kaushik**, S. Jain, and M. Kumar, "Slow Light Assisted Electrical Tuning in Hollow Optical Waveguide via Carrier Depletion in Silicon and Indium Tin Oxide Sub-Wavelength Gratings", **Journal of Optical Society of America B**, vol. 37, no. 8, pp.2360-2365, June 2020. **(Impact Factor-2.3)**
10. S. Jain, S. Rajput, **V. Kaushik**, S. Srivastava, and M. Kumar, "Efficient Optical Modulation with High Data-Rate in Silicon based Laterally Split Vertical p-n Junction", **IEEE Journal of Quantum Electronics**, vol. 56, no. 2, pp. 1-7, April 2020. **(Impact Factor-2.384)**
11. S. Jain, S. Rajput**, V. Kaushik,** and M. Kumar, "High Speed Optical Modulator based on Silicon Slotted Rib Waveguide", **Optics Communication**, vol. 434, pp. 49-53, January 2019. **(Impact Factor-2.125)**

B2. In referred conferences (08):

1. S. Jain, **V. Kaushik, S.** Rajput, and M. Kumar, "Silicon-based Broadband Reflector for On-chip Photonic Devices", International Symposium on Integrated Functionalities-**ISIF 2017,** Delhi University, New Delhi, India, December 2017.
2. S. Rajput, P. Babu, **V. Kaushik**, L. Singh, S. Jain, and M. Kumar, "High Extinction Ratio in Silicon-ITO Heterojunction based Optical Modulator", Conference on Laser and Electro-Optics Pacific Rim **CLEO-PR-2020**, Sydney, Australia, August 2020.
3. S. Rajput, **V. Kaushik**, S. Jain, and M. Kumar, "Electrically Tunable Absorption in Hollow Waveguide for Optical Modulation",

International Conference on Optics and Electro-optics **ICOL-2019,** IRDE DRDO, Dehradun**,** India, October 2019.

4. S. Rajput, **V. Kaushik,** S. Jain, and M. Kumar, "Graphene based High Speed Silicon Slotted Optical Phase Modulator", The International Conference on Fiber Optics and Photonics- **Photonics 2018**, Indian Institute of Technology Delhi, India, December 2018.
5. S. Rajput, **V. Kaushik,** S. Jain, and M. Kumar, "Ultra-low Loss Slow Light in Si-ITO based Hollow Core Waveguide", International Symposium on Integrated Functionalities-**ISIF 2017,** Delhi University, New Delhi, India, December 2017.

TABLE OF CONTENTS

LIST OF FIGURES

LIST OF TABLES

ACRONYMS

Al	Aluminium
CMOS	Complementary Metal Oxide Semiconductor
DI	De-Ionized
DSO	Digital Storage Oscilloscope
DUT	Device Under Test
EBL	Electron Beam Lithography
ENZ	Epsilon Near Zero
EO	Electro Optic
ER	Extinction Ratio
FDE	Finite Difference Eigen
FDTD	Finite Difference Time Domain
FEM	Finite Element Method
FG	Function Generator
FKE	Franz-Keldysh Effect
HCG	High Contrast Grating
HCW	Hollow Core Waveguide
IC	Integrated Circuit
IL	Insertion Loss
In	Indium
IPE	Internal Photoemission
ITO	Indium Tin Oxide
I-V	Current-Voltage
MZI	Mach-Zehnder Interferometer
NIR	Near Infra-Red
NRZ	Non-Return to Zero

OSA	Optical Spectrum Analyzer
PIC	Photonic Integrated Circuit
PMMA	Poly (methyl methacrylate)
QCSE	Quantum Confined Stark Effect
RCWA	Rigorous Coupled Wave Analysis
RIE	Reactive Ion Etching
SEM	Scanning Electron Microscopy
Si	Silicon
SiO_2	Silicon Dioxide
SMF	Single Mode Fiber
SMU	Source Measure Unit
SOI	Silicon on Insulator
SWG	Sub-wavelength Grating
TCO	Transparent Conducting Oxide
TE	Transverse Electric
TLS	Tunable Laser Source
TM	Transverse Magnetic
UV	Ultraviolet
RIE	Reactive Ion Etching
SEM	Scanning Electron Microscopy
ZnO	Zinc Oxide

NOMENCLATURE

ε	Dielectric Constant
λ	Wavelength
$h\nu$	Photon Energy
n	Refractive Index
n_{eff}	Effective Refractive Index
Λ	Grating Period
ϕ	Phase of the electro-magnetic wave
q	Electronic Charge
α	Attenuation Coefficient
β	Phase Constant
ω	Angular Frequency
ω_p	Plasma Frequency
k	Wavenumber
n_g	Group Index
v_g	Group Velocity
Φ_B	Potential Barrier
$Evac$	Vacuum level Energy
E_c	Conduction Band Energy
E_v	Valance Band Energy
E_g	Energy Band gap
E_F	Fermi Level Energy

ABSTRACT

Active Photonic Devices based on Two-Dimensional Electron Gas in Engineered Semiconductor Heterojunction

by

Vishal Kaushik

Optoelectronic Nanodevice Research Laboratory,
Discipline of Electrical Engineering,
Indian Institute of Technology Indore

Supervisor: Dr. Mukesh Kumar

As electronics-based technologies reach their performance bottlenecks, the research community is shifting its focus from electrons to photons. Photons enjoy various advantages over the electrons, such as wider bandwidth, higher speeds, and almost negligible propagation loss. Silicon emerges as the workhorse for Photonic Integrated Circuits (PIC) owing to its high refractive index, excellent mechanical properties, along with the availability of stable native oxide and already existing mature CMOS industry. While silicon has excellent passive optical properties and has been employed for low-loss optical interconnects, resonators, and directional couplers. Realizing highly efficient active photonic functionalities with silicon has proven to be immensely challenging. In order to fully harness the tantalizing prospects that photonics offer, several electro-optic elements of a typical integrated optical link such as LASERS, optical modulators and photodetectors needs to be realized on a single chip. Thus, recently other best-in-class materials have been actively investigated for their excellent optical functionalities that can complement silicon to exploit the benefits of photonics to its fullest via hybrid integration configuration. Wide bandgap semiconductors like Zinc Oxide (ZnO) have been exploited for their superior tunable optical properties. Besides possessing a direct and wide bandgap, ZnO exhibits a large exciton binding energy (60 meV), amenity to wet chemical etching, high thermal conductivity, and radiation hardness. Additionally, ZnO allows bandgap engineering

offering the possibility of realizing ZnO based heterojunction with smaller lattice mismatch, providing ZnO edge over its counterparts. Moreover, several reports have experimentally realized highly dense 2-Dimensional Electron Gas (2-DEG) at the interface of ZnO based heterojunctions. 2-DEG in ZnO based heterojunction exhibits several exquisite properties of 2-D materials due to confined charge carriers, such as high speed, high probability of quantum transition due to high density of charge carriers. Nevertheless, as ZnO has a bandgap of 3.36 eV it exhibits dynamic tunability in UV part of the spectrum, hindering its applications in visible and Infrared region.

In this thesis ZnO based heterojunctions are investigated for sub-bandgap operations for implementing various essential opto-electronic elements like guidance, control, and detection of optical power on an on-chip platform. We demonstrate broadband optical modulation in visible spectrum employing a sub-bandgap approach in ZnO based heterojunction. The device utilizes high density confined charge carriers shows tunable absorption via optical lifting in regions well below its bandgap. The proposed device is optimized for high quantum efficiency and demonstrates high extinction ratio of around 8 dB for visible spectrum with a 3dB bandwidth of around 115 nm. Wide bandgap semiconductor with a sub-bandgap modulation approach thus offers an ideal platform for broadband modulation in visible region. Furthermore, by maintaining high charge carrier density this approach can, in principle be used for different spectral range spanning from Infrared to visible region just by changing CBO.

Subsequently a sub-bandgap photodetector employing a CdZnO-MgZnO heterojunction is experimentally realized. The reported photodetection is based on metal-less internal photoemission via optical excitation in 2D electron gas (2DEG) present at the bottom of the conduction band offset in the heterojunction. Role of 2D confinement and a higher momentum offered by the proposed platform in improving the internal quantum efficiency is also highlighted with the help of a physical model and a responsivity of 8.5 mA/W is experimentally reported at a wavelength of 532 nm. Building on to the linear frequency response of internal photo emission via 2-DEG we propose a novel approach to experimentally validate broadband wavelength detection on an on-chip platform with simple fabrication process. The proposed device also utilizes an additional reference junction for coherent common mode rejection. We report sensitivity of 0.96μA/nm for a broad wavelength-range of 280 nm from 660 to 940 nm. Simple fabrication process, efficient intensity noise cancelation along with heat resistance and radiation hardness of ZnO makes the proposed platform simple, low-cost and efficient alternative for several applications such as optical spectrometers, sensing, and Internet of Things (IOTs).

Finally, we realized voltage tunable localized surface plasmon resonance in ZnO nanoparticles at 1730 nm (Near Infrared [NIR]). The proposed non-metallic on-chip platform exploits Epsilon-Near-Zero (ENZ) property of heavily doped ZnO nanoparticles while modulation doping alters boundary conditions confining free charge carriers pushing their plasmonic behavior in NIR regime. The novel device uses highly doped ZnO nanowire grown inside anodized aluminum template. The novel work is first of its kind (to the best of our knowledge) offering voltage tunability of localized surface plasmon resonance in NIR region of the spectrum via an on-chip platform. These findings give fresh insights into semiconductor plasmonics and can fundamentally expand its domain by opening new avenues allowing applications which were initially unthinkable.

Chapter 1

Introduction to Hybrid Integrated Photonics

1.1 From Electrons to photons

The advent of information age has transformed our way of living and exponentially increased our data appetite. The entire world is interconnected by wires, optical cables, and electromagnetic waves from free space. Terabits of data on one hand, flows from one corner of the world to another over the network, almost instantaneously. On the other hand, information of this magnitude is stored and retrieved from the miniature silicon chip, with increasing capacity. The effort to store ever-larger amounts of data on ever-smaller chips, as well as the quest to transmit that information over the longest distance in the quickest time feasible is never-ending and is likely to continue until the full potential [1] [2]is reached. Information technology investigates all options for increasing information capacity, starting with the creation to the consumption of information. From the stage of its conceptualization, research in the field of semiconductor technologies has seen tremendous pace. These rapid advancements have played a critical role in driving the Integrated Circuit (IC) technologies towards high speed and miniaturization. Continuous strides towards satisfying highly competitive market demands over the years have pushed the technology to its limits.

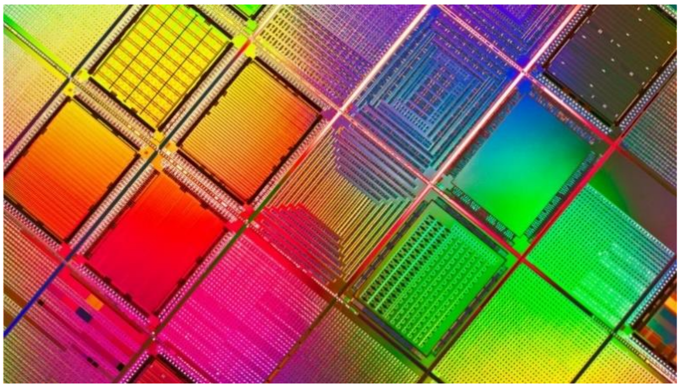

Fig. 1.1: 2 nm technology demonstrated by IBM. Image Credit: IBM

With recent demonstrated of 2 nm technology by IBM as shown in Fig. 1.1, further miniaturization to cater to the ever-increasing demand of the market would require dealing with unique challenges on fundamental level[3]. The wire connections between the chips are affected by Resistor-Capacitance delays and need an activation energy of 1pJ, which is dissipated via the Joule effect. It becomes increasingly challenging to keep up with the heat dissipation requirements, when the size of single transistors shrinks, increasing transistor density [4]. To make matters worse, increased integration which translates to smaller wires with a higher resistance. Figure 1.2 depicts power dissipation requirements in CPU with respect to increasing integration density in comparison to a hot plate and a nuclear reactor.

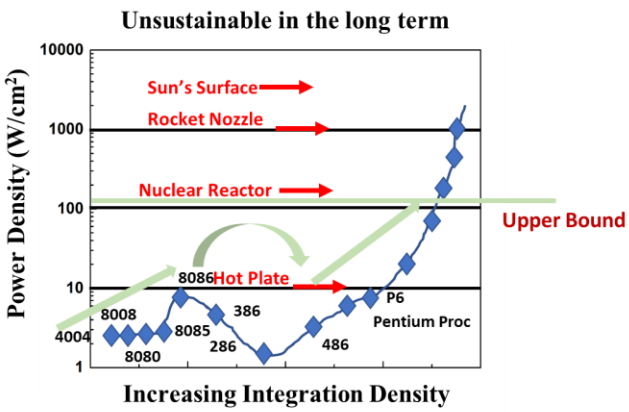

Fig. 1.2: Power dissipation requirements with respect to increasing integration density. Source: Intel

To maintain the pace of scaling research community is shifting their focus from electrons to photons. Photons enjoy various advantages over the electrons such as wider bandwidth higher speeds a comparative analysis is shown with the help of fig. 1.3. Fibre-optic communication systems have bandwidths of the order of one terahertz, whereas electronic systems have bandwidths of only a few hundred kilohertz [5][6]. Consequently, photons can carry a great amount of information at much higher speeds in a dielectric medium than an electron can in a metallic wire.

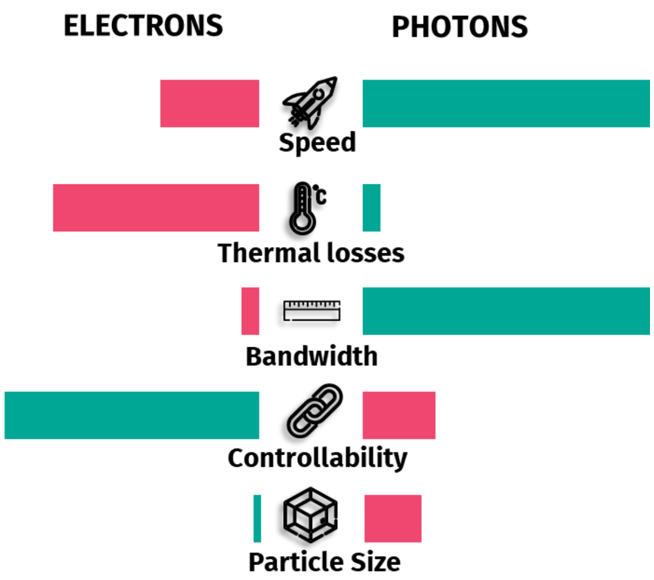

Fig. 1.3: A comparative analysis of electrons vs photons on the basis of speed, thermal losses, bandwidth, controllability, and particle size.

Furthermore, light particles (or photons) do not interact as strongly as electrons, reducing energy losses. While century-old long-distance copper cables are being replaced by optical cables for efficient transmission of huge amount of data. The bottlenecks in handling and processing of all that data has resulted in a hiatus in the progress seen in conventional data networks. Thus, the next logical question that inevitably accompanies this quest is how to solve the information processing bottlenecks over nanometre size devices. Therefore, the transition to photonics-based communications did not stop with long-haul lines. The shift in paradigm was soon realised in the short range as well. Although rack-to-rack optical connections are already commercially available, the paradigm shift is propagating further down, to the chip ladder. All of this is not conceivable if the VLSI interfaces between the photonic and microelectronic worlds do not progress in tandem. Thus, as electronics-based technologies are reaching their performance bottlenecks, photonics is increasingly seen as an alternate tool for next generation of communication, computing etc.

1.2 Photonic Integrated Circuits

A Photonic Integrated Circuit (PIC) is a highly disruptive technology that operates in the Near Infrared (NIR) and visible regions of the electromagnetic spectrum and allows highly efficient chip to chip communication. PIC is a complex circuit platform where a number of optical components such as multiplexer, de-multiplexer, optical modulators, photodetectors, optical amplifiers, filters, splitters are incorporated on a single chip, and it utilizes light source to drive discreet optical components.

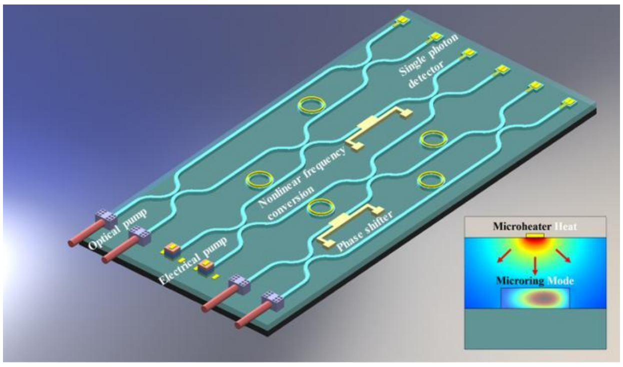

Fig. 1.4: A comparative analysis of electrons vs photons on the basis of speed, thermal losses, bandwidth, controllability, and particle size. Image Credit: Ali Adibi, Georgia Institute of Technology.

Fig. 1.4 displays integrated photonic platform consisting of an optical source, a routing circuit, and photodetectors. PICs provides a solution to the limitations of electronic integrated circuits like narrow bandwidth, data transmission speed, heating effects due to joule effect. The major application areas of PICs are data communications, sensing, defense and aerospace industries, biomedical applications such as lab-on-a-chip devices etc. On-chip integration of nanoscale optical devices, with its CMOS compatibility along with Dense Wavelength Division Multiplexing (DWDM) offers low-loss and high channel capacity [7][8][9]. As a result, there's a significant interest in exploiting this technology to meet the interconnect demands for future systems. Thus, the search for faster and less energy hungry platform has placed PIC at the centre of enhanced research focus.

1.2.1 Silicon Photonics

Study and application of integrated opto-electronic system which employs silicon as an optical medium is referred to as "Silicon Photonics". These operate in the spectral infrared region of 1.55 µm wavelength which is typically used in most fiber-optic telecommunication systems. The on-chip light source is produced by various hybrid silicon lasers. The data is then transmitted from data center to the on-chip optical modulators to write the data on optical carrier. The modulated light wave is combined using wavelength-division multiplexing method through an on-chip optical multiplexer and then transmitted to the receiver through a fiber by using appropriate fiber-to-chip coupling methods. Once the optical signal reaches the receiver, an on-chip de-multiplexer splits the signal based on their wavelengths and on-chip photodetectors are used to convert the optical signals to digital signals.

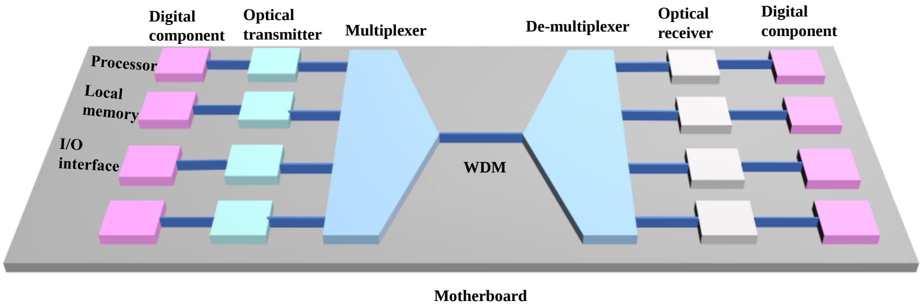

Fig. 1.5: Design for the on-chip core-to-core optical interconnect system.

The next step for silicon photonics based on-chip optical interconnect is to integrate the optical transmission line on the motherboard to support core-to-core optical transmission. In figure 1.5, a possible design for the on-chip core-to-core optical interconnect system is shown.

The embedded system has the ability to break the data transmission bottleneck on the motherboard and improve the performance of local processors. Such silicon-based structures are fabricated over the top of a silica layer and is popularly known as Silicon on Insulator (SOI). It normally comes with 2 ~ 3 μm thick buried oxide layer (BOX) and 220 ~ 250 nm crystalline silicon device layer. Using silicon as an optical medium and complementary metal-oxide semiconductor fabrication processing technology, silicon photonics allows tighter monolithic integration of many optical functions within a single device.

1.2.2 Need for Hybrid Integration

The rapid development of silicon photonics is undeniable. However, several constraints due to the material property still persists which require further research. Primarily, indirect bandgap of silicon renders it difficult to be used as a gain material and hybrid structures are generally adopted to realize on-chip optical sources. Also realizing highly efficient active photonic functionalities with silicon has proven to be immensely challenging. In order to fully harness the tantalizing prospects that photonics offer, several electro-optic elements of a typical integrated optical link such as LASERS, optical modulators and photodetectors needs to be realized on a single chip. The weak electro-optic effect, slow device performance, absence of second-order nonlinearity, and temperature sensitiveness in Si have led to low electro-optic coupling and a larger device footprint for such imperative applications. Thus, hybrid integration has become essential for fabricating advanced integrated photonic circuits harnessing the most favorable properties of multiple material platforms.

1.3 Choice of Material for Hybrid Photonic Integrated Circuits

Recently various best-in-class materials have been actively investigated for their excellent optical functionalities that can complement silicon to exploit the benefits of photonics to its fullest via hybrid integration configuration. Some of these materials are discussed below:

1.3.1 Lithium Niobate

Lithium niobate ($LiNbO_3$) has emerged one of the most popular materials for electro-optic devices and nonlinear optical devices in the fast-growing field of integrated photonics. It comprises a unique set of exciting electro-optic properties such as: a high electro-optic (EO) coefficient ($r_{33} = 30.8 \times 10^{-12}$ m/V at $\lambda = 0.63$ μm), high intrinsic IInd order nonlinearities ($d_{33} = -33$ pm/V at $\lambda = 1.064$ μm), and a large transparency window (350 nm – 5500 nm). Lithium niobate (LiN) has attracted a lot of attention since the 1970s [10][11].

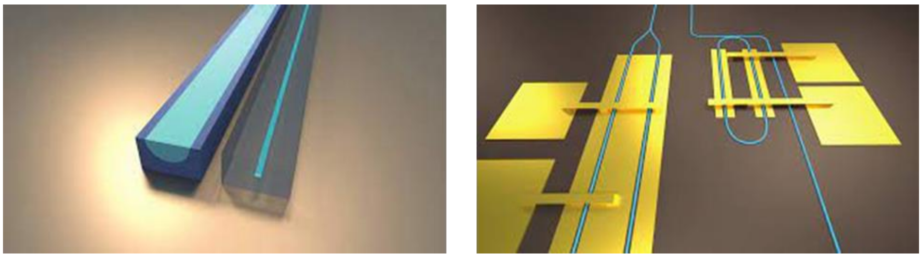

Fig. 1.6: Schematics of a traditional ion-diffused LN waveguide (left) and an optical modulator embedded in SiO2 (right).

However, most of its industrial success has been limited to devices made from bulk LiN crystals in the form of free-space or fiber-coupled components using ion-implanted waveguides. Recent advancements in bonding of single crystal thin films of LiN onto silicon substrates (LNOI), opens a new avenue to explore the advantages of LiN in the context of PICs and to benefit from their miniaturization, cost reduction, scalable manufacturing, and integration.

In an LNOI platform we can combine high performance active EO components such as modulators, phase shifters and tunable cavities with unique optical nonlinearities at a wide range of wavelengths to achieve truly novel functionalities and PIC designs that are beyond the capabilities of any PIC platform commercially available today. The heterogeneous integration of lithium niobate with SOI waveguides has attracted significant interest, which enabled electro-optical tunable resonators Mach-Zehnder modulators and Mid-IR modulators. Fig. 1.6

shows the schematics of a LiN based waveguide and modulator on SOI platform.

1.3.2 III-V Semiconductors

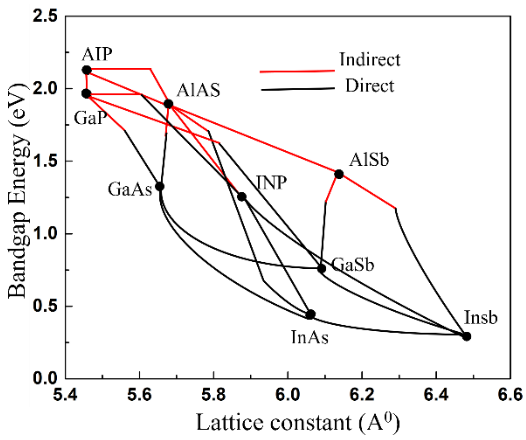

Fig. 1.7 Bandgap energies and lattice constants of most common III-V semiconductors

Most widely used semiconductors for optoelectronic device applications are compounds formed between elements of group III and group V of the periodic table. The bandgap energies and lattice constants of commonly used III-V semiconductors are shown in Fig. 1.7. These compound semiconductors find applications in different optoelectronic devices based on the parameters. The bandgap of the compound semiconductors can be engineered by alloying them. Bandgap engineering enables formation of heterojunctions that is critical for designing high-performance optoelectronic device like lasers [12][13].

InGaAsP alloys lattice matched to InP are widely used for fabricating various opto-electronic devices such as lasers, semiconductor optical amplifiers, modulators for long haul fiber communications owing to their bandgap energies in the low dispersion, low loss window for the optical fibers. However, poor temperature sensitivity of InP based lasers have prompted research in the direction of fabrication of long wavelength (~1.3 μm) lasers based on GaAs and its alloys. Another important application of GaAs based

1.3.3 Group-III Nitride

Group III-nitride semiconductors such as, Gallium Nitride and Aluminum Nitride are wide bandgap semiconductors with important optoelectronic applications. III-nitrides have outstanding electrical, thermal and optoelectronic properties which enable a broad range of technological applications including high speed and high-power electronics, blue/UV light emitting and laser diodes [14][15][16]. GaN is particularly notable for realizing high-speed device and AlN is an important material for making piezoelectric resonators.

Table 1.1. *Comparison of the electronic and optical properties of Si, GaN and AIN at 300 K.*

	Si	GaN	AlN
[17][18][19]Crystal structure	Diamaond cubic	Wurtzite or zinc-blende	Wurtzite or zinc-blende
Refractive index	3.47	2.43	2.11
Bandgap (eV)	1.12	3.4	6.2
Thermo-optic coefficient	$1.8x10^{-4}$	$6.0x10^{-5}$	$2.3x10^{-5}$
Thermal conductivity (W/m.K)	130	130	285
* All data refer to T= 300 K.			

In Table 1.1, the electronic and optical properties of Si, GaN and AlN are compared. These materials have a large refractive index (n = 2.43 for GaN; n = 2.11 for AlN) at the telecom wavelengths (1550 nm), which can enable compact-sized photonic waveguides. Both the materials can be found in either wurtzite or zinc blende structures, they are non-centrosymmetric and can hence give rise to significant second order optical nonlinearity. It has been reported that to have second-order optical susceptibility on the same order of that of lithium niobate.

Compared with silicon, Group III-Nitride semiconductors provide an additional benefit by having a large electronic bandgap (3.4 eV for GaN; 6.2 eV for AlN), and thus it not only provides suppression of two photon absorption but also allows for wideband operation from ultra-violet to infrared (IR) wavelengths.

1.3.4 2D-materials

As a consequence of the superior electronic and optical properties, two-dimensional (2D) materials have been extensively studied in recent years. Owing to their unique and significant properties, 2D materials have found applications in various fields of novel photonic devices including photodetectors, optical absorbers, optical modulators, fiber lasers and so on. These materials, through their self-limiting character, bloomed to be emerging candidates with their remarkable capability to deviate the present research from the nanometer scale to two-dimensionality by supplementing innumerable research opportunities to explore the photonics on which they are based. The major factor behind the popularity of 2D materials is the tunability of their band gap ranging from insulator to metal based on their layer thickness and this advantage can be employed in broadband photonic device applications. Graphene for example enjoys exceptionally high charge carrier mobility and is thus useful in realizing broadband and high-speed devices. Fig. 1.8 shows the Graphene's hexagonal atomic structure. Optical and electrical characteristics of graphene can be actively controlled via application of

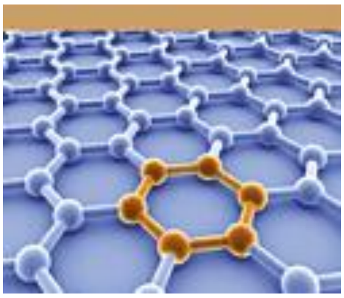

Fig. 1.8 Schematic illustration of Graphene's hexagonal atomic structure. Image Credit: IOP Science

either electrostatic or magnetostatic bias. The latter feature enables graphene devices to support very slow waves at different frequencies, resulting in miniaturized devices. However, there are some obstacles about graphene that hinder achieving its intriguing properties, including its fabrication technology, its contact with other materials.

1.3.5 Transparent Conducting Oxides

Transparent conducting oxides (TCOs) such as Sn-doped In_2O_3 (indium tin oxide, ITO), Al-doped ZnO, and Sb-doped SnO_2 are widely applied as transparent electrodes for liquid crystal displays (LCDs), organic light-emitting diodes (OLEDs), and solar cells. In addition, TCOs are applicable to transparent optoelectronics because they have the unique features of optical transparency in the visible region and controllable electrical conductivity, from almost insulating to degenerate semiconducting ($\sim 10^4$ S/cm) behavior[20][21]. Novel functions may be integrated into the materials since oxides have a variety of elements and crystal structures, providing great potential for realizing a diverse range of active functions.

Transparent conducting oxides (TCOs), for instance, Indium Tin Oxide (ITO) and Aluminum-doped Zinc Oxide (AZO), are oxide semiconductors conventionally used in optoelectronic devices such as flat panel displays and in photovoltaics. However, the application of TCOs has been restricted to transparent metals, notwithstanding the fact that TCOs are n-type semiconductors. The primary reason is the lack of p-type TCOs, because many of the active functions in semiconductors originate from the nature of the pn junction.

1.4 Zinc Oxide for Integrated Photonics

As a novel material of II-VI semiconductor, zinc oxide (ZnO) exhibits exciting opto-electronic properties. Significant improvement in the quality of ZnO single-crystal substrates and epitaxial films in previous decade has stimulated considerable amount of research interest in ZnO. Fig. 1.9 shows bulk crystal of ZnO. The prospect of using ZnO as a complement or alternative to GaN in optoelectronics has driven many research groups worldwide to focus on its semiconductor properties, trying to control the unintentional n-type conductivity and to achieve p-type conductivity. Being a TCO, the optical response of ZnO is governed by density of free charge carriers as well as carrier mobility, which is controlled through the addition of n-type dopants [22][23]. The free carrier concentration in ZnO can be high enough so that it exhibits metal-like behavior in the near-infrared (NIR) and mid-infrared (MIR) ranges which can be exploited for subwavelength light manipulation [24].

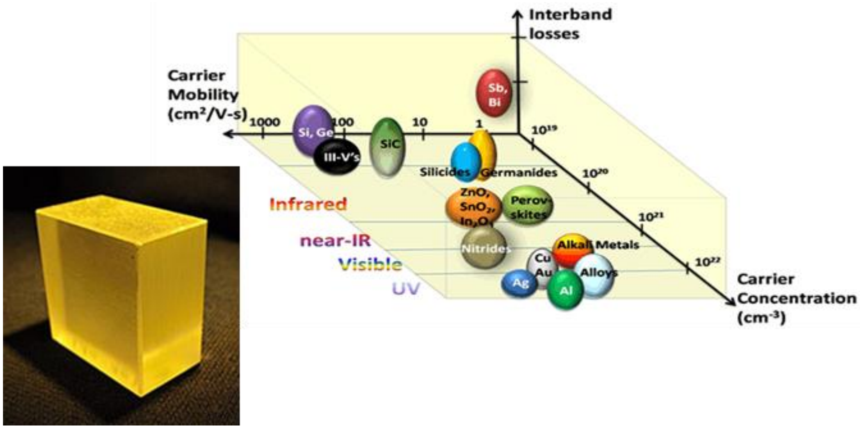

Fig. 1.9 ZnO bulk crystal (in left) Comparison of different conducting materials on the basis of charge carrier concentration, carrier mobility and Inter-band losses (in right).[25]

Moreover, in contrast to the optical properties of noble metals, which cannot be tuned or changed, the permittivity of TCOs can be adjusted via doping and/or fabrication process, providing certain advantages for designing various plasmonic and nanophotonic devices. Importantly, TCOs like ZnO possess a unique property of having a small negative real part of the permittivity at the telecommunication wavelengths. Structures that exhibit such near-zero permittivity (epsilon-near-zero [ENZ];) in the optical range can have a plasmonic resonance accompanied by slow light propagation. Fig. 1.9 plots different commonly used ENZ materials with respect to carrier mobility, carrier concentration and inter-band losses. Thus, conditions for enhanced light–matter interactions can be created. Also, the ZnO dopped with elements such as Mg and Cd allows realization of the band gap engineering and may help in development of several kinds of the light emitting components in UV, blue or even in green part of the spectrum. Few such exciting properties of ZnO are discussed below.

1.4.1 Properties

Direct and wide bandgap: At low temperatures, the bandgap of ZnO is 3.44 eV, whereas at room temperature, it is 3.37 eV. The respective bandgap values in case of GaN are 3.50 eV and 3.44 eV. The direct wide bandgap of ZnO allows various applications in opto-electronics in the blue and UV spectrum region such as laser diodes, LEDs, and detectors. Several reports have demonstrated optically pumped lasers in ZnO based nanocrystal, thin films, platelets, and nanowires. Although realization p-n homojunction are also recently reported however, there still exist serious doubts on their reproducibility and stability.

Large exciton binding energy: ZnO has a free exciton binding energy of 60 meV, which is more than half of its counterpart i.e. GaN [26][27]. Such a large exciton-binding energy suggests the possibility of efficient excitonic emission at room temperature. The enormous exciton binding energy makes ZnO a material of choice for opto-electronic devices exciton-based functionalities, as the exciton-oscillator strength is generally much stronger as compared to the e-h transitions in direct band-gap semiconductors.

Large non-linear optical coefficients: ZnO crystals and thin films exhibit second- and third-order non-linear optical behavior, suitable for non-linear optical devices. The linear and non-linear optical properties of ZnO depend on the crystallinity of the samples. ZnO films grown by laser deposition, reactive sputtering and spray pyrolysis show strong second-order non-linear response. Third-order non-linear response has recently been observed in ZnO nanocrystalline films [102]. The non-linear optical response in ZnO thin films is attractive for integrated non-linear optical devices.

Large piezoelectric constants: In some materials, application of mechanical stress generates potential difference and vice-versa. Such materials are known as piezoelectric materials and can be used as actuators, sensors and transducers. The strong piezoelectric is mainly attributed to the lack of symmetry in the crystal structure of ZnO (i.e. wurtzite) along with its large electromechanical coupling. Growth of uniform thickness of ZnO films with excellent piezoelectric properties have been extensively reported via Physical Vapor Deposition (PVD), sol-gel, sputtering and spray pyrolysis.

Strong luminescence: ZnO, owing to its exceptional luminescence in the part of visible spectrum is an excellent material for applications in phosphor [28][29]. The emission spectra are characterized by a broad peak with width of 0.8 eV at 495 nm. Additionally, the inherent n-type nature of ZnO offers it advantage for various application in areas such as field emission and vacuum fluorescent displays. The source and mechanism of luminescence in ZnO is still not fully established however, recently in several reports green luminescence is attributed Zn vacancies.

Amenability to wet chemical etching: Semiconductor device fabrication processes greatly benefit from the amenability to low-temperature wet chemical etching. It has been reported that ZnO thin films can be etched with acidic, alkaline as well as mixture solutions. This possibility of low-temperature chemical etching adds great flexibility in the processing, designing and integration of electronic and optoelectronic devices.

Radiation hardness: Radiation hardness is important for applications at high altitude or in space. It has been observed that ZnO exhibits exceptionally high radiation hardness even greater than that of GaN, the cause of which is still unknown.

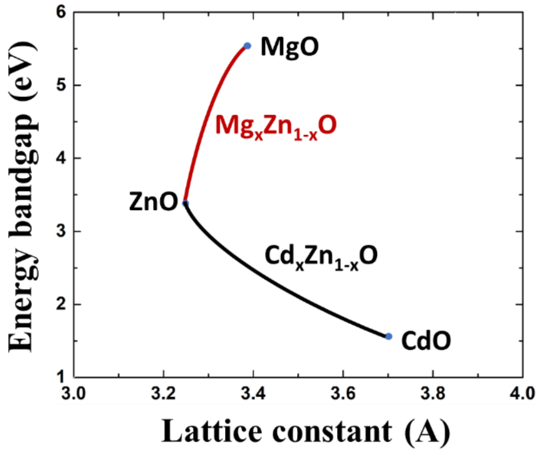

Fig. 1.10 Bandgap of ZnO, MgO and CdO with respect to their lattice constants.

1.4.2 Bandgap Engineering in ZnO:

Electronics and opto-electronics industry commonly employ semiconductor heterojunctions to provide potential barriers and quantum wells that tune and control carrier transport. Tailoring the composition of the material is the most widely used method to alter the band gap of the materials in the so called "bandgap engineering" to realize semiconductor heterojunctions. Bandgap engineering in ZnO can be achieved by doping ZnO with atoms of Mg and Cd. While, adding Mg to ZnO increases the band gap, whereas Cd decreases the band gap, like the effects of Al and In in GaN. Although MgO and CdO crystallize in the rocksalt structure, for moderate concentrations the $Mg_{1-x}Zn_xO$ and $Cd_{1-x}Zn_xO$ alloys assume the wurtzite structure of the parent compound, while still leading to significant band-gap variation. Fig. 1.10 shows bandgap and lattice constants of MgO, ZnO and CdO [30].

1.4.3 Two-Dimensional Electron Gas in ZnO Based Heterojunction:

A heterostructure is formed when two materials with different bandgap are deposited over one another keeping their individual properties intact. In case of presence of a large band gap difference at the interface of such heterostructures, an energy discontinuity is created

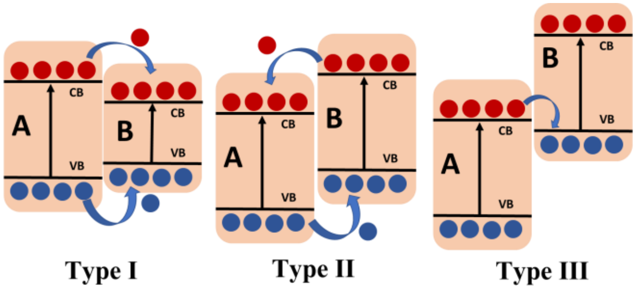

Fig. 1.11 *Types of electronic band alignment in semiconductor heterojunction.*

in the energy band spectrum at the interface. Fig 1.11 depicts different types of semiconductor heterojunctions based on the alignment of their bands. For centrally band aligned heterostructures with either material being undoped or *n*-type doped, the energy discontinuity makes the energy band to bend in the formation of a notch in the conduction band and a valley in the valence band at the interface, both of which are formed in the lower band gap material. Fig. 1.12 visualizes a band diagram of a heterostructure that yields such band gap discontinuity. In case the notch formation in the conduction band lies below fermi energy level, the energy states lying below fermi energy level have the potential to accommodate electrons free from the influence of the lattice atoms of either material, forming a quantum potential well. Such energy states are called two-dimensional energy states (2-DES) as they can accommodate two-dimensional electron gas (2-DEG). Therefore, this notch's depth defines the ability of the heterostructure to accommodate 2DEG. The notch's depth is defined by the conduction band discontinuity (ΔEc) or the conduction band offset, which in turn is dependent upon the difference in the band gap of two materials known as bandgap discontinuity (ΔEg). Considering the case of ZnO based heterostructure with MgZnO being the high band gap material (barrier layer) and ZnO being the low band gap material (buffer layer). The content of magnesium in the barrier layer defines the bandgap of MgZnO. In case of MgZnO/ZnO heterostructure, ΔEc is calculated as $\Delta E\text{c} = 0.9 \times \Delta E\text{g}$. While MgZnO/ZnO heterostructure has shown to induce a high sheet

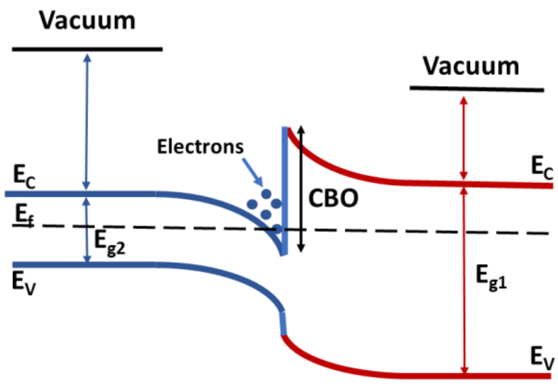

Fig. 1.12 Electronic band diagram of a typical centrally aligned semiconductor heterojunction along with confined charge carriers

density (n_s) (~ 10^{13} cm^{-2}) 2-Dimensional Electron Gas (2-DEG) at room temperature by Tampo *et al* [31] the Mg composition required to achieve such high n_s has been as high as 0.6 in barrier layer MgZnO, which is difficult to fabricate without the occurrence of phase separation. This implies that for lower Mg composition in barrier layer, higher 2-DEG density is very difficult to achieve in MgZnO/ZnO heterostructure. Ding *et al.* [32] has proposed $Be_yMg_xZn_{1-x-y}O$ as the barrier layer to circumvent this limitation and has achieved 2-DEG density comparable to that achieved in the case of $Mg_{0.6}Zn_{0.4}O$/ZnO heterostructure achieved by utilizing y = 0.2 and x = 0.26 [32]. Benharrats *et al* [33]. have shown that 2-DEG can be increased further with the use of CdZnO/ZnO heterostructure [34]. Although the use of CdZnO/ZnO, BeZnO/ZnO, or BeMgZnO/ZnO heterostructures are beneficial for enhancing 2-DEG density compared to that in MgZnO/ZnO, the main drawback of all these structures is that the polarization in ZnO buffer does not change significantly. Therefore, any improvement in 2-DEG density is solely governed by the change in the polarization in barrier layer. A possible option to circumvent this limitation proposed in this work is to alloy CdO in the buffer layer, which would result in MgZnO/CdZnO heterostructure, instead of MgZnO/ZnO or CdZnO/ZnO. This provides an opportunity to modulate the barrier as well as buffer layer polarization components towards enhanced n_s, which otherwise has been restricted to barrier layer only. Therefore, this approach explores the possibility of achieving high 2-DEG density in low-cost large-area-electronics compatible sputter grown MgZnO/CdZnO heterostructure towards opto-electronic functionalities.

1.5 Semiconductor Nanostructures for Enhanced Light-Matter Interactions:

Nanophotonics encompasses a wide range of nontrivial physical effects including light-matter interactions that are well beyond diffraction limits and have opened up new avenues for a variety of applications in light harvesting, sensing, luminescence, optical switching, and media transmitting technologies [35][36][37]. Recently, growing expertise of fusing nanotechnology and photonics has become fundamental, arising outskirts, challenging basic experimentation and opportunities for new technologies in our daily lives, and played a central role in many optical systems. It entails the theoretical study of photon's interactions with matter at incredibly small scales, known as nanostructures, in order to prepare nanometer scale devices and accessories for processing, development, slowing down, influencing, and/or regulating photons through comprehending their behavior while interacting with or otherwise traveling via matter. This multidisciplinary field has also made an impact on industry, allowing researchers to explore new

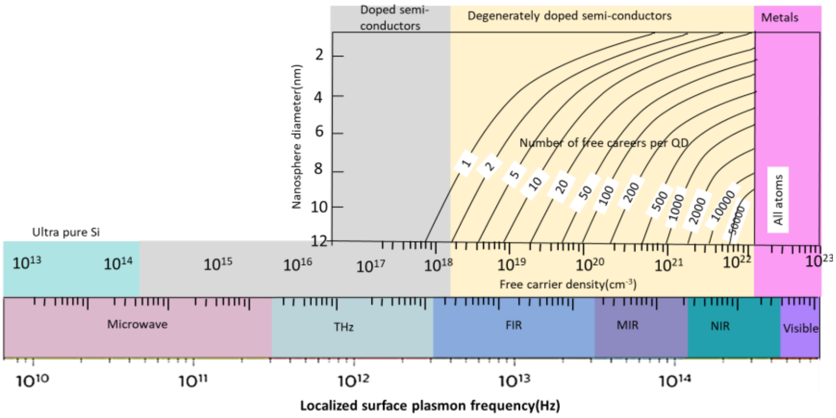

Fig. 1.13 *LSPR frequency for different particle size of semiconductor nanocrystals calculated using Drude model.*

horizons in design, applied science, physical science, chemistry, materials science, and biomedical technologies.

Recent advancements in heavily doped Epsilon-Near-Zero (ENZ) material nanocrystals have supplemented immense research opportunities for examining collective charge carrier oscillations and their interaction with light at very fundamental level. Latest findings demonstrating Infrared (IR) absorption bands in heavily doped semiconductor nanocrystals similar to that shown in metallic nanostructures have proved plasmonic resonance to be a ubiquitous signature of free charge carriers instead of just being associated with optical response of metals. Prospects of realizing plasmonic resonance with semiconductors has opened up new windows of opportunities where plasmonics will provide enhanced light-matter interaction while semiconductors will allow dynamic tunability. The plasmonic response of nanoparticle in particular displays enhanced sensitivity to small change in charge carriers. Theoretically the electro-optic sensitivity can be estimated as $1/r^3$, which means smaller the nanoparticle is greater the sensitivity of its LSPR frequency, to change in charge carrier concentration becomes. Since metal nanoparticles contains a sizable number of charge carriers, achieving dynamic modulation by inducing a significant change in its carrier density becomes impractical. Semiconductor q-dots owing to wide band of carrier densities are thus ideal choice for realizing various active device functionalities using tunable plasmonics. Fig. 1.13 shows Drude model based two-dimensional plot depicting correlation between LSPR frequency and free charge carrier density in semiconductor nanoparticles [24].

1.6 Organization of Thesis:

The thesis is organized into seven chapters starting with an introduction to hybrid integrated photonics devices, literature review of past work and problem formulation followed by 4 major chapters on original research work done and the final chapter on conclusion and the future scope.

Chapter 2. Recent Trends in Bandgap Engineered Photonic Devices: Second chapter consists of a brief literature review on the band gap engineering in semiconductor heterojunction, optical properties of 2-Dimensional Electron Gas, sub-bandgap modulation and photodetection, and semiconductor nanostructures for plasmonic resonance. The chapter concludes by highlighting the problem formulation for the dissertation.

Chapter 3. **Broadband Optical Modulation in Zinc Oxide based Heterojunction:** This chapter describes experimental demonstration of a broadband, electro-absorptive modulator which utilizes bandgap engineering in ZnO based heterojunction for sub-bandgap operation. Tunable absorption via optical lifting of confined electrons across the potential barrier in the ZnO based heterojunction is studied. The device is optimized for high quantum efficiency and demonstrates high extinction ratio for broad range of wavelength in IR-visible region.

Chapter 4. Efficient Sub-Bandgap Photodetection via Two-Dimensional Electron Gas: This chapter features experimental demonstration of a sub-bandgap photodetection via 2-D electron gas in ZnO based heterojunction. Internal photoemission via optical excitation of confined electron gas formed at the heterojunction in a metal-less device is studied. Role of improved momentum matching across ZnO based heterojunction for superior Internal Quantum Efficiency (IQE) in the proposed structure is discussed with the help of a physical model explaining the underlying the mechanism of device operation.

Chapter 5. On-chip Nanophotonic Broadband Wavelength Detector with 2D-Electron Gas: This chapter explores the wavelength sensitive internal photo response of 2DEG at the semiconductor heterojunction for wavelength detection. The novel device employing two semiconductor heterojunctions take the advantage of wavelength sensitive photocurrent along with a reference junction current for common mode rejection. Several benefits such as simple fabrication, on-chip compatibility and broadband operation of the proposed device are highlighted. Finally, the chapter concludes by comparing the proposed device with other best-in-class for applications in optical spectrometer, sensing and Internet of Things (IOTs).

Chapter 6. Voltage Tunable Plasmonic Resonance in ZnO based Nanostructures: This chapter investigates plasmonic resonance in non-metallic on-chip platform using heavily doped Epsilon-Near-Zero (ENZ) material (Zinc Oxide) nanoparticles. Plasmonic response of smaller nanoparticles exhibits enhanced sensitivity to change in free charge carrier concentration. The proposed design uses highly doped ZnO nanowire grown inside anodized aluminum template. Effect of modulation doping via applied voltage bias on plasmonic response of the nanoparticles is studied. Voltage tunability of localized surface plasmon resonance in NIR region of the spectrum via an on-chip platform can fundamentally expand the domain of semiconductor plasmonic and open up new avenues allowing applications which were initially unthinkable.

Chapter 2

Recent Trends in Bandgap Engineered Photonic Devices

2.1 High Density of Two-Dimensional Electron Gas in ZnO Based Heterojunction

H. Tampo et.al-2006 [38] reported two-dimensional electron gas in Zn polar ZnMgO/ZnO heterostructures grown by radical source molecular beam epitaxy. Elemental Zn and RF radical oxygen were used as group II and group VI sources, respectively. Zn polar ZnO layers on c-plane sapphire were grown by controlling the thickness of the MgO buffer, located between the ZnO layer and the sapphire substrate. The thicknesses of the MgO buffer and the Zn-MgO and ZnO layers were 10 nm, 100 nm, and 1 μm, respectively, as shown in Figure 2.1. The Mg composition was determined based on reflectance measurements.

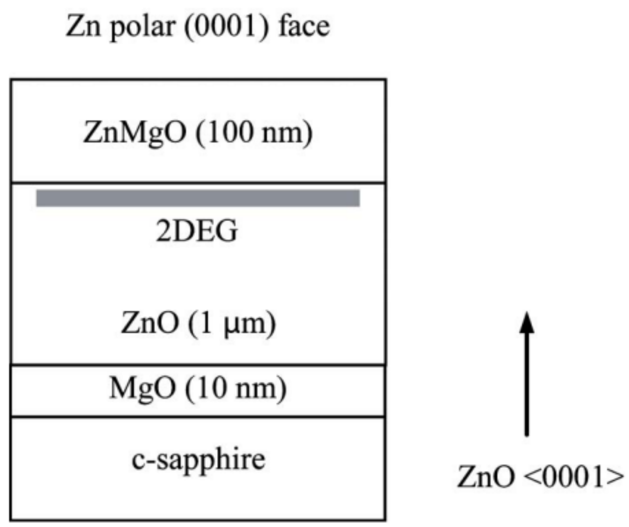

Figure 2.1: (Color online) Layer structure for a Zn polar ZnMgO/ZnO heterostructure. The growth direction is <0001> for Zn polarity.

The polarity of the ZnO layers was determined by anomalous dispersion x-ray diffraction measurements, a method which is both simple and nondestructive. The electrical properties of the ZnO films were measured using Hall effect measurements with a van der Pauw geometry and a magnetic field of 0.77 T. Hall measurements were conducted over the temperature range of 4–300 K using a continuous flow helium cooling system. The electrical properties were also investigated using capacitance-voltage (C-V) measurements for a 30 nm ZnMgO layer with Pt Schottky contacts.

The electron mobility of the ZnMgO/ZnO heterostructures dramatically increased with increasing Mg composition and the electron mobility (μ~250 cm^2 /V s) at RT reached a value more than twice that of an undoped ZnO layer (μ~100 cm^2 /V s). The carrier concentration in turn reached values as high as ~ 1 x 10^{13} cm^{-2} and remained nearly constant regardless of Mg composition. Strong confinement of electrons at the ZnMgO/ZnO interface was confirmed by C-V measurements with a concentration of over 4 x 10^{19} cm^{-3}. Temperature-dependent Hall measurements of ZnMgO/ZnO heterostructures also exhibited properties associated with well-defined heterostructures. The Hall mobility increased monotonically with decreasing temperature, reaching a value of 2750 cm^2 /V s at 4 K. Zn polar "ZnMgO on ZnO" structures are easy to adapt to a top-gate device. These results open new possibilities for high electron mobility transistors based upon ZnO-based materials.

J.D. Ye et.al-2010 [39] reported the formation of two-dimensional electron gas (2DEG) at the $Zn_{1-x}Mg_xO$/ZnO interface grown by metal-organic vapor phase epitaxy on sapphire substrates. The existence of the 2DEG is confirmed by the observation of Shubnikov–de Haas oscillations and the integer quantum Hall effect. In particular, the $Zn_{0.8}Mg0_{0.2}O$/ZnO heterostructure shows a high Hall mobility of 2138 cm^2/V s with a carrier sheet density of 3.51×10^{12} cm^{-2} at 1.4 K.

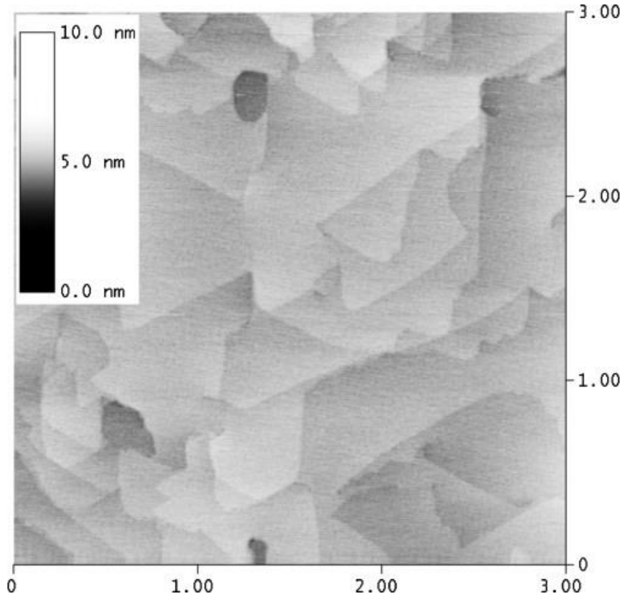

Figure 1.2: AFM image of Zn0.83Mg0.17OZn0.83Mg0.17O epilayer with thickness of 27 nm on ZnO template.

We attribute the origin of 2DEG to be the donor states on ZnMgO surface. The dependence of carrier sheet density of 2DEG on ZnMgO layer thickness and Mg composition (x) are also investigated. If ZnO layer was the origin of the 2DEG, then the carrier concentration would be independent of $Zn_{1-x}Mg_xO$ layer thickness as well as x composition. The 2DEG density is also not proportional to the $Zn_{1-x}Mg_xO$ layer thickness, which suggests that the effect of donors in ZnMgO layer is not so important.

2.2 Electronic and Optical Properties of 2-Dimensional Electron Gas

H.S. Kwack et.al-2005 [15] investigated the optical properties and carrier dynamics of the two-dimensional electron gas (2DEG) in $Al_{0.4}Ga_{0.6}N$/GaN single heterostructures grown by metalorganic chemical vapor deposition by means of photoluminescence (PL), PL excitation, and time-resolved PL spectroscopy. Shubnikov-de Haas oscillations were clearly observed at 1.5 K, confirming the existence of a 2DEG. An additional 2DEG PL emission appeared at about 40 meV below the GaN band-edge emission and persisted up to about 100 K, while this peak disappeared when the top Al0.4Ga0.6N layer was removed by reactive ion etching. We observed abrupt PLE absorption at GaN band edge energy and approximately 50-ps delayed risetime compared to GaN and AlGaN emissions, indicating effective carrier transfer from the GaN flatband and AlGaN regions to the heterointerface. Even though the 2DEG emission is a spatially indirect (slow) recombination, a fast decay component of ~0.2 ns is found to be dominant in 2DEG emission because of the fast exhaustion of photogenerated holes in GaN flatband region via spatially direct (fast) GaN recombination. From the results, we explain the carrier generation, transfer, and recombination dynamics and the relationships between 2DEG, GaN, and $Al_{0.4}Ga_{0.6}N$ emissions in undoped $Al_{0.4}Ga_{0.6}N$/GaN single heterostructures.

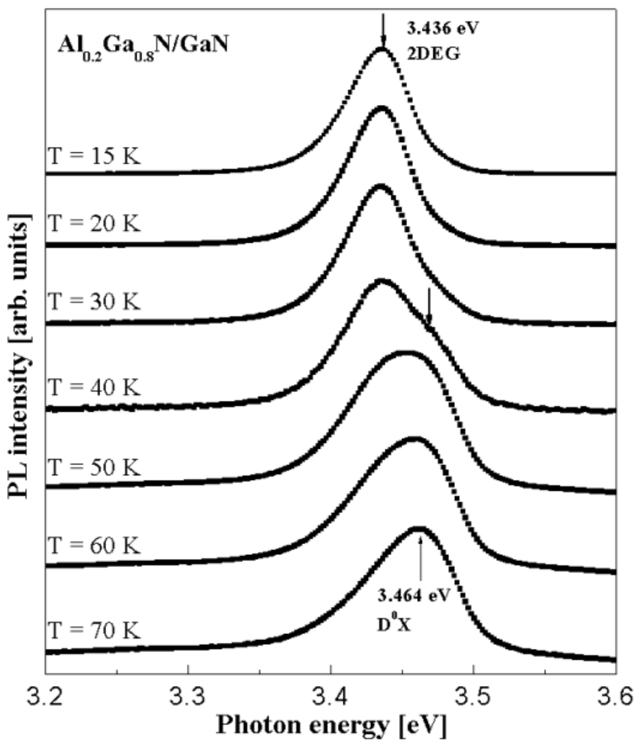

Figure 2.2: Temperature-dependent photoluminescence of an $Al_{0.2}Ga_{0.8}N$/GaN heterostructure.

Y.S. Park et.al-2003 [40] have studied optical properties related to a two-dimensional electron gas at an AlGaN/GaN heterostructure. Figure 2.4 exhibits the PL spectra of an as-grown Al-GaN/GaN heterostructure sample measured at different temperatures ranging from 15 to 70 K. They have reported photoluminescence spectra related to the two-dimensional electron gas confined at the AlGaN/GaN heterointerface. The PL peak related to recombination between the two-dimensional electron gas and photoexcited holes is located at 3.436 eV at 15 K, which is 28 meV below the bound exciton (D^0X) emission in GaN. The 2DEG-related PL was identified by measuring the PL of the structure as functions of the light intensity and the temperature and comparing the results with those for GaN exposed via etching.

2.3 Intensity Modulators and Key Parameters

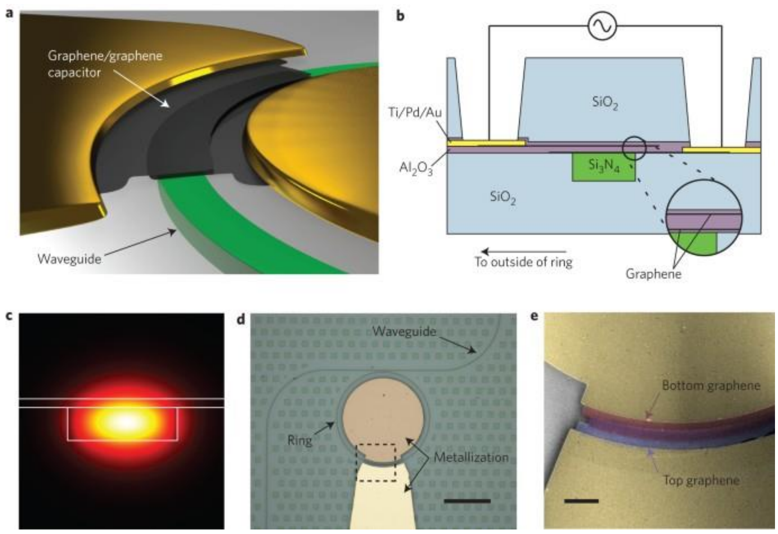

Figure 2.3: Graphene electro-optic modulator with 30 GHz bandwidth

C.T. Phare et.al-2015 [41] reported that graphene has generated exceptional interest as an optoelectronic material because of its high carrier mobility and broadband absorption promise to make extremely fast and broadband electro-optic devices possible. Electro-optic graphene modulators previously reported, however, have been limited in bandwidth to a few gigahertz because of the large capacitance required to achieve reasonable voltage swings. Here, we demonstrate a graphene electro-optic modulator based on resonator loss modulation at critical coupling that shows drastically increased speed and efficiency. Our device operates with a 30 GHz bandwidth and with a state-of-the-art modulation efficiency of 15 dB per 10 V. We also show the first high-speed large-signal operation in a graphene modulator, paving the way for fast digital communications using this platform. The modulator uniquely uses silicon nitride waveguides, an otherwise completely passive material platform, with promising applications for ultra-low-loss broadband structures and nonlinear optics.

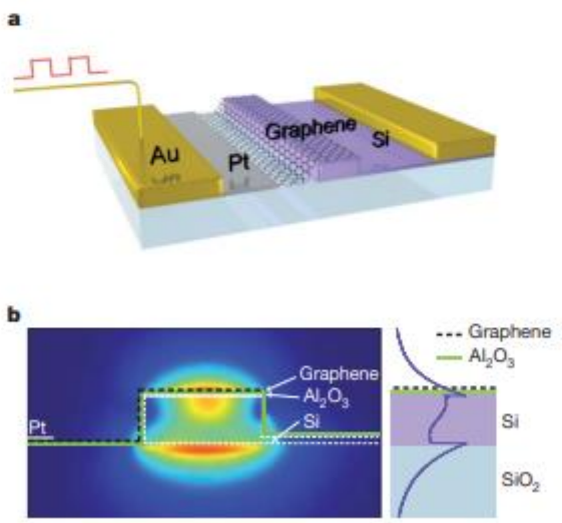

Figure 2.4: A graphene-based waveguide-integrated optical modulator. (a) Three-dimensional schematic illustration of the device; a monolayer graphene sheet is on top of a silicon bus waveguide. (b) Left, cross-section of the device, with an overlay of the optical mode plot, calculated by finite element simulation.

M. Liu et.al-2011 [42] reported the first waveguide-integrated graphene-based electro-absorption modulator, in which modulation is achieved by actively tuning the Fermi level of a monolayer graphene sheet. The structure of the electro absorption modulator is schematically illustrated in Fig. 2.5. A 50-nm-thick Si layer was used to connect the 250-nm-thick Si bus waveguide and one of the gold electrodes. Both the silicon layer and the waveguide were shallowly doped with boron to reduce the sheet resistance. A spacer of 7-nm-thick Al2O3 was then uniformly deposited on the surface of the waveguide by atom layer deposition. A graphene sheet grown by chemical vapour deposition (CVD) was then mechanically transferred onto the Si waveguide. The cross-sectional view of the device structure and the optical field distribution of the guided mode are shown in Fig. 2.5 (b). The thin silicon layer and the platinum electrode adjacent to the waveguide have negligible effect on the mode profile. The gigahertz graphene modulator demonstrates a strong electro-absorption modulation of 0.1 dB/μm and operates over a broad range of wavelength, from 1.35 mm to 1.6 mm, under ambient conditions.

2.4 Sub-bandgap Photodetection via Internal Photoemission

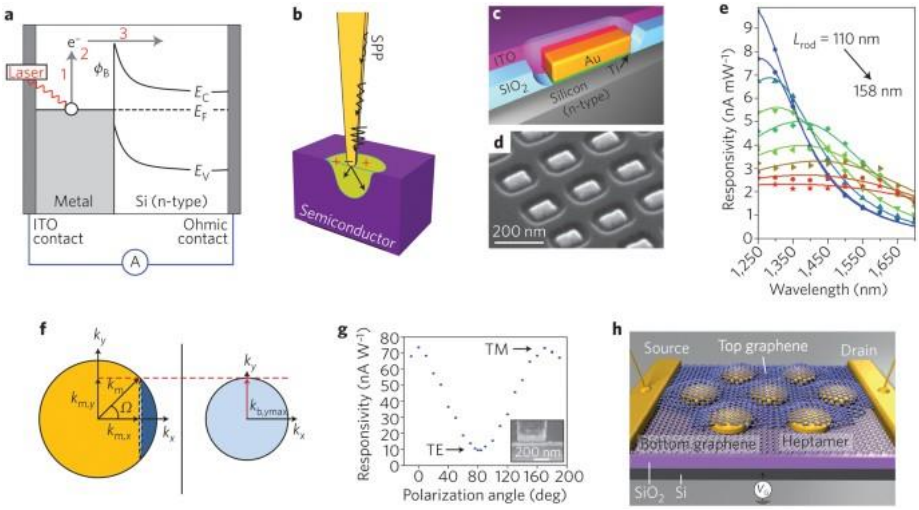

Figure 2.5: Plasmon induced hot carrier science and technology.

M.L. Brongersma et.al-2015 [43] stated that the The discovery of the photoelectric effect by Heinrich Hertz in 1887 set the foundation for over 125 years of hot carrier science and technology. In the early 1900s it played a critical role in the development of quantum mechanics, but even today the unique properties of these energetic, hot carriers offer new and exciting opportunities for fundamental research and applications. Measurement of the kinetic energy and momentum of photo ejected hot electrons can provide valuable information on the electronic structure of materials. The heat generated by hot carriers can be harvested to drive a wide range of physical and chemical processes. Their kinetic energy can be used to harvest solar energy or create sensitive photodetectors and spectrometers. Photoejected charges can also be used to electrically dope two-dimensional materials. Plasmon excitations in metallic nanostructures can be engineered to enhance and provide valuable control over the emission of hot carriers. This Review discusses recent advances in the understanding and application of plasmon-induced hot carrier generation and highlights some of the exciting new directions for the field.

I. Goykhman et.al-2014 [44] reported a model for quantum efficiency of guided mode plasmonic enhanced silicon Schottky detectors. Plasmonic enhanced Schottky detectors operating on the basis of the internal photoemission process are becoming an attractive choice for detecting photons with sub bandgap energy. Yet, the quantum efficiency of these detectors appears to be low compared to the more conventional detectors which are based on inter-band transitions in a semiconductor. Hereby we provide a theoretical model to predict the quantum efficiency of guided mode internal photoemission photodetector with focus on the platform of silicon plasmonic.

2.5 Two-Step Anodization as a Template for Semiconductors Nanostructure

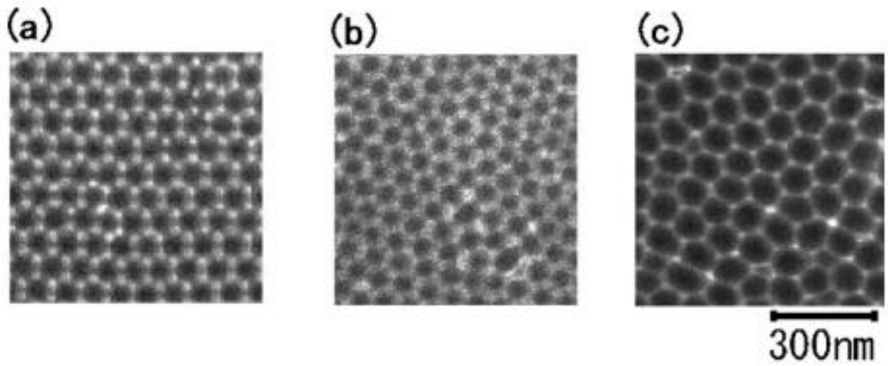

Figure 2.6: SEM images of the underside of nanoholes obtained by different acids at the same anodic oxidation conditions of 36 V and 2 h.

(a) An acid mixture containing 0.3 M sulfuric acid and 0.3 M oxalic acid. (b) 0.3 M sulfuric acid. (c) 0.3 M oxalic acid. Plasmon induced hot carrier science and technology.

S. Shingubara et.al-2004 [45] reported the possibility of fabricating a highly regular nanohole array using different acid mixtures for the anodic oxidation of aluminum was investigated. The regularity of a nanohole array formed using a 1:1 sulfuric/oxalic acid mixture was quantified. Excellent regularity was obtained at around an anode voltage of 32 to 36 V. Cell pitch of the nanohole array at 36 V was 73 nm, which falls between those obtained using sulfuric acid ~65 nm at 28 V and oxalic acid ~95 nm at 40 V. The present results strongly suggest that the pitch of the regular nanohole array can be varied by changing the ratio of the different acids.

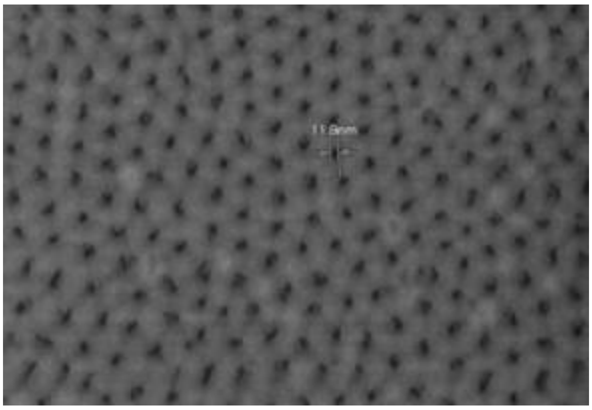

Figure 2.7: SEM images 12 nm pore diameter self-ordered anodic alumina templates

C.V. Manzano et.al-2014 [46] demonstrated Ordered anodic aluminum oxide (AAO) templates with pores of 12 nm in diameter and aspect-ratios (length-to-diameter) of >1000 is prepared by a simple two-step anodization process under mild-anodization conditions. Such a low diameter pores are consequence of the reduction of the dielectric constant of the electrolyte together with the effect of increasing the electrolyte viscosity. We show that the temperature has a strong impact on reducing the pore diameter, as provokes the increase of viscosity of the medium and thus the hindering of the diffusion of species involved in the widening of pores. Moreover, we manage to stop the AAO growth process at the pore nucleation stage and we show that 8 nm in diameter pores are originally formed under these conditions. The presented ultra-narrow pore templates may allow for the preparation of ordered arrays of high aspect-ratio ultra-small one-dimensional (1D) nanostructures that could be useful to explore quantum phenomena and integrate quantum-devices.

2.6 Plasmon Resonance in Semiconductor Nanostructures

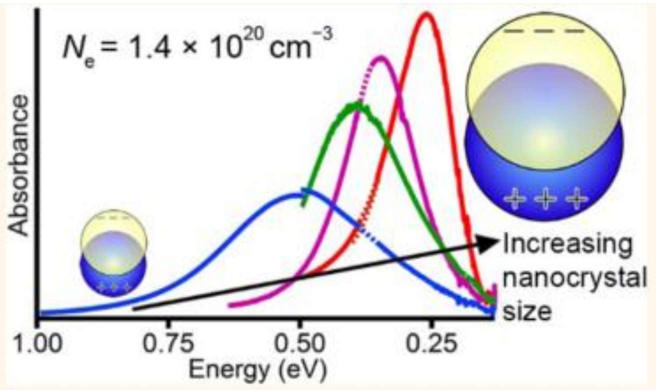

Figure 2.8: Charge-Tunable Quantum Plasmons in Colloidal Semiconductor Nanocrystals

Alina M. Schimpf et.al-2014 [47] demonstrated charge-tunable quantum plasmons in colloidal semiconductor nanocrystals. Nanomaterials exhibiting plasmonic optical responses are impacting sensing, information processing, catalysis, solar, and photonics technologies. Recent advances have expanded the portfolio of plasmonic nanostructures into doped semiconductor nanocrystals, which allow dynamic manipulation of carrier densities. Once interpreted as intraband single-electron transitions, the infrared absorption of doped semiconductor nanocrystals is now commonly attributed to localized surface plasmon resonances and analyzed using the classical Drude model to determine carrier densities. Here, we show that the experimental plasmon resonance energies of photodoped ZnO nanocrystals with controlled sizes and carrier densities diverge from classical Drude model predictions at small sizes, revealing quantum plasmons in these nanocrystals. A Lorentz oscillator model more adequately describes the data and illustrates a closer link between plasmon resonances and single-electron transitions in semiconductors than in metals, highlighting a fundamental contrast between these two classes of plasmonic materials.

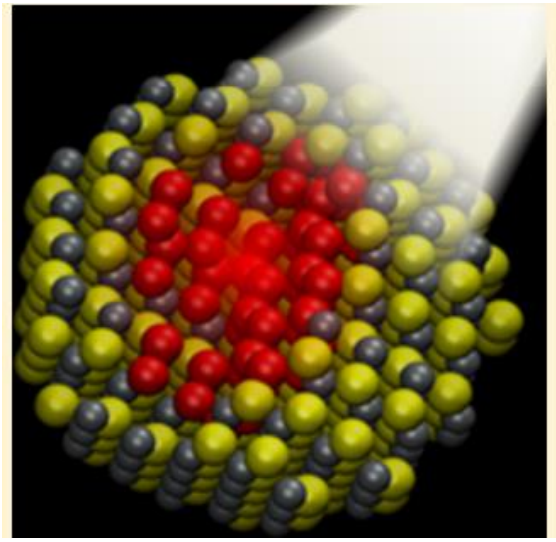

Figure2. 9: Plasmon Resonances of Semiconductor Nanocrystals

Jacob A. Faucheaux et.al-2014, [24] reported plasmon resonances of semiconductor nanocrystals: physical principles and new opportunities. The discovery of localized surface plasmon resonances (LSPRs) in doped semiconductor nanocrystals has opened a new regime in plasmonic. We address both the technological and fundamental advances made possible by the realization of LSPRs in semiconductor nanocrystals. LSPRs were originally thought to be specific only to metallic nanostructures, but since their manifestation in semiconductor nanostructures, LSPRs are being seen as ubiquitous optical signatures of charge carriers. As fingerprints of a charge carrier collection, LSPRs of semiconductors are emerging as optical probes of processes that involve carrier dynamics, including redox reactions, electrochemistry, phase transitions, and photocatalysis. Unlike their electrical counterparts, LSPRs allow remote contactless probing and minimal device design.

Ultrasmall semiconductor quantum dots are now enabling access to plasmon resonances of a handful of charge carriers, allowing us to ask fundamental questions regarding the lower limit of charge carriers needed to sustain a plasmon resonance, the emergence of a collective mode from a single-electron transition, and the effect of quantum confinement on plasmon resonances. These fundamental issues are discussed here, along with the need for new physical models required to capture the unique aspects of semiconductor LSPRs.

2.7 Motivation and Objectives

In the first chapter we have discussed the need for hybrid integrated circuit platform and choice of materials. We have also discussed the advantages offered by plasmon resonance for high performance opto-electronic devices like modulator and photodetector. Consequently, after conducting a deep literature survey on the previous works related to novel waveguiding schemes, state-of-the-art optical modulators, and photodetectors, we observed certain areas with significant scope of improvement. Thus, there are two major motivations for this thesis work. First is to conceptualize a sub-bandgap approach to exploit active photonic functionalities of Zinc Oxide in the spectral region well below its bandgap for realizing different major building blocks of photonic integrated circuits. Second one is to realize plasmonic resonance in ZnO nanoparticle in Near Infrared (NIR) region for enhanced light-matter interaction in beyond diffraction limit regime while bypassing the lattice mismatch issue faced in hybrid integration.

Based on the above discussions, following are the objectives of the research work carried out for this thesis:

- Experimentally realizing sub-bandgap optical modulation in visible-IR region via two-dimensional electron gas in ZnO based heterojunction.
- Design, fabricate and characterize ZnO heterojunction based sub-bandgap photodetection with high quantum efficiency.

- Demonstrate broadband wavelength detection on an on-chip platform using 2-dimension electron gas in ZnO heterojunction.
- Finally, the aim is to surpass the diffraction limit while enhancing light-matter interaction by demonstrating the plasmonic resonance in ZnO nanoparticles based on-chip compatible platform.

Chapter 3

Broadband Optical Modulation in Zinc Oxide based Heterojunction

3.1 Introduction

The optical modulator, which constitutes an essential part of optical communication and optical interconnects, can limit the performance of the optical communication link. Silicon forms the backbone of the electronic industry owing to the advances in complementary metal-oxide-semiconductor (CMOS) technology. Recently, silicon has found its way to enable various photonic functionalities. However, silicon still struggles with its unimpressive opto-electronic properties attributed to its indirect bandgap and low electro optic coefficient. A large amount of research has been focused to come up with alternative (best in class) materials to build efficient integrated photonic devices. Presently, electro-refractive and electro-absorptive based approaches are being used to achieve modulation. The electro-refractive approach typically utilizes control over the real part of material permittivity with the help of plasma dispersion or free carrier absorption. However, due to the low electro-optic coefficient of silicon, such devices struggle with a large device footprint and high capacitance [48][49][50][51][52][53] which consequently raises the power consumption. This can be overcome by employing resonator-based designs such as ring resonators; however, they demand a significant quality factor resulting in a rigorous fabrication process and a narrowband modulation [54] [55] In contrast, electro absorptive modulators (EAMs) utilize the change in the imaginary part of the refractive index with the help of the Franz–Keldysh or quantum confined Stark effect (QCSE) in a germanium-based quantum well [56] [57]. This works by shifting the band-edge peak or exciton peak in quantum well structures with the help of the applied electric field. Although the QCSE provides a high extinction ratio at lower voltages, it nevertheless suffers from an inherently narrowband spectral range coupled with a finite bandgap of germanium. There have been several reports on high-speed intensity modulators based on inter sub-band (ISB) transitions in quantum well structures; however, modulation in a communication regime requires a large conduction band difference which attracts large strain due to high doping concentration. Some reports have shown broadband modulation in graphene-based modulators but with a low extinction ratio and stringent fabrication processes [42] [58]. An increasing number of Internet users demand implementation of broadband upgradation on a shared-access network, creating major implications for the requirement of broadband functionality of optical modulators. However, a narrow energy bandgap of commonly used semiconductors, along with a limited operational range of conventionally employed modulation scheme, i.e., resonator based or QCSE, demands a fresh approach towards modulation. A wide bandgap semiconductor such as zinc oxide (ZnO) and gallium nitride (GaN) with a sub-bandgap modulation approach could enable guidance and modulation on a much broader range of the spectrum. The spectral limit for operating wavelength due to the bandgap of different commonly used semiconductors is illustrated in the Fig. 1(a). Besides possessing a direct and wide bandgap, ZnO can also form a heterojunction with a smaller lattice mismatch by alloying with MgO and CdO in moderate concentration [58] [59]. Enhanced efforts invested in the study of ZnO material system have led to a greater understating of the nature of impurities and its electrical behavior. However, achieving a stable p-type ZnO still remains a major challenge. Its high exciton energy, high saturation velocity, and amenability to wet etch, along with the prospects of achieving stable p-type behavior, offers ZnO an edge over its counterpart.

This chapter suggests a simpler and more controllable sub-bandgap approach by proposing the use of a wide bandgap semiconductor based on a ZnO heterojunction for broadband EAM. The proposed concept utilizes the presence of high-density two-dimensional electron Gas (2DEG) at the bottom of the conduction band offset (CBO) in a heterojunction offering a unique model for optical modulation in regions well below the material bandgap. The idea is to use this CBO as a potential barrier where photons can be used to optically lift the electrons across the barrier as opposed to the ISB transition in a quantum well, where a large CBO is required to achieve modulation in an infrared spectrum. Optical lifting has been shown to allow broadband modulation capability, even in a visible region with a comparatively lower CBO. Its broadband capability originates from the fact that this phenomenon employs the transition of electrons across the barrier instead of transitions between two quantum states providing more effective electronic control over the wider spectrum. An extinction ratio of 8 dB is obtained in the proposed optical modulator based on a MgZnO-CdZnO heterojunction. A broadband operation is realized where an extinction ratio of around 7–8 dB is reported over a wide wavelength range of 527–646 nm. The reported results pave the way to realize an optical modulator with a ZnO-based heterojunction for a broadband EAM.

3.2 Device Design and Working Principle

Figure 3.1 (b) shows the proposed design of the optical modulator based on ZnO. The light is guided in the MgZnO-CdZnO heterojunction-based rib waveguide. The thickness of the bottom (cladding) MgZnO is 200 nm, while that of the rib is 500 nm. A 2 µm wide and 5 mm long rib is considered, along with the contact pad and connection patches. A thermally grown oxide on the top silicon of the silicon wafer is utilized to avoid any leakage of optical power into the high-index silicon substrate, as shown in Fig. 3.1 (b). The rib provides a perfect structure for modulation as optical power when guided, as an optical mode shows much greater interaction with the junction which can excite electrons in the confined 2DEG. Applying voltage across the junction would allow change of the 2DEG density which would result in tuning the rate of optical lifting. This allows electrical control over the device's absorption and, thus, optical modulation.

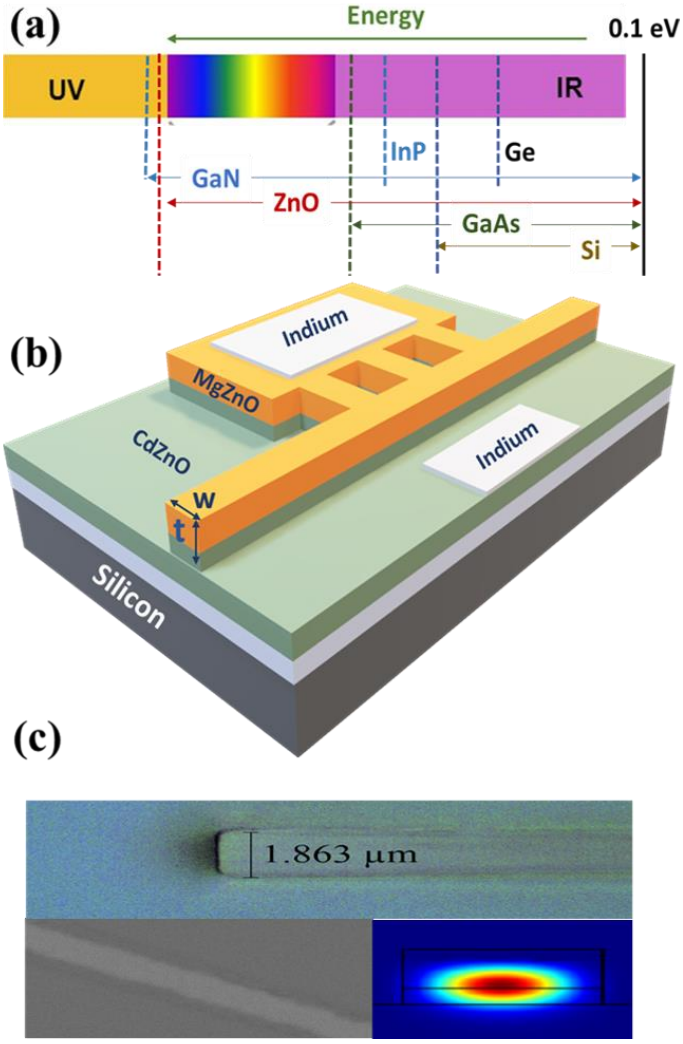

Figure 3.1: (a) Operational ranges of popular semiconductors. ZnO and GaN inherently possess broader spectral ranges because of their wide bandgaps. (b) Schematic representation of the proposed optical modulator. Light is guided in the rib made up of MgZnO-CdZnO with a thickness t and width w of 600 nm and 2 µm, respectively. (c) Optical field distribution in the rib at the bottom right corner, along with the optical and SEM images of the top view of the fabricated device.

3.3 Tuning Quantum Transitions of Confined Charge Carriers

Photoemission of electrons from metal surfaces has been treated by Fowler's hypothesis with the assumption that the quantum efficiency (QE) of such transitions is proportional to the number of available electrons with enough energy to overcome the potential barrier [60][61][62][63]. Thus, the quantum transmission probability (η_i) can be approximated as:

$$\boldsymbol{\eta_i \approx \frac{C_F(h\upsilon - q\phi_B)^2}{h\upsilon}} \quad \ldots\ldots\ldots\ldots\ldots\ldots\ldots\ldots\ldots\ldots\ldots\ldots\ldots\ldots\ldots\ldots\ldots \quad \mathbf{(3.1)}$$

where C_F is Fowler's emission constant and is specific for different devices, hν is the photon energy, and $q\psi_B$ is the potential barrier for electrons. This relation is only valid near threshold energy, i.e., CBO < hν < CBO + 1.5 eV; for higher energies, the estimation of photoemission becomes increasingly complicated [63]. Given the exponential relation, the QE peaks for the photon energy of the CBO + 1.5 eV. Metals are frequently used for photoemission, particularly due to their high density of electrons nevertheless; high associated optical loss limits their use for the application in optical modulation as metals reduce optical propagation distance significantly. Although the study of photoemission for other heterojunctions, for example, semiconductor-insulators and semiconductor-semiconductor junctions is scarce, there are some studies that suggest similar dependence in semiconductor-semiconductor junctions also [64],[65]. These devices, however, suffer from low current due to the low density of electrons in semiconductors and insulators compared to the metals. The proposed model deals with the low-density carrier problem by employing a semiconductor heterojunction with a high density of 2DEG which can provide high charge carrier density without absorbing a substantial amount of optical power, paving the way for successful implementation of low-power optical modulation in a sub-bandgap regime.

3.4 High Density 2DEG in ZnO Based Heterojunction

High-density 2DEG formation in ZnO-based heterojunction has been reported in several reports [66][67]. Although its actual source and mechanism of formation is still an outstanding issue, several reports attribute the high sheet carrier concentration in ZnO-based heterojunction to the strong electronic polarization effect present at the heterojunction [66][67]. Considering the importance of sheet carrier density in optical transitions, an MgZnO and CdZnO composition is

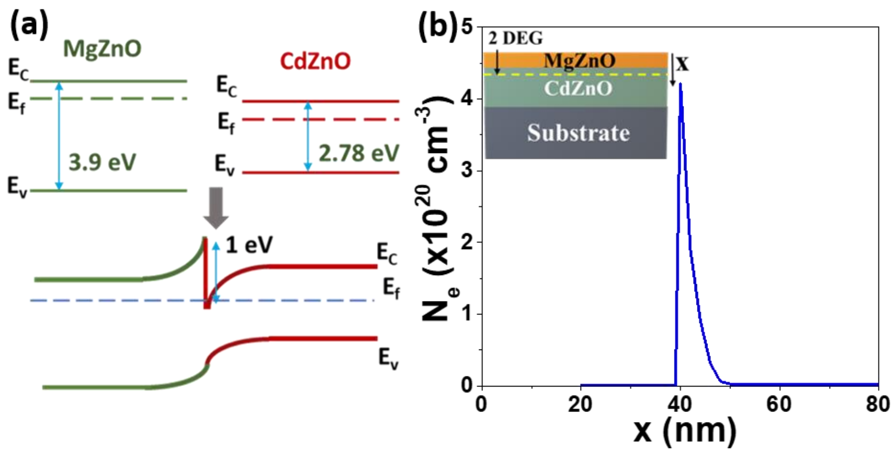

Figure 3.2: (a) Formation of 2DEG. (a) Energy band diagram of the heterojunction. The CBO for the junction is estimated to be 1 eV. (b) Carrier profile obtained using C-V measurement of the $Mg_{0.3}Zn_{0.7}O$ and $Cd_{0.3}Zn_{0.7}O$ heterojunction where x is the distance from the top surface, as shown in the inset. The peak in the carrier concentration (Ne) depicts the presence of 2DEG at the heterojunction.

felicitously chosen to obtain a high density of electrons at the heterojunction. Electron density of $> 10^{13}$ cm^{-3} has been reported for a $Mg_{0.3}Zn_{0.7}O$ and $Cd_{0.3}Zn_{0.7}O$ heterojunction using dual ion beam sputtering (DIBS) [67]. Device fabrication begins with the thermally grown native oxide over a thoroughly cleaned silicon wafer. Subsequently, a thin layer of $Cd_{0.3}Zn_{0.7}O$ with 300 nm $Mg_{0.3}Zn_{0.7}O$ of 400 nm thickness is deposited onto the oxidized silicon wafer using DIBS. The carrier concentration for MgZnO and CdZnO is measured separately and is found to be 8×10^{18} and $3 \times 10^{18} cm^{-3}$, respectively.

Alloying ZnO with MgO enhances its bandgap, while alloying CdO reduces it; UV visible spectroscopy of the MgZnO and CdZnO was performed, and bandgaps of 3.9 and 2.78 eV were directly measured with the help of Tauc plot. The Fermi energy difference in both the layers necessitates a transfer of electrons from MgZnO to the CdZnO layer bending the electronic bands, as shown in Fig. 3.2 (a), and forming a high density of confined electron gas. Another deposition of 40 nm $Mg_{0.3}Zn_{0.7}O$ was carried out over 300 nm $Mg_{0.3}Zn_{0.7}O$ to perform C-V measurement to confirm the presence of 2DEG using platinum Schottky contact and an indium contact. The charge carrier density is plotted against the distance from the top surface in Fig. 3.2 (b). The peak in carrier density confirms the presence of a high electron density concentration at 40 nm below the top surface which corresponds to the MgZnO-CdZnO junction, as depicted in the inset. A 2 µm wide and 5 mm long ZnO waveguide, along with contact pad and connecting patches, is then patterned. The device structure is finally obtained with the help of wet etching for 500 nm, and the remaining bottom 200 nm CdZnO forms the bottom contact.

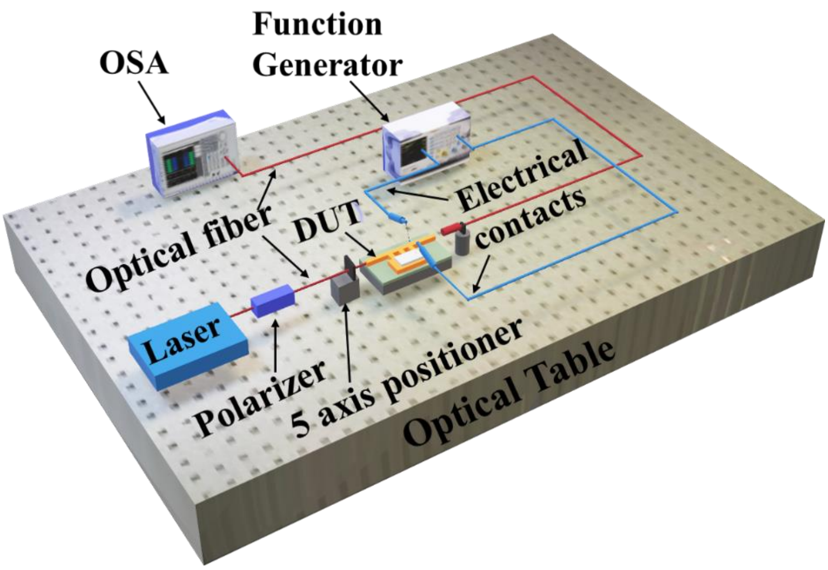

Figure 3.3: Schematic representation of the optical characterization setup. The device under test (DUT) is excited with various wavelengths (1550, 647, 561, and 532 nm) using a polarization controller (PC) via

butt coupling, and its opto-electronic response is measured on an optical spectrum analyzer by applying voltage across the device.

3.5 Electro-Optic Characterization

An optical characterization setup is arranged as illustrated in Fig. 3.3. The device is mounted on a three-axis positioner and light is butt coupled from fiber on a five-axis positioner into the waveguide. The output is then transmitted to an optical spectrum analyzer after the application of voltage bias. To examine the photoelectric properties of the device, its photocurrent for different wavelengths is measured. Optical signals with wavelengths of 1550, 647, 561, and 532 nm are excited into the waveguide, and the respective current response is measured by applying a voltage bias on the MgZnO layer and CdZnO connected to the ground. The photocurrent was measured for both the TE and TM polarization; however, only TM polarization has shown a substantial increment in photocurrent, as shown in Fig. 3.4. It shows the expected response wherein photons only above threshold energy enhances the photocurrent. Such a behavior establishes the presence of a potential barrier for electrons which can also be perceived by an energy band structure of the heterojunction shown in the inset of Fig. 3.4. The observed potential barrier is consistent with the expected CBO in a ZnO-based material system where ΔE_C is given as $0.9 \times \Delta E_g$ [[66][67]]. According to the relation, the estimated value of the CBO for the given composition is 1 eV.

To further investigate the absorbing effect of the electronic transitions, voltage-dependent transmission power is measured and plotted against applied bias in Figs. 3.5 (a) – 3.5 (d) for different wavelengths. For 1550 nm, a small change of −0.6 dB in the optical power has been observed at the output for 0 to 8 V of applied bias. The scale on Y axis of Fig. 3.5 (a) is taken to be consistent with the scales in Figs. 3.5 (b)–3.5 (d) for clarity of comparison.

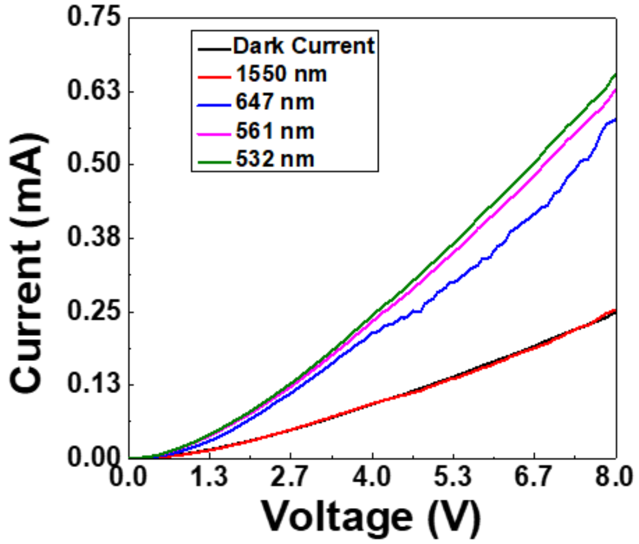

Figure 3.4: I-V characteristics of the device under different excitation conditions. Dark current and photocurrent for 1550, 647, 561, and 532 nm TM polarized light with respect to the voltage applied at MgZnO layer and CdZnO connected to the ground.

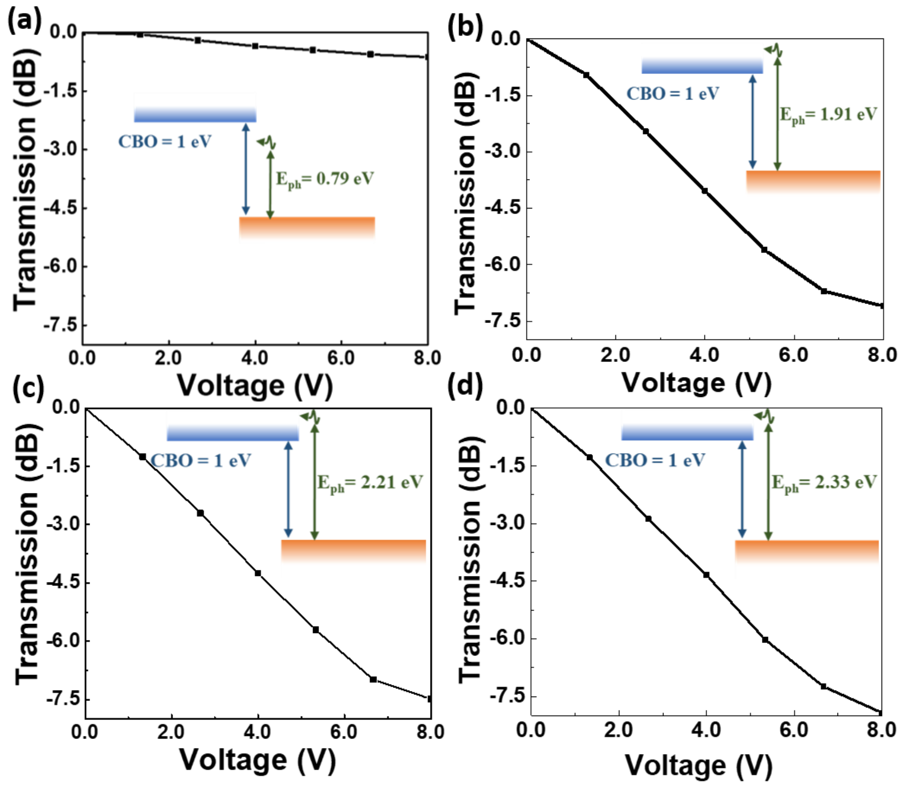

Figure 3.5: Electro-optic behavior of the device. Optical transmission of the waveguide against the applied bias for different wavelengths of light: (a) 1550, (b) 647, (c) 561, and (d) 532 nm. Inset: CBO and photon energy (Eph) for the given wavelength.

Such a low loss for 1550 nm can be due to the essential nature of quantum confined electrons (2DEG) in a single quantum well. Since the photon energy is below the barrier height, the electrons in single quantum well have only quantized available states, thus they exhibit strong absorption only at specific frequencies and absorption is low for other frequencies. Additionally, free carrier absorption in highly doped semiconductors can show charge carrier concentration-dependent absorption at infrared frequencies, as predicted by the Drude model. On the other hand, for 647, 561, and 532 nm TM polarized light, the optical transmission power decreases with the increasing voltage, as their corresponding photon energies of 1.91, 2.21, and 2.33 eV are well above the potential barrier, as shown in Figs. 3.5 (b) – 3.5 (d) and their insets, respectively. Optical transmission is related to the density of charge carriers, as well as the (hν−CBO). Figures 3.5 (b) – 3.5 (d) display the relation of photocurrent with hν; as for any given voltage, the current will depend on the wavelength of the light.

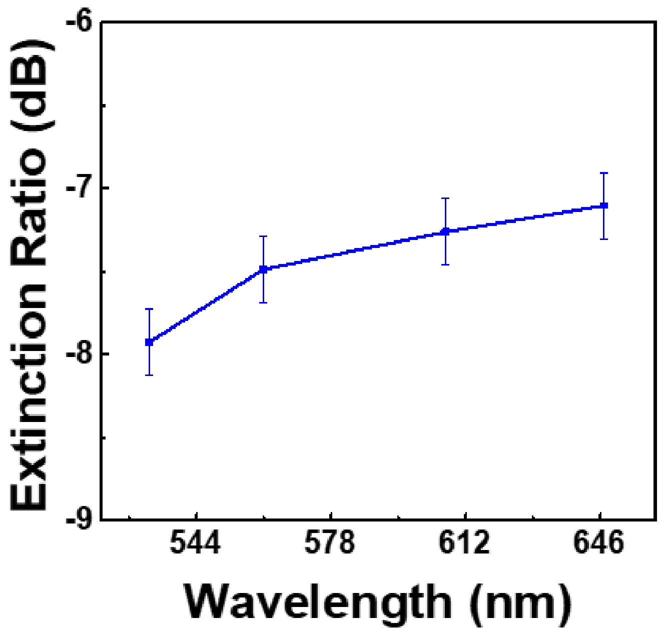

Figure 3.6: Extinction ratio of the device for different wavelengths at 8 V depicting broadband functionality of the device.

However, for a specific frequency, by varying the voltage we are essentially tuning the 2DEG concentration and, thus, modulating the transmission of light. A positive applied bias on MgZnO increases the electron population in 2DEG which, in turn, enhances the QE of the device increasing the optical absorption. A closer look at Fig. 3.4 also reveals an increment in photocurrent of the device for above threshold excitation. A direct relation between the photocurrent and the absorption is evident, thereby substantiating our previous assumption of photons lifting the electrons across the CBO barrier. Additionally, since the energy bandgap of CdZnO and MgZnO is sufficiently higher than the energy of photons, the possibility of photocurrent due to electron hole pair generation in bulk materials is ruled out. Thus, it can be confidently concluded that the optical power is utilized in optically lifting the electrons across the CBO barrier. The extinction ratios of the device for different wavelengths are measured and shown to have 115 nm broadband operation with extinction above 7 dB, as depicted in Fig. 3.6. A clear increment in the extinction ratio with increasing voltage and photon energy is shown in Fig. 6, which can be attributed to the enhanced QE due to an increase in 2DEG density with voltage.

3.6 Summary

To summarize, the modulation capability of ZnO-based heterostructure over a broad range of wavelength via optical lifting is successfully demonstrated. The heterostructure is optimized to obtain a high density of electrons, and operational frequency is appropriately chosen to attain higher QE. The presence of high-density 2DEG and a CBO are confirmed with the help of C-V measurement. Increasing photocurrent with decreasing optical transmission with applied bias for photons above threshold energy confirms the absorption of photons via optical lifting. The application of positive voltage at the donor layer enhances the density of charge carriers which, in turn, results in enhanced QE. Since the QE depends on the number of available electrons, as suggested by Fowler's hypothesis and can be observed as increased photocurrent and decreased optical transmission. A maximum extinction ratio of 8 dB is achieved for a wavelength range of 115 nm via optical lifting. Thus, this Letter provides an exciting alternative to the conventional narrowband EAM. Utilizing optical lifting as a sub-bandgap approach on a direct and wide bandgap ZnO provides an ideal platform for broadband modulation. By maintaining high charge carrier density this approach, in principle, can be used for different spectral range spanning, from Infrared to a visible region just by changing the CBO.

Chapter 4

Efficient Sub-Bandgap Photodetection via Two-Dimensional Electron Gas

4.1 Introduction

Past decade has seen immense advancement towards on- chip integration and miniaturization of optical communication systems as an alternative to conventional electronic integrated circuits. Optical communication system utilizes [68][7][69][50] light signals where data is encoded and distributed over waveguides instead of metal based electronic interconnects. To fully utilize the benefits of Photonic Integrated Circuits (PIC), development of several essential passive and active devices is imperative. Silicon has always been a preferred choice of material due to a well-established CMOS fabrication technology and a variety of photonic devices such as low loss waveguide, optical modulators [70][52][6][71][72][73][74] and optical cavity with high quality factor based on Si have already been demonstrated. However, indirect bandgap and unimpressive opto-electronic properties of Si [75],[49] have pushed for the search of other (best in class) materials to realize various photonic functionalities that are imperative for the development of optical communication systems. Photodetectors (PD) is one of such basic building blocks of optical communication system which performs optical to electrical conversion of the optical signal. Zinc oxide (ZnO) is widely used in photodetection and it gained enormous attention for various opto-electronic functions owing to its novel properties such as high saturation velocity, high excitonic energy and amenability to wet etch. [28] However, its wide bandgap limits its photodetection capability to UV region, as photons with energy lower than their bandgap are unable to generate photo response. In order to explore photodetection for longer wavelengths sub-bandgap photodetection approach needs to be explored. Internal photoemission

(IPE) in Metal-Semiconductor Schottky junction holds immense potential for detecting low energy photons [76],[77] Hot carriers in metals are photo-excited and consequently emitted across the potential barrier.

The major disadvantage of Semiconductor-Metal IPE is its low Quantum Yield (QY), [78],[79] and is typically found to be <1%. This is largely attributed to the momentum mismatch between electronic states in metals and semiconductors resulting in reflection of photoexcited charge carriers at the junction [78], and rapid thermalization of electrons in metals. Surface Plasmon Polaritons (SPP) has also been utilized for field enhancement [6][28] due to plasmonic mode confinement at metal semiconductor Schottky junction. Its role in enhancing IQE has been extensively studied for various Metal-Semiconductor plasmonic structure [80][81][82][83][84][85][86][87][88][89][90]. These devices, however, also struggle with unimpressive IQE of ≈ 1% as the broad energy distribution of hot carriers in plasmonic mode results in rapid thermalization. This limits availability of electrons with sufficient momentum in lateral direction to escape towards the collector side. recently it has been shown that inserting 2D materials like single layer Graphene between metal and silicon enhances its IQE [91][92][93][94][95][96]. Although exact reasons for the improvement in the efficiency is still unknown, high absorption of optical energy along with 2 D nature of monolayer graphene are considered some of the main reason behind the improvement in its IQE. However, even with the extraordinary properties of Graphene, most of the reported responsivity value for Graphene based IPE (without plasmonic enabled field enhancement) [96],[97] photodetector is still in few mA/W. Such an unexpected low value can be attributed to the specular reflection that photoexcited electrons encounter at the Graphene-Silicon junction due to momentum mismatch in both the layers and thus the transmission probability is limited to 11%. Mediocre efficiency with complex fabrication makes graphene rather unattractive choice for photodetection. Any improvement in momentum matching between emitter and collector for such 2D emitters will result in many folds enhancement of the IQE. Semiconductor heterojunctions also contain 2 D confined charge carriers right next to the junction barrier and thus can potentially be used as an emitter in IPE based photo detection. As such structures are typically realized with two materials having similar lattice, they usually have high momentum matching between the two semiconductors. Study on IPE in Semiconductor heterojunction junction is scarce [97] because semiconductors in general were not considered best suitable option as they produced very low current due low charge carrier concentration in semiconductors as compared to metals [64][65]. However, modulation doping in carefully chosen heterojunctions, can induce high doping concentration at the semiconductor junction barrier improving the responsivity of the device.

Present work reports a sub-bandgap IPE based photodetection in MgZnO and CdZnO heterojunction with 2-DEG as an emitter. The heterojunction provides a unique platform where the confined electrons could absorb photons to escape across the quantum well. The rib waveguide of CdZnO provides strong optical confinement which assists in realizing enhanced electro-optic coupling. The reported heterojunction, on one hand, provides a high density of 2-DEG carrier concentration in close proximity to the junction without the associated metallic loss. On the other hand, similar momentum in MgZnO and CdZnO allows high electron escape probability from 2-DEG to MgZnO with minimum reflection 2-DEG based emitters can thus overcome the limitations associated with both metal and graphene-based emitters resulting in improved IQE. The proposed model thus offers an effective alternative for sub-band photodetection with simple and cost-effective fabrication. IQE of 14% is obtained for the proposed design using a theoretical model. A responsivity of 8.5 mA/W is experimentally obtained in the proposed CdZnO-MgZnO heterojunction-based photodetector. The improved efficiency in non-plasmonic mode comes at the back of low loss and efficient carrier transport offered by 2D confined electrons in heterojunction. The reported work paves the way to realize efficient sub band photodetection with wide bandgap semiconductors.

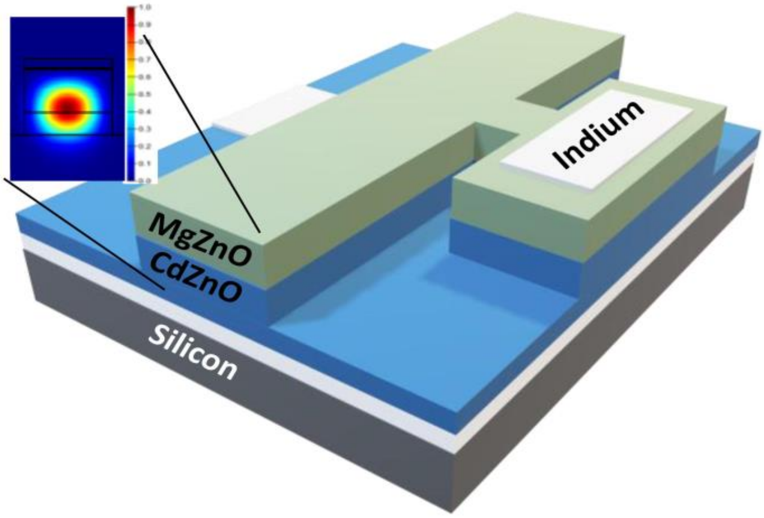

Figure 4.1: Schematic of the proposed photodetector with 3D illustration of the structure. Light is guided in a 2 μm wide and 600 nm thick rib waveguide made up of CdZnO-MgZnO heterojunction which causes the creation of 2DEG. Optical field distribution inside the rib is also shown in the inset.

4.2 Device Design Employing 2-DEG

Fig. 4.1 depicts a 3D schematic of the proposed zinc oxide-based photodetector. A thermally grown native oxide is also utilized on the of top silicon wafer to avoid any leakage of the guided optical power in the high refractive index substrate. A rib waveguide is made up of a CdZnO-MgZnO heterojunction so that the guided light can interact efficiently with the junction. The rib waveguide is 5 mm long and 2 μm wide and is shown along with contact pad. The thickness of the rib and that of the bottom cladding is 500 nm and 200 nm respectively. The inset shows optical field distribution in the rib waveguide. The Finite Difference Eigen Mode (FDE) Solver in Lumerical mode solution is employed for the modal analysis of optical waveguide at 532 nm wavelength.

4.3 Working Principle of Sub-Bandgap Photodetector via Two-Dimensional Electron Gas

Present work utilizes a sub-bandgap approach for photodetection in ZnO based structure for visible and infrared region. The proposed scheme employs the presence of a 2 D confined electron gas near to the conduction band offset (CBO) in CdZnO-MgZnO heterojunction. MgO and CdO in ZnO allows effective bandgap engineering in ZnO, [98] [22][99] wherein alloying CdO and MgO reduces and enhances its bandgap respectively. When layers with different work functions come into contact charge transfer takes place from higher bandgap material, bending the electronic energy bands in a way to form a potential well in the conduction band with a highly dense 2-DEG as shown in Fig. 4.2 (a). The junction forms a highly dense confined electron gas in the lower bandgap semiconductor at the bottom of the CBO offset due to charge transfer. The high concentration of confined charge carriers can be employed to realize an efficient photodetector similar to IPE where Conduction band offset (CBO) impedes the flow of charges across the junction with a potential barrier proportional to the bandgap difference of the two semiconductors [100] [101]. Photons above threshold energy could excite electrons across the potential barrier generating photocurrent. MgZnO and CdZnO heterojunctions is judiciously optimized to simultaneously have high density of 2D confined charge carriers along with large momentum matching between adjacent semiconductors. The proposed device offers densely confined electrons near the heterojunction with quantized momentum and high transmission probability owing to low momentum mismatch between MgZnO and CdZnO. The proposed device thus provides effective solution for the lingering problem in metal-graphene based emitter where photoexcited electrons experience specular reflection upon emission to the collector side.

4.4 Optical Excitation of Electrons Confined in Two Dimensions

Carrier dynamics across 2D and 3D materials is an active topic of research and several reports have highlighted the benefits of using such structures [102]. Uriel Levy *et al.* analyzed photoemission in Si-G junction by modelling the role of multiple reflection of electrons at graphene interface and the transmission probability of electrons across the Si-G junction [103]. This report has delved into the dependence of the IQE on transmission probability (T) of electrons at the Si-G junction. We have plotted the quantum efficiency against T in Fig. 4.2 (b), and it is observed that IQE is a strong function of transmission probability for lower value of T as can be seen in Fig. 4.2 (b). In 2 D quantum well structure formed via modulation doping at the heterojunction of two semiconductors with different bandgap, motion of electrons is restricted in one dimension i.e. perpendicular to the junction by potential wall as shown in Fig. 4.2 (a), quantizing the allowed available energy state inside the W. The motion of such charge carriers in the direction parallel to the heterojunction is similar to the motion in bulk solid and can thus be treated with the conventional effective mass and 1-electron approximation theorem. The potential in the structure can thus be described as a sum of quantum well term V(z) and the periodic term V (x, y). However, in the direction perpendicular to the junction the motion of electrons can be described by $E_{\perp}$ as given in eq4.1. [104][105]The electron energies of the emitter (2-DEG in this case) can thus be considered as a superimposition of the periodic solutions obtained for the 2–D periodic potential and the quantum well energies for quantized bound states energies.

$$E_n\left(k_x, k_y\right) = E_{n,z} + \frac{\hbar^2\left({k_x}^2 + {k_y}^2\right)}{2m^*} = E_{n,z} + E_{\perp}$$

$$E_{\perp} = \frac{\hbar^2 {k_{\perp}}^2}{2m^*}$$

………………………………………………… (4.1)

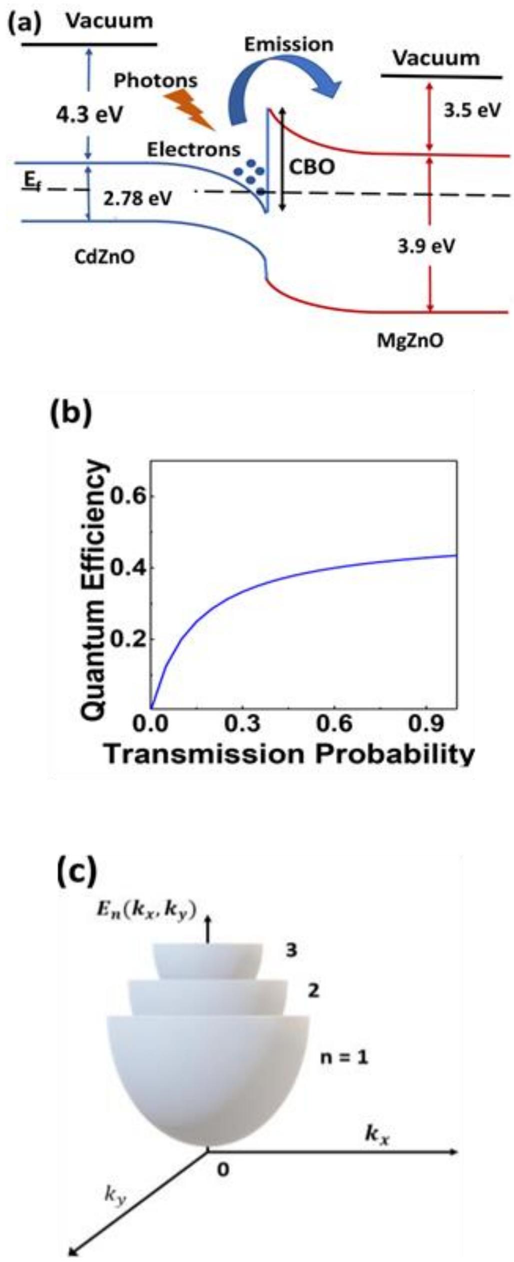

Figure 4.2: (a) Electronic band diagram of the CdZnO-MgZnO. E_c is the Conduction band which forms a quantum well which confines the electrons in the direction perpendicular to the junction. (b) Theoretical Internal Quantum Efficiency of IPE against transmission probability in 2-D structures. QE shows strong dependence on transmission probability for its lower values. (c) Allowed momentum states for 2D confined electrons. Electrons have continuous momentum in direction parallel to the junction however in the direction perpendicular to the junction momentum is quantized and are represented by n.

A plot of the energy level with different sub bands corresponding to different value of n is shown in Fig. 4.2 (c). The energy bands associated with each state (n) are called sub-bands and the quantum well energy associated with this (E_n) can be described precisely with (k_x, k_y) = (0, 0) as shown in the figure. While the momentum of these charge carriers' parallels to the junction remains like that of the bulk material, it is also quantized in the direction perpendicular to the junction. Several studies suggest that the necessary and sufficient condition for the escape of charge carriers is that there must be a component of their momentum perpendicular to the junction after excitation. Every electron in energy levels above n = 0 have momentum in the direction perpendicular to the junction as far as transmission probability of electrons across the junction is concerned which in general provides 2D materials an edge over their counterparts.

Electrons have high thermalization rate in metals and 2-DEG with a thermalization time (τ_{th}) of roughly 10 fs. However, unlike metals, electrons confined inside a quantum well like the 2-DEG are reflected back and forth from the potential walls, which allows multiple attempts for excited electrons to be emitted across the junction before they lose their energy to thermalization. The multiple attempts allow enhanced probability of transmission of the photo excited electrons across the junction. Considering the round-trip time 2a/v = 3 fs; where a is the quantum well width and v is saturation velocity 2a/v ≈ 3 fs; where a is the quantum well width and v is the saturation velocity in ZnO which is taken ≈ 2.5 × 107 cm/s [106][107] and the transmission robability (T) is considered ≈ 0.2 [108] due to high optical matrix element between MgZnO and CdZnO, the effective emission time is estimated as $\tau_{em} = \tau_{rt}/(2T) \approx 25$ fs. The enhancement in quantum efficiency is given by $\boldsymbol{\eta = \frac{1}{2}\frac{\tau_{th}}{\tau_{th}+\tau_{em}} \approx 14\%}$. Such a huge enhancement comes on the back of multiple reflection and momentum matching between CdZnO and MgZnO as opposed to the Si-M junction.

4.5 Device Fabrication

Highly dense 2-DEG has already been reported in ZnO based heterojunction. Although, the actual source and exact mechanism of formation of high sheet carrier concentration in such structures are still an outstanding issue, various reports link its origin to the presence of strong electronic polarization effect at the heterojunction. Composition of MgO and CdO is felicitously chosen considering the significance of high charge carrier density in optical transitions. Electron density >10^{13} for $Mg_{0.3}Zn_{0.7}O$ and $Cd_{0.3}Zn_{0.7}O$ heterojunction has been reported using Dual Ion Beam Sputtering (DIBS). Band gap of Mg_xZnO_{1-x} increases almost linearly with MgO concentration can be estimated as $E_g(x) = E_g(0) + 2.145x$ which comes out to be around 4 eV for x = 0.3. Similarly, for $Cd_{0.3}Zn_{0.7}O$ a band gap is estimated to be around 2.78 eV. The electron affinity of MgZnO as well as CdZnO is assumed to linear dependence on the MgO and CdO content varying from 1.7 to 4.3 eV for MgO and 4.3 to 4.5 for CdO. Corresponding value for Mg0.3Zn0.7O is 3.52 eV and for Cd0.3Zn0.7O is 4.4 eV [109]. The value of ΔEC is usually estimated to be 0.9 × ΔEg, where ΔE_g is the bandgap difference of the 2 layers, in the reported work ΔE_g = 1.12 eV (3.9–2.78 eV) and thus ΔE_C is calculated to be around 1 eV with the given expression.

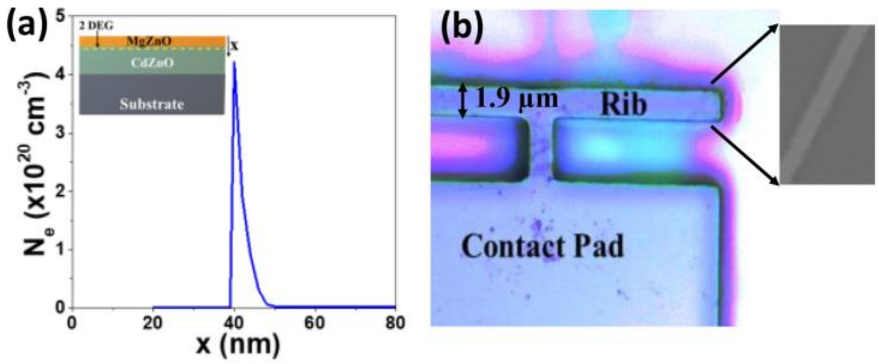

Figure 4.3: (a) Carrier Profile of $Mg_{0.3}Zn_{0.7}O$ and $Cd_{0.3}Zn_{0.7}O$ obtained using C-V measurement of the hetero junction, where x is the distance from the top surface. The peak in carrier concentration (N_e) depicts the presence of -DEG at the heterojunction. (B) Optical and SEM images of the fabricated device. High resolution optical image of an edge of the

device is shown where a rib of width 2 μm running along with the contact pad. The inset shows SEM image of a portion of the rib waveguide.

To fabricate the device native oxide is thermally grown over a clean silicon wafer. A thin layer of $Cd_{0.3}Zn_{0.7}O$ with 300 nm followed by deposition of 400 nm thick $Mg_{0.3}Zn_{0.7}O$ is subsequently deposited with the help of Dual Ion Beam Sputtering (DIBS) onto the oxidized silicon wafer. Hall measurements is separately performed for both the deposited layers and a sheet carrier concentration of 3×10^{18} and 8×10^{18} is measured for CdZnO and MgZnO using Indium contacts in Van der Pauw geometry. To confirm the presence of a high density 2 DEG at the heterojunction a C-V measurement is performed over a sample with 40 nm $Cd_{0.3}Zn_{0.7}O$ deposited on a 300 nm $Mg_{0.3}Zn_{0.7}O$ with the help of platinum Schottky contact and an ohmic indium contact. The free electron density in CdZnO is plotted against vertical distance from the top of the surface as shown in Fig. 4.3 (a). Peak in the carrier concentration validates the presence of a highly dense electron sheet at 40 nm depth from the top, this corresponds to the CdZnO-MgZnO junction as depicted in the inset of Fig. 4.3(a). A 5 mm long and 2 μm wide ZnO waveguide is patterned along with a contact pad with the help of Heidelberg Instruments DWL66 + Maskless lithography system. The structure is then wet etched for 500 nm and final device is obtained after PR removal; the remaining bottom 200 nm is intentionally left to form the bottom contact. Fig. 4.3 (b) shows an optical image of the top view of the fabricated device. The figure displays an edge of the device where a rib of width around 2 μm is shown running along with the contact pad. The inset shows SEM image of a portion of the rib waveguide.

4.6 Device Characterization

For optoelectronic characterization photocurrent was measured for TM polarized visible and near IR light with wavelengths of 1550, 647, 561, 532 nm. To observe just Sub-bandgap photocurrent excitation wavelengths is chosen so that their photonic energy is lower than the bandgap of both the materials. The fabricated device is fixed on a 3-axis

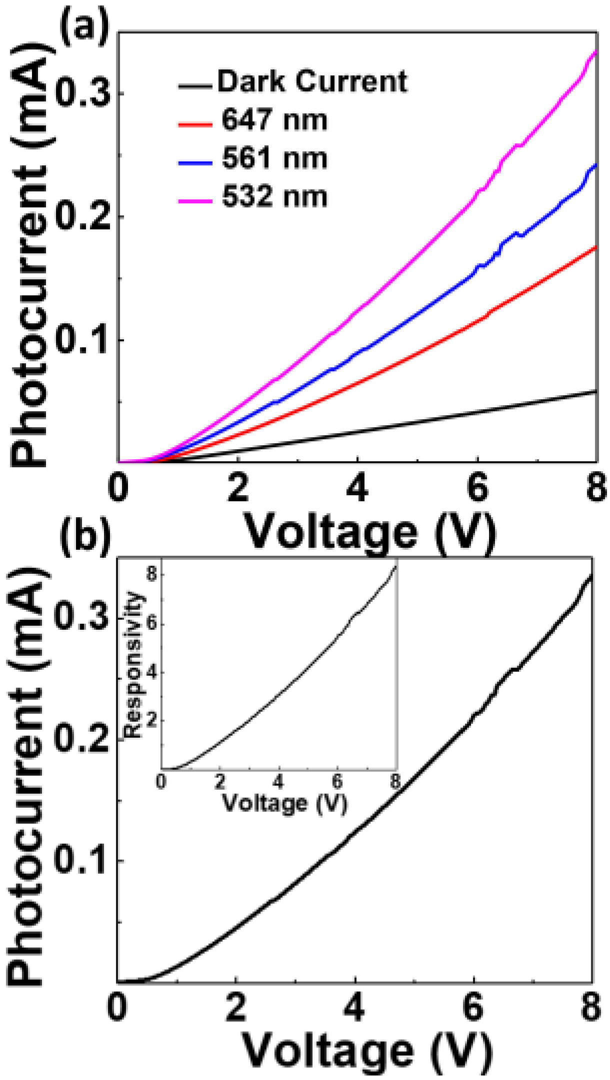

Figure 4.4: (a) Photocurrent for different wavelength of light. Dark current along with the photocurrent. For TM polarized 647, 561, 532 nm wavelength light vs voltage applied on MgZnO with CdZnO connected ground. (b) Photocurrent for 532 nm light vs applied voltage. Responsivity vs voltage for 532 nm light is shown in the inset.

positioner stage using a vacuum holder and the optical power is butt coupled from the laser source to the waveguide via a polarization controller with the help of an optical fiber. The fiber is aligned with the facet of the waveguide with the help of a 5-axis positioner under a microscope stage on an optical table. Light is then coupled to a photodetector from the output of the waveguide using a similar optical fiber. The optical coupling was subsequently optimized by adjusting the alignment of fibers and the waveguide with the help of micro positioner stage to obtain maximum power reading at the output. To test opto-electronic response I-V characteristic of the device is measured by placing the electrical probes onto the contact pads of the device with the help of micro manipulators under the microscope. A DC steady state characterization is done using a continuous wave (CW) laser and a standard BNC cable to connect the electrical probes with the SMU unit.

I-V response for different wavelengths of 1550, 650, 561 and 532 nm TM polarized light is measured. For 1550 nm wavelength the device does not shows any significant photo response as the corresponding photonic energy is lower than the CBO. The photoexcited electrons thus fail to overcome the potential barrier, limiting the photocurrent at 1550 nm. On the other hand, the device shows impressive photocurrent for 650, 561 and 532 nm wavelengths and their I-V curve is plotted in Fig. 4.4 (a). It can be clearly observed that the photo current is higher for lower wavelengths of light at any given voltage, which is distinctive characteristic of IPE as reported in several previous studies [60]. Moreover, since the photon energy of the input light is far less than the band gap of CdZnO and MgZnO, possibility of photocurrent generation due to electron hole pair generation can be ruled out. The photocurrent is shown to increase with the applied voltage as more charge carriers are induced in the 2-DEG because of band bending at the heterojunction with increasing voltage. A high photocurrent of 0.35 mA with responsivity of 8.5 mA/W is measured for 532 nm at 8 V as shown in Fig. 4.4 (b). Since the IQE of the device is proportional to the density of charge carriers at the emitter side (2DEG in this case) the photocurrent is expected to increase with the applied voltage. When a positive voltage is applied on the collector side more electrons are accumulated in the 2 DEG which increases the density of carrier concentration at the emitter side and in turn enhances the photocurrent. A significant dark current is also observed as displayed in Fig. 4.4 (a) which varies almost linearly with the applied voltage and can be attributed to the thermionic emission by the 2 DEG across a narrow potential barrier. While high doping at the collector side provides higher QE and responsivity it also increases the associated thermionic emission due to narrowing of the potential barrier. The increment in photocurrent and responsivity with the applied bias strictly follow increase in the density of 2-DEG density. This is in agreement with the fowler's hypothesis according to which the QE is proportional to the number of available charge carriers at the emitter side. A high responsivity of 8.5mA/W is observed for the device which is also consistent with the theoretical model discussed above.

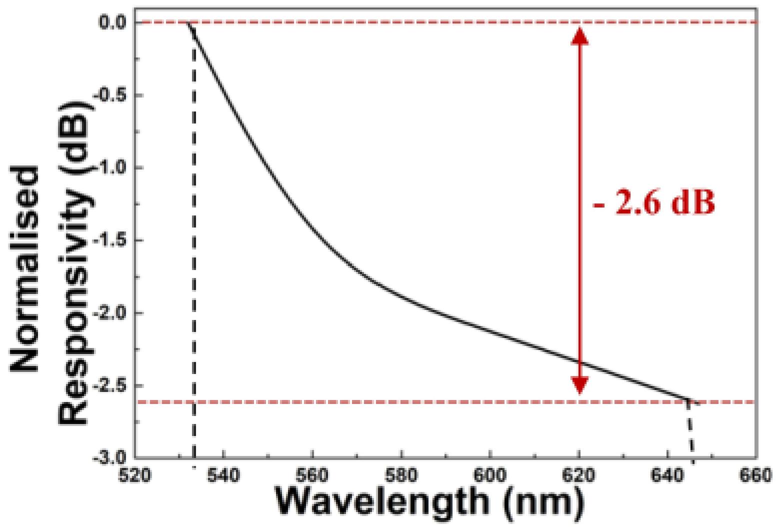

Figure 4.5: (a) Bandwidth of the device. Wavelength dependent normalized responsivity for 8 V.

A high responsivity and QE of the device is clear indicative of how strong the transmission probability is a function of momentum matching across the barrier. Normalized responsivity of the device is also plotted as a function of wavelength in Fig. 4.5 for a bias voltage of 8V. Highest responsivity is achieved at 532 nm and it decreases as the wavelength increases. Wavelengths lower than 532 are not considered as their respective photon energy could exceed the bandgap of CdZnO. A 3 dB bandwidth of 115 nm is obtained for the device as displayed in the figure. A comparison of metal and 2DEG as emitter in IPE is shown in the Table 4.1 where it can be noted that the proposed 2DEG based photodetector shows a higher IQE and responsivity as compared to the metal and graphene based non-plasmonic sub-bandgap photodetectors.

High absorption coupled with the low transmission probability makes metals a poor choice for emitter in IPE. 2DEG on the other hand exhibits no such metallic losses, also the presence of single family of materials in emitter and collector sides makes sure that the momentum is conserved which could be the main reason behind such a high IQE of 2DEG based photodetector.

Table 4.1: Comparison of Sub-bandgap photodetection in different materials, responsivity, IQE and dark current in IPE has been compared for different emitters

Parameters	**Responsivity**	**IQE**	**Dark Current**
Si-M based IPE	1.38 mA/W	<<1%	30 nA
Si-G based IPE	1 mA/W	10%	20 nA
2-DEG based IPE (This work)	8.5 mA/W	14%	30 μA
Si-G plasmonic schottky photodetector	0.4 A/W	Not available	3 μA

4.7 Conclusion

To summarize, sub-bandgap photodetection capability in ZnO based heterojunction is demonstrated. The proposed device exhibits an efficient metal-less photoemission in CdZnO-MgZnO heterojunction. A physical model based on 2D materials is utilized for a better understanding of the basic mechanism of internal photoemission in 2D confined electrons. 2DEG at the heterojunction is shown to exhibit two pronged benefits where, on one hand, a uniform momentum distribution in CdZnO and MgZnO ensures high transmission probability of photoexcited electrons across the barrier. On the other hand, 2D confinement of electrons provides multiple attempts by back-and-forth motion of the electrons in the presence of potential barriers at both ends, enhancing their interaction time at the potential barrier. A responsivity of 8.5 mA/W for a wavelength of 532 nm with a 3 dB bandwidth of 115 nm is reported in a metal-less structure which is obtained with simple fabrication process without involving 2D materials e.g. graphene which requires complex fabrication process. Responsivities of different sub-band photodetection are also compared. The reported device shows a high responsivity as compared to silicon-metal junction and to non-plasmonic graphene-silicon photodetectors. Although, plasmonic enhanced Si-G photodetectors still have the best responsivity due to field enhancement in plasmonic modes, use of metals is generally avoided due to the associated optical losses. Field enhancement without metals can be achieved in the reported device structure with the help of photonic crystals and slow light effect. The proposed scheme can be useful in realizing photodetection at visible wavelengths which may find application in visible light communication.

Chapter 5

On-chip Nanophotonic Broadband Wavelength Detector with 2D-Electron Gas

5.1 Introduction

As electronics-based technologies are reaching their performance bottlenecks, research community is shifting their focus from electrons to photons. Photons enjoy various advantages over the electrons such as wider bandwidth higher speeds [70][110][111][112]. Integrated photonics has witnessed immense interest as it carries the promise of significant reduction of size, weight, manufacturing costs, and power consumption while improving reliability, in comparison to the assembling and packaging of multiple discrete photonics components [[113][74][114][115][52][116]. Wavelength sensitive detector with low intensity noise is a technology that is used in several fields of research or engineering where spectral information is essential. Hence, low cost, on-chip wavelength detectors which can be extremely useful in the fields of sensing, Internet of Things (IOTs), communication and environmental monitoring have attracted the attention of the researchers in recent years. Thus, enormous amount of research efforts has been concentrated on the development of different types of spectral filters such as dispersive and absorptive spectrum filters. On one hand, dispersive filters utilize optical interference owing to difference between optical path-length for different wavelengths, some examples of such filters include Fabry–Perot cavities, gratings, and photonic crystals. In order to achieve the desired optical path-difference bulky dispersive filters are typically required. Such systems are not compatible with on-chip photonics, or when the system is size, weight and power (SWaP) constrained. In addition to this, strong dependence on the angle of incident light is another limitation for such system as it requires the use of collimation optics, further adding to bulk of the system. On the other hand, semiconductor-based filters offer on-chip compatible alternative which relies on materials with wavelength selective absorption or resonant structure such as photonic crystal cavities. Nevertheless, to achieve high spectral resolution it is inevitable to integrate complex geometries with very low fabrication tolerance; additionally broadband operation is achieved by employing multiple layers of different materials. This not only increases the complexity but also leads to excessive production costs [117][118][119]. Another approach that uses 2D materials is gaining a lot of attention due to their unique opto-electronic properties such as ultrahigh responsivity, fast photo response and broad detection range. However, issues such as lack of maturity in large scale growth of high-quality film along with concerns related with pattering and highly quality Ohmic contacts damages the wide appeal that 2DM enjoy. In addition to this most of the devices are usually susceptible to atmospheric noise due to linearity constrains in amplitude domain. Internal photoemission in metal– semiconductor Schottky junctions has drawn a lot of interest owing to its capability for photodetection in subbandgap regime [60][120][76][121]. Frequency dependence of quantum yield (Y) in such devices has been thoroughly studied and shown to be dependent on frequency with a relation $Y \propto (h\nu - \phi_\beta)^\gamma$ where ϕ_β is the potential barrier at the interface and γ is number ranging from 1 to 3 [121]. Internal photoemission display near linear frequency response with respect to frequency for a wide range of spectrum provided γ for the system is close to 1. These structures suffer from low responsivity due to poor internal quantum efficiency [79][122][91]. Lately introduction of 2D materials with plasmonic mode is being actively pursued to enhance the responsivity to several orders of magnitude however, the associated metallic losses and momentum mismatch severely hinders their application [123][124][125][126][127]. Recently sub bandgap photodetection utilizing two-dimensional electron gas (2-DEG) in semiconductor heterojunction has been shown to exhibit high responsivity where high density of 2-D confined electrons absorbs photons energy to jump across the conduction band offset (CBO) at the heterojunction as shown in Figure 5.1 (b). Wide bandgap semiconductors like ZnO offer higher barrier height useful for applications in visible and infrared (IR) region [128][99][129][130][131]. Zinc oxide exhibits bandgap engineering when alloyed with MgO and CdO. Its bandgap can be increased or decreased with increasing percentage of MgO and CdO, respectively [102][132][133][108]. Bandgap engineering in ZnO based alloy has been used to demonstrate heterojunctions with very high density of 2-DEG confined at the junction barrier. The electronic band diagram of the heterojunctions is shown in Figure 5.1 (b) where high density of confined electrons is present on both junction barriers. With applied bias across the junction the current is restricted due to potential barrier present in the conduction band. However, as light is incident at the junction electrons gains sufficient energy to overcome the barrier and drive photocurrent as shown in Figure 5.1(b). Tightly confined electron gas exhibited in the proposed ZnO based heterojunctions shows low losses while offering superior momentum matching which paves the way for low reflection as compared to their metal counter parts. ZnO-heterojunction based platform with high density of 2-DEG on one hand, offers superior internal quantum efficiency (IQE) over traditional emitters like metals [102],[108]. On the other hand, it also displays almost linear relationship between photocurrent and photonic energy for a broad range of frequency spectrum. Since the current is dependent on two variables i.e., frequency and amplitude, two such heterojunctions must be employed to distinguish and eliminate the contributions of light intensity for error free wavelength detection.

We report (in proof-of-principle) a broadband, on-chip optical wavelength detector in part visible part IR region with potential applications in the fields of optical spectrometer, sensing, and demodulation of wavelength modulated optical signals. The proposed approach utilizes multiple asymmetric heterojunctions of ZnO based material system to achieve wavelength detection of the incident light. Thermal resistance and radiation hardness of ZnO makes the device suitable for operation in harsh environment. Additionally, the device is

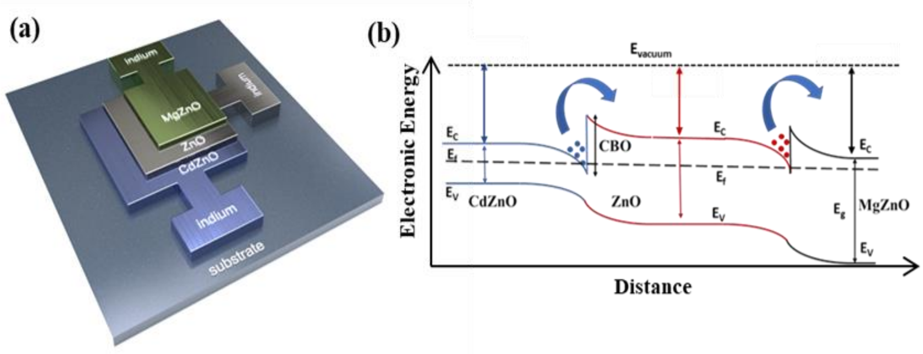

Figure 5.1: (a) Schematic of the proposed nanophotonic device for wavelength detection. Active layers CdZnO-ZnO-MgZnO forming two heterojunctions at the interface of CdZnO-ZnO and ZnO-MgZnO along with individual contact pads enabling application of bias voltage. (b) Electronic band diagram of the double heterojunction along with confined charge carriers. Horizontal axis represents distance from the substrate along the thickness of the deposited layers and vertical axis represents the electronic energy. Conduction band offset at both the junctions are 0.54 and 0.56 eV.

engineered to reduce intensity dependence of the photoemission current via 2-DEG formed at the ZnO based heterojunctions. Linear dependence on frequency, simple fabrication process along with low dependence on intensity of the light makes the proposed approach very simple and effective for reducing intensity-based noise. Where most platforms use different materials or resonators for targeting different part of the spectrum, the proposed approach uses bandgap engineering with same material system. Present work employs three different bandgap materials (i.e., CdZnO–ZnO– MgZnO) forming two heterojunctions. Materials have been carefully engineered to reduce intensity dependence from the current difference of both the junctions. This difference current display reduced intensity dependence along with maintaining linear frequency response. A particular multiplication factor is introduced to further reduce the intensity dependence of the device. This could pave the way for relatively simple, on-chip, low noise wavelength detection. Transparent nature of 2-DEG on one hand ensures equal exposure of light over both the junctions and thus provides a spatially and temporally coherent reference photocurrent which is used to compensate for the intensity noise. On the other hand, high density of 2-DEG offers high IQE along with high photocurrent making it a perfect platform for applications in wavelength demodulation, sensing, IOT etc.

5.2 Design and Band Structure of Nanophotonic Broadband Wavelength Detector with 2D-Electron Gas

The schematic diagram of the device is shown in Fig. 5.1 (a), where three active layers of ZnO based compound semiconductor alloy (CdZnO-ZnO-MgZnO) are shown. Initially a layer of Cd0.3Zn0.7O with thickness and band gap of 100 nm and 2.78 eV respectively, is deposited over silicon wafer using Dual Ion Beam Sputtering (DIBS) system. The thickness and band gap of the layer is experimentally confirmed with the help of Atomic Force Microscopy (AFM) and UV visible spectroscopy respectively. The deposited layer is then patterned with the help of direct UV laser writer PICOMASTER 100 and the structure is subsequently wet etched in diluted HCl solution. Similarly, 100 nm thick layers of ZnO and $Mg_{0.25}Zn_{0.75}O$ with bandgaps of 3.36 eV and 4 eV respectively are deposited, patterned, and etched to obtain the final device. The deposited layers form two heterojunctions of CdZnO-ZnO and ZnO-MgZnO. Patterning is done in a way so that each layer is connected to individual electrodes which allow collection of photocurrents through each junction. The conduction band offset for these heterojunctions can be estimated with the formula CBO = 0.9*ΔEg, where ΔEg is the bandgap difference of the materials [[131][102]]. CBO of 0.54 eV and 0.56 eV is estimated using the above criteria while, the presence of confined charge carriers with a density of 2.3×10^{20} and 1.8×10^{20} respectively is experimentally confirmed with help of capacitance-voltage graph. Fig. 5.2 (a) shows the optical image of the fabricated device. The active region of the device consists of the layers of CdZnO-ZnO-MgZnO which are deposited one over the other forming dual heterojunctions and each layer is individually connected to a contact pad.

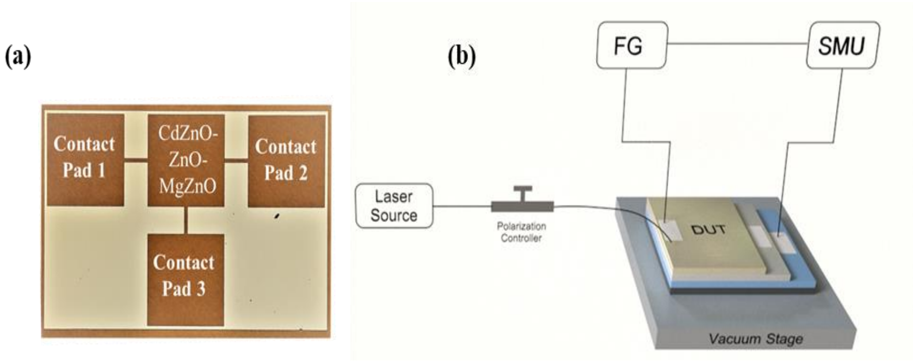

Figure 5.2: (a) Optical image of the fabricated device. CdZnO-ZnO-MgZnO layer deposited over each other and connected to an individual contact pad. (b) Setup for opto-electronic characterization of the Device Under Test (DUT). Both the junctions are biased using Signal Measurement Unit (SMU) and Function Generator (FG) and optically excited with photonic energies from 0.8 to 1.87 eV using different laser source.

5.3 Wavelength Dependent Photocurrent

The internal photoemission current from both the junctions shows no photocurrent for photons with energy lower than the CBO at the junction. Photons with energy higher than the CBO drive photocurrent which is linearly dependent on two parameters i.e., photon energy/frequency and intensity of light incident as shown in eq.5.1 and 5.2. Where the height of CBO determines the threshold frequency for photoexcitation of confined charge carriers above the barrier height and the density of 2-DEG defines the starting point and slope of linearity. Present approach works equivalent to how two equations are used to solve two unknowns. The contribution of light intensity can be reduced by taking difference current which is taken by subtracting the junction currents as given by eq. 5.3. To reduce the intensity component further to almost zero a suitable multiplication factor (k) is introduced before subtraction as can be seen in eq. 5.4.

$$I_1 = m_1\left(\hbar\nu - \phi_\beta\right) + n_1 A \ldots\ldots\ldots\ldots\ldots\ldots\ldots\ldots\ldots\ldots\ldots\ldots\ldots\ldots\ldots(5.1)$$

$$I_2 = m_2\left(\hbar\nu - \phi_\beta\right) + n_2 A \ldots\ldots\ldots\ldots\ldots\ldots\ldots\ldots\ldots\ldots\ldots\ldots\ldots\ldots(5.2)$$

$$I_d = (m_1 - m_2)\left(\hbar\nu - \phi_\beta\right) + (n_1 - n_2)A \ldots\ldots\ldots\ldots\ldots\ldots\ldots\ldots\ldots\ldots(5.3)$$

$$I_d = (m_1 - km_2)\left(\hbar\nu - \phi_\beta\right) + (n_1 - kn_2)A \ldots\ldots\ldots\ldots\ldots\ldots\ldots\ldots\ldots\ldots(5.4)$$

Where A is the intensity of light, ϕ_β is the potential barrier in conduction band at the junction and m and n represents the slopes. The multiplication factor k is judiciously chosen to be n_1/n_2, so that the coefficient of intensity (i.e., $n_1 - k*n_2$) becomes zero.

5.4 Device Measurement

Fig. 5.2 (b) depicts the setup for opto-electronic characterization of the device where the Device under Test (DUT) is placed on top of a vacuum stage and the optical power is irradiated vertically using a continuous wave (CW) laser source. The laser output is connected to a polarization controller via optical fiber through which light is further delivered with the help of optical fiber whose other end is mounted over a 3-axis positioner. The fiber is aligned vertically with respect to the plane of the DUT using a 3-axis positioner as shown in Fig. 5.2 (b) and the whole setup is placed under a microscope stage on an optical table. Light is then illuminated over the DUT and subsequently the optical coupling is optimized by aligning the fiber and the DUT with the aid of micro positioner stage. Opto-electronic response of the device is obtained by providing potential bias to the device through 2-channel Signal Measurement Unit (SMU) while the DUT is illuminated with optical power. Standard BNC cables are connected to the contact pads of the device via electrical probes as shown in the Fig. 5.3 (a) and I-V characteristic of the device is obtained and plotted for with an optical excitation of 650 nm wavelength. Further photocurrents of both the junctions are measured for different light intensities with a fixed voltage bias of 6 V, where the photonic energy is higher than the potential barrier at both the junctions. The photocurrent shows strict linear behavior with respect to the intensity of the light with a slope and responsivity of 1.1

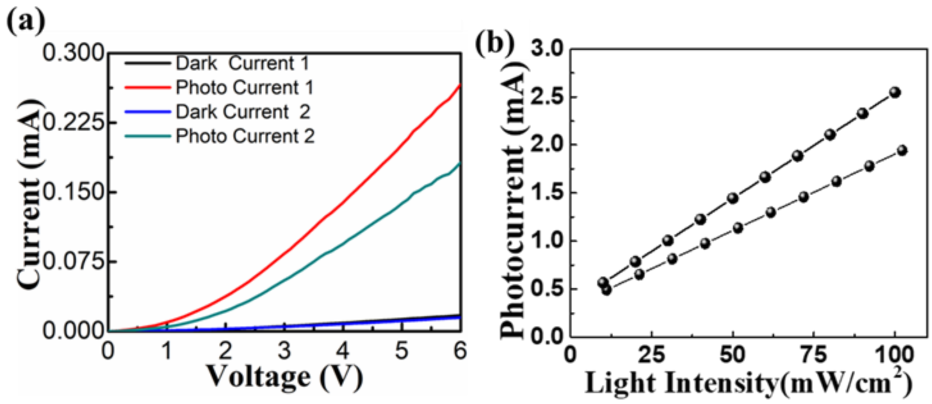

Figure 5.3: (a) Opto-electronic response of the device. (a) Dark current and photocurrent of the device for both the junctions with optical excitation from 650 nm wavelength. Dark current and Photocurrent 1 and 2 corresponds to CdZnO-ZnO and ZnO-MgZnO interface respectively (b) Photocurrent of junction 1 and 2 with respect to intensity of the incident light.

mA/3dB and 25 mA/W respectively, as shown in Fig. 5.3 (b).

Fig. 5.4 (a) shows the photocurrent response of both the junctions with respect to the energy of incident photon energy ranging from 0.8 to 1.87 eV, where each junction is biased at 6 V. The energy range of the incident photons is well below the corresponding bandgap of any layer, ruling out any contribution of photocurrent due to electron hole pair generation. The photocurrent of both the junctions displays almost linear response for a broad range of frequencies of the incident photons as shown in Fig. 5.4 (a). Junction 1 exhibits higher photocurrent as compared to junction 2 this may be attributed to the fact that it contains higher density of 2-DEG as compared to junction 2 as probability of photoexcitation is directly proportional to the charge density at the interface. The difference between the photocurrent from both the junctions is plotted against photon energy in fig. 5.4 (b) which displays a similar linear dependency over frequency for broad wavelength range of 300 nm.

To take into consideration the effect of noise due to intensity fluctuation from external factors fig. 5.4 (b) is plotted, for a range of light intensity with ±5 dB intensity variations around intensity of 90 mW/cm^2. Wavelength sensitivity is calculated by taking the slope from fig. 5.4 (b), where an average change in photocurrent of around 0.96 µA can be seen for corresponding change of 1 nm of wavelength respectively. Thus, wavelength sensitivity of 0.96 µA/nm is reported for a broad wavelength-range of 280 nm. Fig. 5.4 (c) shows difference photocurrent with a multiplication factor of 1.42 for photocurrent in junction 2. According to eq. 4 to remove intensity component from its coefficient (i.e., n_1 - k*n_2) should be zero thus multiplication factor (k) is chosen to be n_1/ n_2, where the individual values of n_1 and n_2 can be taken from fig. 5.3 (b). To demonstrate intensity noise cancellation in wavelength

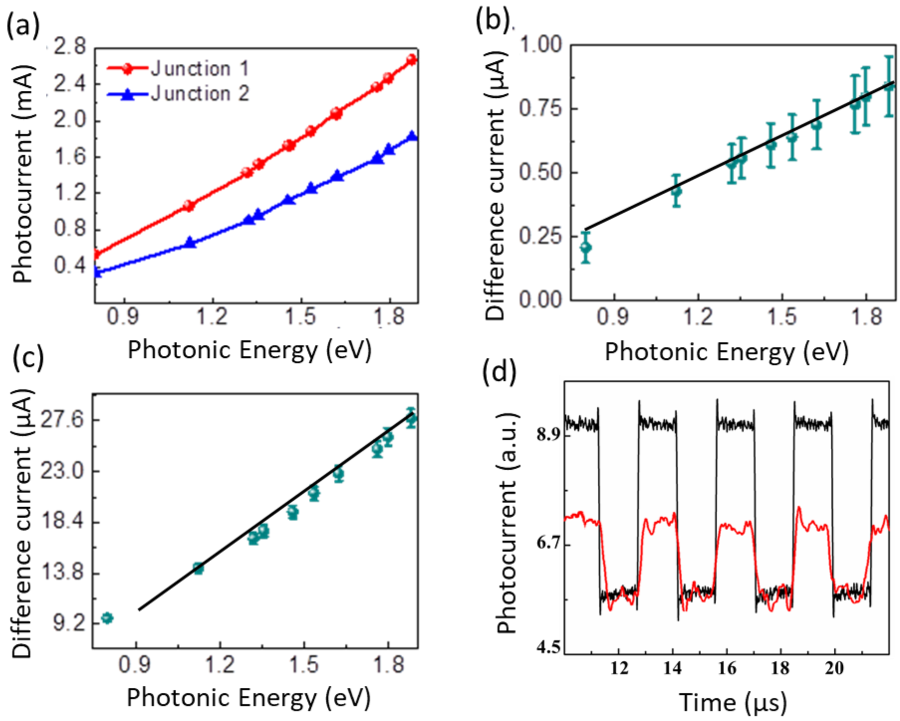

Figure 5.4: Frequency response of the device. (a) Junction current for different frequencies with a voltage bias of 6V across the junction. Difference photocurrent response with respect to the photonic energy of the incident light at 6 V bais (b) without multiplication factor. (c) With multiplication factor of 1.42. The error bar represents current fluctuations due to variation in light intensity of ± 5 dB. (d) Dynamic response for a laser pulse (650 and 780 nm wavelength) with a frequency of 330 KHz. Trace in red and black denotes dynamic response for 780 nm and 650 nm respectively.

dependent photocurrent fig. 5.4 (c) is also plotted with error bars. Comparing fig. 5.4 (b) and 5.4 (c) it can be clearly seen that the error margin due to 5 dB fluctuations in intensity is reduced after a *photo*

multiplication factor of 1.42 is introduced, offering higher resolution. Fig. 5.4(c) also shows that although, multiplication factor improves the noise performance, it also reduces the wavelength responsivity creating a trade-off. Finally, dynamic response of the proposed device is plotted in fig. 5.4 (d) where device is excited by a square pulse of laser with a period of 3 µs and 50% duty cycle for 650 and 780 nm with corresponding light intensities of 70 mW/cm^2 and 90 mW/cm^2 respectively. The current response is plotted in arbitrary units clearly demonstrating wavelength detection capability of the device in parts of visible and IR regime. The speed of the device can be calculated with the help of rise time and fall time of the dynamic response and it comes out to be around 3.6 MHz. The speed as well as responsivity of the device can be enhanced by increasing density of the 2-D confined electron gas. This however will increase the dark current as thermionic emission increases due to thin potential barriers at higher doping, resulting in a tradeoff between speed of the device with dark current. Thus, higher speed would result in larger dark current increasing Noise Equivalent Power (NEP).

5.5 Discussion

Table 5.1 provides a comparison between different types of photodetection techniques [134-146][117][119], with potential spectrum detection capabilities. Conventionally used Avalanche Photo Diode (APD) or Photomultiplier Tube (PMT) based detectors exhibits impressive responsivity they however, either hide spectral information of the signal or needs to be couple with bulky frequency scanning components. Limited channels for detection inhibit parallel detection of broadband optical signal along with high spectral resolutions. Another common approach to achieve the same employs dispersion optics which are again either bulky or requires complex designs with extremely low fabrication tolerance. As an alternate semiconductor based absorptive filters have been investigated due to their compactness and on-chip compatibility. The approach utilizes different materials with wavelength selective absorption along with broadband tunable filters. High resolution, broadband spectrum detection with semiconductors can be achieved only by incorporating high quality-factor resonators and multiple layers of different materials respectively. This not only increases the complexity but also leads to excessive production costs. A different approach i.e., superconducting nanowire based photodetection while displaying ultrabroadband functionality, obscure all the spectral information. 2D Materials (2DM) have been recently attracting enormous amount of interest owing to their impressive opto-electronic properties. Riding on the back of ultrahigh responsivity, fast photo response and broad detection range, 2DM have become a material of choice for wide range of applications. However, issues such as lack of maturity in large scale growth of high-quality film along with scalable deposition of contacts with highly ohmic character hinders wide scale use of these materials.

Table 5.1 Comparison of different wavelength detection techniques [11-15, 38-48]

Wavelength Detection Techniques	Spectral Bandwidth	Responsivity	Wavelength Resolution	Remarks
Avalanche photodiode	≈ 800 nm	10 A/W	NA	Excellent responsivity, obscure spectral information
Dispersion optics	≈ 1000 nm	NA	≈ 1- 2 nm	Either incompatible for on-chip applications or, requires complex fabrication
Colloidal Q-Dot	300 nm	NA	≈ 1- 2 nm	Incompatible with on-chip photonics
Semiconductor nanostructure	10 nm	NA	2-3 pm	Excellent wavelength resolution, low fabrication tolerance and narrow bandwidth
Superconducting Nanowires	> 1000 nm	NA	Cannot provide spectral information	Ultra-broadband, obscure spectral information
2D Material	≈ 1000 nm	> 10 A/W	NA	Very high responsivity, growth of large area, high quality, 2D layers is still challenging
Present Work	300 nm	25 mA/W	Few nanometers	Simple fabrication, broadband low responsivity

Present work demonstrates, in proof-of-principle, a novel and innovative wavelength detection technique on an on-chip platform with simple fabrication approach. Employing difference in potential barrier and charge carrier concentration in 2-DEG for wavelength specific photocurrent allows bypassing the need for complex geometries and depositing different materials. Different conduction band offset can be used to target different part of the spectrum which can be achieved by changing the MgO and CdO concentration with respect to ZnO. Additionally, presence of a reference junction on the same device provides spatial and temporally coherent photocurrent for performing excellent common mode rejection. It simultaneously makes the device more immune to the noise present in the channel by reducing the intensity dependence of the device. Although the proposed work lacks in speed and responsivity, it is a step forward in the right direction and offers a powerful platform for wavelength detection after further improvements. The major reason for slow speed can be the low mobility of sputtered ZnO films (typically 5-30 $cm^2/(V.s)$) therefore, device would greatly benefit from material engineering for achieving higher mobility. Also thickness of the layers can be reduced for efficient charge transport. Optimized layer thickness along with enhanced mobility will considerably reduce the carrier transit time offering higher speed of the device. Also, surface engineering such as addition of nanorod antennas can reduce reflections and enhance the responsivity of the proposed device. A thorough analysis of the material and design engineering is thus required for further improvement in its responsivity and speed [146].

5.6 Conclusion

To summarize, wavelength detection capability of the proposed ZnO based dual heterojunction has been experimentally demonstrated for part-visible part-IR region of spectrum over a broad range of frequencies. Internal photoemission via highly dense 2-DEG in ZnO based heterojunction shows linear dependence with respect to frequency and intensity of the incident light. The active region of the device consisting of layers of CdZnO-ZnO-MgZnO, deposited on top of each other incorporates two heterojunctions CdZnO-ZnO and ZnO-MgZnO. Photoemission current via 2-D electron gas formed at both the junctions exhibit linear frequency response. Difference of both the photoemission currents after an appropriate multiplication factor, also displays linear frequency response along with reduced sensitivity to intensity of the light for a broad range of frequencies. This could pave the way for broadband, low noise wavelength detection in optical regime with simple fabrication process. High density of confined electron gas offers enhanced IQE and ensures equal exposure at both the junctions making it ideal platform for on-chip wavelength detection. Wavelength sensitivity of 0.96 µA/nm is reported in the present work. The proposed device can be useful in the fields of optical spectroscopy, sensing, IOT and wavelength demodulation for optical communication.

Chapter 6

Voltage Controlled Plasmonic Resonance in Semiconductor Nanostructures

6.1 Introduction

Semiconductor nanoparticles have been extensively studied for applications in electronic and opto-electronic domain such as Q-dot LEDs, bio-sensing, solar cells photovoltaics. Recent advancements in heavily doped Epsilon-Near-Zero (ENZ) material nanocrystals have supplemented immense research opportunities for examining collective charge carrier oscillations and their interaction with light at very fundamental level. Latest findings demonstrating Infrared (IR) absorption bands in heavily doped semiconductor nanocrystals similar to that shown in metallic nanostructures have proved plasmonic resonance to be a ubiquitous signature of free charge carriers instead of just being associated with optical response of metals [24][147]. Prospects of realizing plasmonic resonance in semiconductor nanoparticles has opened up new windows of opportunities with conjunction of enhanced light-matter interaction offered by plasmonic resonance along with dynamic tunability of semiconductors. The plasmonic response of nanoparticle in particular displays enhanced sensitivity to small change in charge carriers. Theoretically the electro-optic sensitivity can be estimated as $1/r^3$, where r is the size of nanoparticle, which means smaller the nanoparticle is greater the sensitivity of its Localized Surface Plasmon Resonance (LSPR) frequency, to change in charge carrier concentration, becomes. Since metal nanoparticles contains a significantly high number of charge carriers, dynamically inducing a significant change in its carrier density becomes impractical. Semiconductor q-dots owing to wide range of carrier densities are thus ideal choice for realizing numerous active device functionalities using tunable plasmonics. Zinc Oxide (ZnO) has

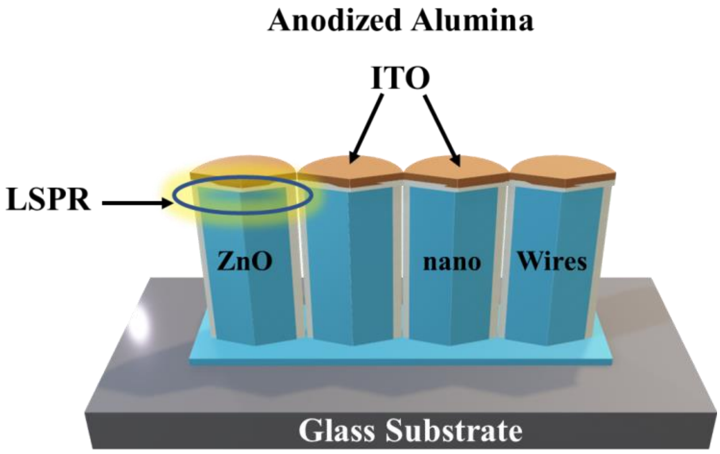

Fig.6.1 Schematic design of proposed device. Zinc Oxide nanowires of diameter 60 nm encapsulated in anodized aluminum oxide. ITO and ZnO base layer work as electrodes. Localized surface plasmon resonance at one end of the nanowires.

been the material of choice as its plasmonic response in Near-Infrared (NIR) is well established. ZnO being an excellent Transparent Conducting Oxide (TCO) has been reported to show Epsilon-Near-Zero condition in NIR region due to very high practically achievable doping levels thus, most of the reports on non-metallic LSPR employs ZnO nanocrystals [47][148]. Voltage induced excess charge carriers in such q-dots can push the plasmonic window for ZnO nanocrystals towards NIR region while dynamic control over its charge distribution can supplement much needed active tunability for realizing several applications in Near Infrared (NIR) region.

Self-assembly is a bottom-up fabrication approach which is commonly used for the synthesis of various semiconductor nanostructures. Colloidal nanocrystals have become the preferred method to synthesize semiconductor Q-dot due to ease of fabrication and better control however, lack of reproducibility in synthesis of high density, ordered nanocrystals and incompatibility with on-chip platform hinders its prospects for various on-chip applications. Additionally, many applications require voltage tunability on an on-chip platform

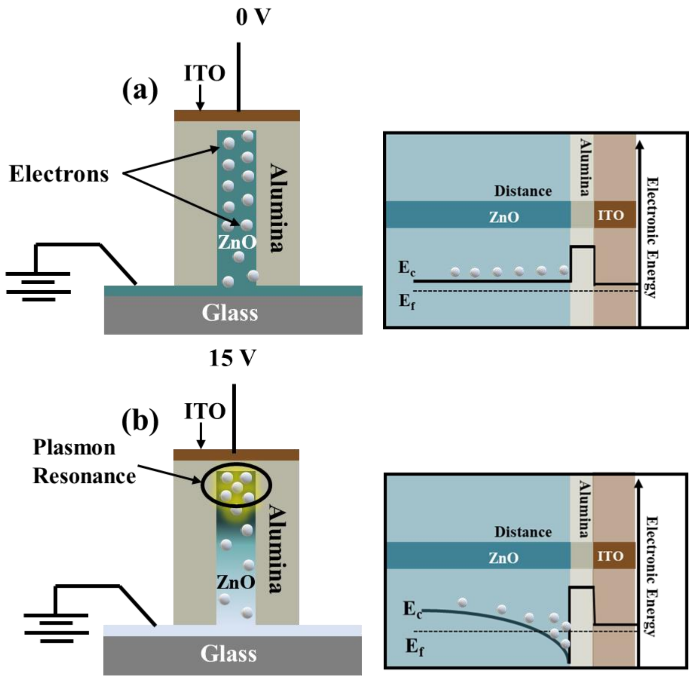

Fig. 6.2 Schematic representation of modulation of charge carrier distribution in individual ZnO nanowire. ***(a)*** *Uniform distribution of charge carriers without application of potential bias across the length of nanowire (left). Electronic band diagram of ZnO nanowire (right).* ***(b)*** *Excess charge carrier accumulation with application of voltage across the nanowire (left). Electronic band diagram of ZnO nanowires with modulation doping following*

where, most of the reported device either completely lacks dynamic tunability or have controls other than applied voltage bias [149][47]. Thus, although the leap is significant, maximum utilization of the technology cannot be achieved without an on-chip platform of LSPR with dynamic tunability via applied potential bias.

Here we demonstrate voltage tunable localized surface plasmon resonance in NIR region on an on-chip platform. The reported device employs voltage induced modulation of charge carrier distribution in 2-Dimensional array of ZnO nanoparticles in anodized aluminum nanowire template. Expanding the portfolio of plasmons into semiconductor can enable tunable plasmonic functionalities with the help of dynamic manipulation of charge carrier distribution which can have exciting applications in spectroscopy, sensing, communication and much more.

6.2 Proposed Device Configuration:

The proposed device consists of an array of Gallium doped ZnO (GZO) nanowires encapsulated in aluminum oxide, with one end of the nanowire connected with the base layer of ZnO as shown in Fig. 1(b). Anodization of aluminum is a bottom-up approach for producing nanopores in aluminum oxide. Present work employs anodized alumina as a template for depositing GZO nanowire as shown in Fig. 6.1. Anodized Alumina Oxide (AAO) provides a perfect template for densely packed, highly ordered array of nanopores formed inside a high-k dielectric. Additionally, simple fabrication and effective control over its feature size allows room for much required structural engineering making it an ideal template for growth of reproducible semiconductor nanostructures in the proposed configuration. A layer of ITO is deposited across the barrier layer of anodized alumina as shown in Fig. 6.1. The base layer of ZnO and ITO are used as electrodes and the device is designed to allow application of voltage across the length ZnO nanowires.

6.3 Tuning Boundary Condition of Free Charge Carriers:

The proposed electronic control via applied bias induces modulation doping which on one hand, attracts excess charge carriers amplifying the free carrier density by bending the electronic energy band of the material. On the other hand, it also modulates the boundary conditions of free charge carriers. Application of sufficiently high positive voltage at ITO (with respect to ZnO base layer) bends the conduction band of the ZnO nanowire enough to provide a significant potential barrier in the conduction band tuning the confinement of the charge carriers from 1-D nanowire to 0-D q-dot as shown with the help of electronic band diagram in Fig. 2 (a) and (b). Thus, the device exhibits high density of charge carriers confined in 0-D, suitable for exciting Localized Surface Plasmon Resonance (LSPR) in NIR range. LSPR frequency depends on charge carrier density in nanoparticles, higher the density of free charge carriers smaller the LSPR wavelength. Metals due

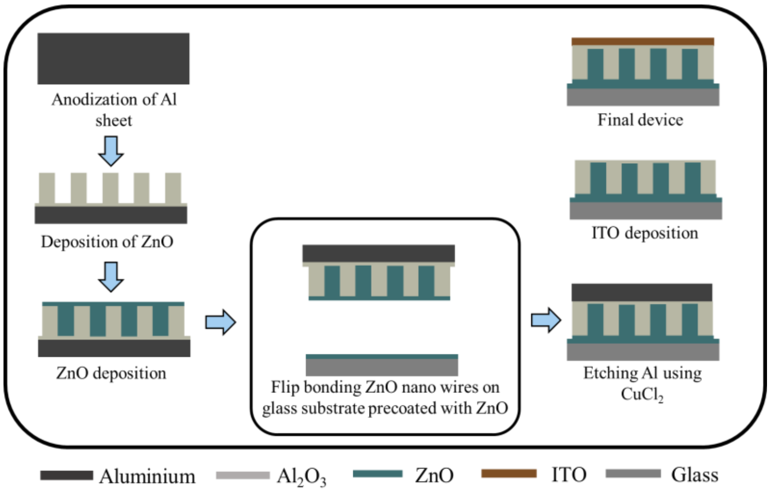

Fig. 6.3 Fabrication flow for the proposed device.

to their extremely high charge carrier concentration shows plasmonic behavior at NIR and visible lights. However, due to comparatively low charge carrier density semiconductor nanocrystals mostly support LSPR in (Mid Infrared) MIR region. Also, although semiconductors can exhibit dynamic tunability of their charge carrier concentrations, replicating such electronic control on nanoparticles mostly seem impractical.

6.4 Proposed Device Fabrication:

To fabricate the structure, initially an aluminum foil (from Sigma Aldrich) with a purity of 99.999% is cleaned in (Deionized) DI water, acetone, and ethanol respectively in a sonicator. The film is then annealed at 450º C in Nitrogen environment for 3 hours to yield a defect free surface. To reduce the surface roughness, the Al foil is subsequently electropolished in a solution of ethanol and perchloric acid with 1:3 ratio by volume under a constant voltage of 15 V for 5 mins, after which the foil is thoroughly cleaned with DI water. To produce highly ordered porous film two-step anodized approach is followed where first step anodization is used to create self-organized porous pattern with high degree of regularity which will be utilized as a template for second step anodization. In order to obtain small pore size, the first step of anodization is carried out at 19 V in an aqueous solution of ethylene glycol and sulfuric acid (50 wt. % and 10 wt. % respectively). After first step anodization the porous oxide layer produced is then etched in an aqueous solution of chromic acid and phosphoric acid (7% and 1.8% by weight) to yield a regular pattern on the Al foil. The second step of anodization with similar parameters is followed for 2 minutes to finally achieve the desired porous structure as depicted in Fig. 3. SEM image of the anodized film where a pore size of around 20 nm in diameter and a period of 60 nm can be clearly seen from Fig. 4(a). After anodization Gallium doped (5%) ZnO is deposited inside the nanoholes formed in AAO using Pulsed Layer Deposition (PLD) system to form dense array of ZnO nanowires inside AAO. Fig. 4(b) shows SEM image of the cross section of the AAO template with ZnO deposited in form of nanowire inside AAO template. XRD plot of the ZnO nanowires deposited inside AAO is shown in Fig. 4(c) which confirms the deposition of ZnO[150][151]._A separate glass substrate is spin coated with Ga doped ZnO via sol-gel method. The AAO assisted ZnO nanowire array is then flip bonded on ZnO coated glass and residual aluminum is etched in a

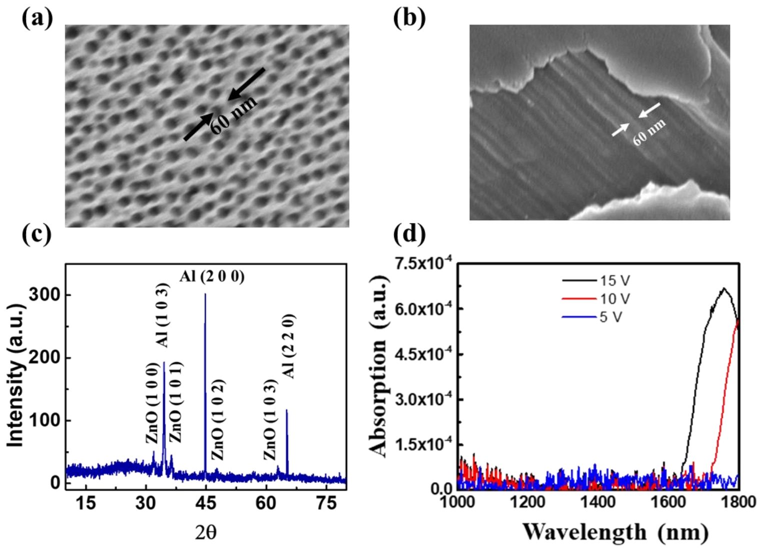

Fig.6.4 Characterization of the proposed device. *(a) SEM image of the anodized aluminum oxide with 60 nm period. (b) SEM image of ZnO deposited inside AAO template.* ***(c)*** *XRD plot of ZnO deposited inside AAO template. (d)* *Absorption spectra of the proposed device with blue shift in absorption peak with respect to the applied voltage.*

solution of $CuCl_2$ leaving an array of ZnO nanowire inside porous alumina oxide over a glass substrate. ITO is deposited over the barrier layer with the help of Sputtering to obtain final device.

6.5 Plasmon Resonance in ZnO Nanostructures:

Dynamic transmission spectrum of the fabricated device is measured with the help of a broadband optical source and an optical spectrum analyzer. The source and detector are aligned for maximum coupling and the proposed device is placed in between them. Electro-optic measurement of the device is conducted by applying a varying voltage bias on ITO with ZnO base layer grounded. Wavelength vs absorption plot of the proposed device is calculated for 5, 10, and 15 V which is shown in Fig. 4 (d) For low applied bias device does not show absorption till 1800 nm however at voltages above 10 V absorption peak starts to emerge which exhibits blue shift with increasing voltage. The enhanced absorption can be attributed to localized surface plasmon resonance in q-dots formed as a result of modulation doping. The observed blue shift can be ascribed to excess charge carrier and stronger confinement at higher voltages.

6.6 Conclusion:

We report voltage tunable LSPR at 1730 nm on a novel on-chip platform. The proposed device employs Gallium doped ZnO nanowires with high carrier concentrations, inducing excess charge carriers via modulation doping, further enhances the charge carrier density to support LSPR in NIR region of the spectrum. Present device is first of its kind (to the best of our knowledge) with voltage controlled plasmonic resonance especially in NIR regime. Adding semiconductors to the coterie of materials which can exhibit plasmonic resonance could redefine the reach of plasmonic. Compatibility with on-chip platform along with the proposed electronic control can radically expand its horizons allowing application in areas which were previously unthinkable such as Reconfigurable Meatsurfaces.

Chapter 7

Conclusion and Future Scope:

From the start of its conception there has been two major motivations for this thesis work. First is to conceptualize a sub-bandgap approach to exploit active photonic functionalities of Zinc Oxide in the spectral region well below its bandgap for realizing different major building blocks of photonic integrated circuits. Second one is to realize plasmonic resonance in ZnO nanoparticle in Near Infrared (NIR) region for enhanced light-matter interaction in beyond diffraction limit regime while bypassing the lattice mismatch issue faced in hybrid integration. The work in this dissertation proposes and experimentally demonstrates electro-absorptive optical modulator, sub-bandgap photodetector and a frequency detector in part visible and part IR region of the spectrum. The proposed devices employing high density 2-Dimensional Electron Gas in ZnO based heterojunction exhibits superior quantum efficiency. Finally, we report an on-chip compatible voltage tunable plasmon resonance in ZnO nanoparticle at NIR region.

The major contribution of the work carried out in this dissertation is as follows:

- The modulation capability of ZnO based hetero structure over a broad range of wavelength via optical lifting is experimentally demonstrated. The hetero structure is optimized to obtain high density of electrons and operational frequency is appropriately chosen to attain higher quantum efficiency. Maximum extinction ratio of 8 dB is achieved for wavelength range of 115 nm via Optical lifting. Utilizing Optical Lifting as a sub-band gap approach on a direct and wideband gap ZnO provides an ideal platform for broadband modulation. By maintaining high charge carrier density this approach can in principle be used for different spectral range spanning from Infrared to visible region just by changing CBO, as for modulation hν must be above CBO.

- Sub-bandgap photodetection with two-dimensional electron-confinement in CdZnO-MgZnO heterojunction is realized. The reported photodetection is based on metal-less internal photoemission via optical excitation in 2D electron gas (2DEG) present at the bottom of the conduction band offset in the heterojunction. A physical model is also employed to explain the underlying mechanism of transmission of electrons across the heterojunction. The rib structure of CdZnO waveguide provides strong optical confinement which leads to an improved electro-optic coupling. A high density of 2DEG, uniform momentum distribution across heterojunction and improved electro-optic coupling result in a responsivity of 8.5 mA/W at a wavelength of 532 nm.
- A novel approach utilizing wavelength sensitive photocurrent across semiconductor heterojunctions to experimentally validate broadband wavelength detection on an on-chip platform with simple fabrication process is reported. The proposed device utilizes linear frequency response of internal photoemission via 2-D electron gas in a ZnO based heterojunction along with a reference junction for coherent common mode rejection. We report sensitivity of 0.96 μA/nm for a broad wavelength-range of 280 nm from 660 to 940 nm. Simple fabrication process, efficient intensity noise cancelation along with heat resistance and radiation hardness of ZnO makes the proposed platform simple, low-cost and efficient alternative for several applications such as optical spectrometers, sensing, and Internet of Things (IOTs).
- Voltage controlled plasmonic resonance (at 1730 nm) in ZnO nanoparticles has been experimentally demonstrated. The device employs modulation doping in heavily doped ZnO nanowires which enables quantum confinement of electrons to 0-D while providing excess charge carriers which in turn shifts the resonance peak to Near infrared (NIR). Anodized aluminum oxide offers an ideal template with low-cost synthesis of nanowire inside a high-k dielectric shell along with effective control over its feature size in

desired range. These findings give fresh insights into semiconductor plasmonics, with significant ramifications for both fundamental investigations of doped semiconductor nanoparticles and exciting future applications due to the additional voltage tunability and on-chip compatibility offered with the proposed work.

Future Scope:

The outstanding properties of the proposed devices in this thesis can enable various promising applications in the future. The sub-bandgap optical modulation and photodetection described in chapter three and chapter four can be realized in IR region of the spectrum by carefully tailoring the bandgap difference with appropriate composition of MgO and CdO. Finally, ZnO nanostructures could be optimized for high-speed voltage controlled plasmonic resonance which can find applications in communication, sensing and much more.

References

[1] T. Darwish and M. Bayoumi, “Trends in Low-Power VLSI Design,” *Electr. Eng. Handb.*, pp. 263–280, Jan. 2005, doi: 10.1016/B978-012170960-0/50022-0.

[2] I. Ratković, N. Bežanić, O. S. Ünsal, A. Cristal, and V. Milutinović, “An Overview of Architecture-Level Power- and Energy-Efficient Design Techniques,” *Adv. Comput.*, vol. 98, pp. 1–57, Jan. 2015, doi: 10.1016/BS.ADCOM.2015.04.001.

[3] “IBM Unveils World’s First 2 Nanometer Chip Technology, Opening a New Frontier for Semiconductors - May 6, 2021.” https://newsroom.ibm.com/2021-05-06-IBM-Unveils-Worlds-First-2-Nanometer-Chip-Technology,-Opening-a-New-Frontier-for-Semiconductors (accessed Jan. 10, 2022).

[4] T. Y. Chiang, B. Shieh, and K. C. Saraswat, “Impact of joule heating on scaling of deep sub-micron Cu/low-k interconnects,” *IEEE Symp. VLSI Circuits, Dig. Tech. Pap.*, pp. 38–39, 2002, doi: 10.1109/VLSIT.2002.1015379.

[5] Y. Q. Bie *et al.*, “A MoTe2-based light-emitting diode and photodetector for silicon photonic integrated circuits,” *Nat. Nanotechnol. 2017 1212*, vol. 12, no. 12, pp. 1124–1129, Oct. 2017, doi: 10.1038/nnano.2017.209.

[6] B. G. Lee, A. Biberman, J. Chan, and K. Bergman, “High-performance modulators and switches for silicon photonic networks-on-chip,” *IEEE J. Sel. Top. Quantum Electron.*, vol. 16, no. 1, pp. 6–22, Jan. 2010, doi: 10.1109/JSTQE.2009.2028437.

[7] J. K. Doylend and A. P. Knights, “The evolution of silicon photonics as an enabling technology for optical interconnection,” *Laser Photonics Rev.*, vol. 6, no. 4, pp. 504–525, Jul. 2012, doi: 10.1002/LPOR.201100023.

[8] P. Dong, “Silicon photonic integrated circuits for wavelength-division multiplexing applications,” *IEEE J. Sel. Top. Quantum Electron.*, vol. 22, no. 6, pp. 370–378, Nov. 2016, doi: 10.1109/JSTQE.2016.2575358.

[9] Y. Ding, H. Ou, J. Xu, and C. Peucheret, “Silicon photonic integrated circuit mode multiplexer,” *IEEE Photonics Technol. Lett.*, vol. 25, no. 7, pp. 648–651, Apr. 2013, doi: 10.1109/LPT.2013.2247394.

[10] A. Liu *et al.*, “A high-speed silicon optical modulator based on a metal-oxide-semiconductor capacitor,” *Nature*, vol. 427, no. 6975, pp. 615–618, Feb. 2004, doi: 10.1038/nature02310.

[11] M. Li, J. Ling, Y. He, U. A. Javid, S. Xue, and Q. Lin, “Lithium niobate photonic-crystal electro-optic modulator,” *Nat. Commun.*, vol. 11, no. 1, Dec. 2020, doi: 10.1038/S41467-020-17950-7.

[12] J. Liu *et al.*, “InAs-Nanowire-Based Broadband Ultrafast Optical Switch,” *J. Phys. Chem. Lett.*, vol. 10, no. 15, pp. 4429–4436, Aug. 2019, doi: 10.1021/ACS.JPCLETT.9B01626.

[13] H. Nguyen-Van *et al.*, “Quantum cascade lasers grown on silicon,” *Sci. Rep.*, vol. 8, no. 1, Dec. 2018, doi: 10.1038/S41598-018-24723-2.

[14] F. Bernardini, V. Fiorentini, and D. Vanderbilt, “Spontaneous polarization and piezoelectric constants of III-V nitrides,” *Phys. Rev. B - Condens. Matter Mater. Phys.*, vol. 56, no. 16, pp. R10024–R10027, 1997, doi: 10.1103/PHYSREVB.56.R10024.

[15] H. S. Kwack *et al.*, “Optical properties and carrier dynamics of two-dimensional electrons in AlGaNGaN single heterostructures,” *Appl. Phys. Lett.*, vol. 87, no. 4, Jul. 2005, doi: 10.1063/1.2000334.

[16] T. Bretagnon *et al.*, “Radiative lifetime of a single electron-hole pair in GaN AlN quantum dots,” *Phys. Rev. B - Condens. Matter Mater. Phys.*, vol. 73, no. 11, 2006, doi: 10.1103/PHYSREVB.73.113304.

[17] S. Ogawa, S. Fukushima, and M. Shimatani, “Graphene plasmonics in sensor applications: A review,” *Sensors (Switzerland)*, vol. 20, no. 12, pp. 1–21, 2020, doi: 10.3390/s20123563.

[18] K. Wang *et al.*, “Ultrafast saturable absorption of two-

dimensional MoS2 nanosheets," *ACS Nano*, vol. 7, no. 10, pp. 9260–9267, Oct. 2013, doi: 10.1021/NN403886T.

[19] J. Yao and G. Yang, "2D material broadband photodetectors," *Nanoscale*, vol. 12, no. 2, pp. 454–476, Jan. 2020, doi: 10.1039/C9NR09070C.

[20] J. Kim, G. V. Naik, N. K. Emani, U. Guler, and A. Boltasseva, "Plasmonic resonances in nanostructured transparent conducting oxide films," *IEEE J. Sel. Top. Quantum Electron.*, vol. 19, no. 3, p. 4601907, 2013, doi: 10.1109/jstqe.2013.2238611.

[21] G. V. Naik, J. Kim, and A. Boltasseva, "Oxides and nitrides as alternative plasmonic materials in the optical range [Invited]," *Opt. Mater. Express*, vol. 1, no. 6, p. 1090, Oct. 2011, doi: 10.1364/ome.1.001090.

[22] "H. Yin, J. Chen, Y. Wang, J. Wang, and H. Guo, "Composi... - Google Scholar." https://scholar.google.com/scholar?hl=en&as_sdt=0%2C5&q=H.+Yin%2C+J.+Chen%2C+Y.+Wang%2C+J.+Wang%2C+and+H.+Guo%2C+"Composition+dependent+band+offsets+of+ZnO+and+its+ternary+alloys%2C"+Scientific+Rep.%2C+vol.+7%2C+2017%2C+Art.+no.+41567.&btnG= (accessed Jan. 08, 2022).

[23] H. Morkoç and Ü. Özgür, *General Properties of ZnO*. 2009.

[24] J. Faucheaux, … A. S.-T. journal of physical, and undefined 2014, "Plasmon resonances of semiconductor nanocrystals: physical principles and new opportunities," *ACS Publ.*, vol. 5, no. 6, pp. 976–985, Mar. 2014, doi: 10.1021/jz500037k.

[25] A. Boltasseva, "Empowering plasmonics and metamaterials technology with new material platforms," *MRS Bull. 2014 395*, vol. 39, no. 5, pp. 461–468, May 2014, doi: 10.1557/MRS.2014.91.

[26] G. Coli and K. K. Bajaj, "Excitonic transitions in ZnO/MgZnO quantum well heterostructures," *Appl. Phys. Lett.*, vol. 78, no. 19, pp. 2861–2863, May 2001, doi: 10.1063/1.1370116.

[27] H. Chen *et al.*, "Two-dimensional electron gas related emissions in ZnMgO/ZnO heterostructures," *Appl. Phys. Lett.*, vol. 99, no.

21, Nov. 2011, doi: 10.1063/1.3662964.

[28] A. Janotti and C. G. Van De Walle, "Fundamentals of zinc oxide as a semiconductor," *Reports Prog. Phys.*, vol. 72, no. 12, 2009, doi: 10.1088/0034-4885/72/12/126501.

[29] M. Lange, C. P. Dietrich, K. Brachwitz, M. Stölzel, M. Lorenz, and M. Grundmann, "Visible emission from ZnCdO/ZnO multiple quantum wells," *Phys. Status Solidi - Rapid Res. Lett.*, vol. 6, no. 1, pp. 31–33, Jan. 2012, doi: 10.1002/PSSR.201105489.

[30] Z. Zolnai *et al.*, "Nondestructive atomic compositional analysis of BeMgZnO quaternary alloys using ion beam analytical techniques," *Appl. Surf. Sci.*, vol. 327, pp. 43–50, Feb. 2015, doi: 10.1016/J.APSUSC.2014.11.067.

[31] H. Tampo *et al.*, "Polarization-induced two-dimensional electron gases in ZnMgO/ZnO heterostructures," *Appl. Phys. Lett.*, vol. 93, no. 20, 2008, doi: 10.1063/1.3028338.

[32] K. Ding, M. B. Ullah, V. Avrutin, Özgür, and H. Morkoç, "Investigation of high density two-dimensional electron gas in Zn-polar BeMgZnO/ZnO heterostructures," *Appl. Phys. Lett.*, vol. 111, no. 18, Oct. 2017, doi: 10.1063/1.4993853.

[33] F. Benharrats, K. Zitouni, A. Kadri, and B. Gil, "Determination of piezoelectric and spontaneous polarization fields in CdxZn1−xO/ZnO quantum wells grown along the polar 〈0001〉 direction," *Superlattices Microstruct.*, vol. 47, no. 5, pp. 592–596, May 2010, doi: 10.1016/J.SPMI.2010.01.007.

[34] H. Yıldırım, "Exciton binding and excitonic transition energies in wurtzite Zn1-xCdxO/ZnO quantum wells," *Superlattices Microstruct.*, vol. 120, pp. 344–352, Aug. 2018, doi: 10.1016/j.spmi.2018.05.045.

[35] I. Alonso Calafell *et al.*, "Giant enhancement of third-harmonic generation in graphene–metal heterostructures," *Nat. Nanotechnol.*, vol. 16, no. 3, pp. 318–324, Mar. 2021, doi: 10.1038/S41565-020-00808-W.

[36] A. M. Schimpf, N. Thakkar, C. E. Gunthardt, D. J. Masiello, and D. R. Gamelin, “Charge-tunable quantum plasmons in colloidal semiconductor nanocrystals.,” *ACS Nano*, vol. 8, no. 1, pp. 1065–72, Jan. 2014, doi: 10.1021/nn406126u.

[37] S. Wang, Y. Zhao, J. Chen, R. Xu, L. Luo, and S. Zhong, “Self-assembled 3D La(OH)3 and La2O3 nanostructures: Fast microwave synthesis and characterization,” *Superlattices Microstruct.*, vol. 47, no. 5, pp. 597–605, May 2010, doi: 10.1016/j.spmi.2010.02.002.

[38] H. Tampo *et al.*, “Two-dimensional electron gas in Zn polar ZnMgO/ZnO heterostructures grown by radical source molecular beam epitaxy,” *Appl. Phys. Lett.*, vol. 89, no. 13, 2006, doi: 10.1063/1.2357588.

[39] J. D. Ye *et al.*, “Two-dimensional electron gas in Zn-polar ZnMgO/ZnO heterostructure grown by metal-organic vapor phase epitaxy,” *Appl. Phys. Lett.*, vol. 97, no. 11, p. 111908, Sep. 2010, doi: 10.1063/1.3489101.

[40] Y. S. Park *et al.*, “Optical Properties Related to a Two-Dimensional Electron Gas at an AlGaN/GaN Heterostructure,” *J. Korean Phys. Soc.*, vol. 43, no. 5 I, pp. 743–746, 2003, doi: 10.3938/JKPS.43.743.

[41] C. T. Phare, Y. H. Daniel Lee, J. Cardenas, and M. Lipson, “Graphene electro-optic modulator with 30 GHz bandwidth,” *Nat. Photonics 2015 98*, vol. 9, no. 8, pp. 511–514, Jul. 2015, doi: 10.1038/nphoton.2015.122.

[42] M. Liu *et al.*, “A graphene-based broadband optical modulator,” *Nature*, vol. 474, no. 7349, pp. 64–67, Jun. 2011, doi: 10.1038/NATURE10067.

[43] M. Brongersma, N. Halas, P. N.-N. nanotechnology, and undefined 2015, “Plasmon-induced hot carrier science and technology,” *nature.com*, 2015, doi: 10.1038/nnano.2014.311.

[44] I. Goykhman, B. Desiatov, J. Shappir, J. B. Khurgin, and U. Levy, “Model for quantum efficiency of guided mode plasmonic enhanced silicon Schottky detectors,” Jan. 2014, Accessed: Jan.

04, 2022. [Online]. Available: http://arxiv.org/abs/1401.2624.

[45] S. Shingubara, K. Morimoto, H. Sakaue, and T. Takahagi, "Self-Organization of a Porous Alumina Nanohole Array Using a Sulfuric/Oxalic Acid Mixture as Electrolyte," *Electrochem. Solid-State Lett.*, vol. 7, no. 3, p. E15, Jan. 2004, doi: 10.1149/1.1644353/XML.

[46] C. V. Manzano, J. Martín, and M. S. Martín-González, "Ultra-narrow 12 nm pore diameter self-ordered anodic alumina templates," *Microporous Mesoporous Mater.*, vol. 184, pp. 177–183, Jan. 2014, doi: 10.1016/J.MICROMESO.2013.10.004.

[47] A. M. Schimpf, N. Thakkar, C. E. Gunthardt, D. J. Masiello, and D. R. Gamelin, "Charge-Tunable Quantum Plasmons in Colloidal Semiconductor Nanocrystals," 2013, doi: 10.1021/nn406126u.

[48] R. A. Soref and B. R. Bennett, "Electrooptical effects in silicon," *IEEE J. Quantum Electron.*, vol. 23, no. 1, pp. 123–129, 1987, doi: 10.1109/JQE.1987.1073206.

[49] M. Lee *et al.*, "Broadband modulation of light by using an electro-optic polymer," *Science (80-.).*, vol. 298, no. 5597, pp. 1401–1403, Nov. 2002, doi: 10.1126/SCIENCE.1077446.

[50] S. Rajput, V. Kaushik, S. Jain, and M. Kumar, "Slow light enhanced phase shifter based on low-loss silicon-ITO hollow waveguide," *IEEE Photonics J.*, vol. 11, no. 1, Feb. 2019, doi: 10.1109/JPHOT.2019.2895699.

[51] C. Gmachl, H. M. ng, and A. Y. Cho, "Intersubband absorption in GaN/AlGaN multiple quantum wells in the wavelength range of [formula omitted]," *Appl. Phys. Lett.*, vol. 77, no. 3, pp. 334–336, Jul. 2000, doi: 10.1063/1.126968.

[52] S. Rajput, V. Kaushik, S. Jain, P. Tiwari, A. K. Srivastava, and M. Kumar, "Optical Modulation in Hybrid Waveguide Based on Si-ITO Heterojunction," *J. Light. Technol.*, vol. 38, no. 6, pp. 1365–1371, Mar. 2020, doi: 10.1109/JLT.2019.2953690.

[53] S. Jain, S. Rajput, V. Kaushik, and M. Kumar, "High speed optical modulator based on silicon slotted-rib waveguide," *Opt. Commun.*, vol. 434, pp. 49–53, Mar. 2019, doi:

10.1016/J.OPTCOM.2018.10.028.

[54] A. Guarino, G. Poberaj, D. Rezzonico, R. Degl'innocenti, and P. Gunter, "Electro-optically tunable microring resonators in lithium niobate."

[55] "Integrated germanium optical interconnects on silicon substrates | Nature Photonics." https://www.nature.com/articles/nphoton.2014.73 (accessed Jan. 07, 2022).

[56] H. Tazawa *et al.*, "Ring resonator-based electrooptic polymer traveling-wave modulator," *J. Light. Technol.*, vol. 24, no. 9, pp. 3514–3519, Sep. 2006, doi: 10.1109/jlt.2006.878514.

[57] C. T. Phare, Y. H. Daniel Lee, J. Cardenas, and M. Lipson, "Graphene electro-optic modulator with 30 GHz bandwidth," *Nat. Photonics 2015 98*, vol. 9, no. 8, pp. 511–514, Jul. 2015, doi: 10.1038/nphoton.2015.122.

[58] H. Yin, J. Chen, Y. Wang, J. Wang, and H. Guo, "Composition dependent band offsets of ZnO and its ternary alloys," *Sci. Rep.*, vol. 7, Jan. 2017, doi: 10.1038/SREP41567.

[59] "Two-dimensional electron gas in Zn polar ZnMgO/ZnO heterostructures grown by radical source molecular beam epitaxy | Request PDF." https://www.researchgate.net/publication/234997879_Two-dimensional_electron_gas_in_Zn_polar_ZnMgOZnO_heterostructures_grown_by_radical_source_molecular_beam_epitaxy (accessed Jan. 04, 2022).

[60] R. H. Fowler, "The analysis of photoelectric sensitivity curves for clean metals at various temperatures," *Phys. Rev.*, vol. 38, no. 1, pp. 45–56, 1931, doi: 10.1103/PHYSREV.38.45.

[61] "Physics of Semiconductor Devices - Simon M. Sze, Yiming Li, Kwok K. Ng - Google Books." https://books.google.co.in/books?hl=en&lr=&id=svYkEAAAQBAJ&oi=fnd&pg=PA3&dq=S.+M.+Sze+and+K.+K.+Ng,+Physics+of+Semiconductor+Devices+(Wiley,+2006).&ots=K9Fu0VASaB&sig=Pt_3swehvRk7Gc88DmF4pu2UfoE&redir_esc=y#v

=onepage&q=S. M. Sze and K. K. Ng%2C Physics of Semiconductor Devices (Wiley%2C 2006).&f=false (accessed Jan. 07, 2022).

[62] R. P.-J. of A. Physics and undefined 1970, “Interface barrier energy determination from voltage dependence of photoinjected currents,” *aip.scitation.org*, Accessed: Jan. 07, 2022. [Online]. Available: https://aip.scitation.org/doi/abs/10.1063/1.1659238.

[63] E. O. Kane, “Theory of photoelectric emission from semiconductors,” *Phys. Rev.*, vol. 127, no. 1, pp. 131–141, 1962, doi: 10.1103/PHYSREV.127.131.

[64] J. S. Helman and F. Sanchez-Sinencio, “Theory of internal photoemission,” *Phys. Rev. B*, vol. 7, no. 8, pp. 3702–3706, 1973, doi: 10.1103/PHYSREVB.7.3702.

[65] L. Apker, E. Taft, and J. Dickey, “Photoelectric emission and contact potentials of semiconductors,” *Phys. Rev.*, vol. 74, no. 10, pp. 1462–1474, 1948, doi: 10.1103/PHYSREV.74.1462.

[66] “Nuclear Magnetic Resonance: Volume 44 - Google Books.” https://books.google.co.in/books?hl=en&lr=&id=iGsoDwAAQBAJ&oi=fnd&pg=PA235&dq=E.+A.+Tampo,+Appl.+Phys.+Lett.+94,+242107+(2009).&ots=BIW1o-IXd5&sig=rytu8IHx6YZEX7ZaKrLu3WyAz90&redir_esc=y#v=onepage&q&f=false (accessed Jan. 07, 2022).

[67] “The Physics of Semiconductor Devices - Google Books.” https://www.google.co.in/books/edition/The_Physics_of_Semiconductor_Devices/WhOGDwAAQBAJ?hl=en&gbpv=1&dq=M.+A.+Khan,+R.+Singh,+S.+Mukherjee,+and+A.+Kranti,+IEEE+Trans.+Electron+Devices+64,+1015+(2017)&pg=PA1275&printsec=frontcover (accessed Jan. 07, 2022).

[68] “J. Roelkens et al., Mater. Today, vol. 10, p. 36, 2007 - Google Search.” https://www.google.co.in/search?q=+J.+Roelkens+et+al.%2C+Mater.+Today%2C+vol.+10%2C+p.+36%2C+2007&hl=en&tbm=bks&ei=yXbYYdTICJKymAWFkoeoCg&ved=0ahUKEwiU0ZrUk6D1AhUSGaYKHQXJAaUQ4dUDCAo&oq=+J.+Roelke

ns+et+al.%2C+Mater.+Today%2C+vol.+10%2C+p.+36%2C+2007&gs_lcp=Cg1nd3Mtd2l6LWJvb2tzEAxQAFgAYKcLaABwAHgAgAHdAYgB3QGSAQMyLTGYAQCgAQKgAQHAAQE&sclient=gws-wiz-books (accessed Jan. 07, 2022).

[69] J. Cardenas, C. B. Poitras, J. T. Robinson, K. Preston, L. Chen, and M. Lipson, "Low loss etchless silicon photonic waveguides," *Opt. InfoBase Conf. Pap.*, 2009, doi: 10.1364/OE.17.004752.

[70] G. T. Reed, G. Mashanovich, F. Y. Gardes, and D. J. Thomson, "Silicon optical modulators," *Nat. Photon.*, vol. 4, no. 8, pp. 518–526, Aug. 2010, doi: 10.1038/nphoton.2010.179.

[71] D. A. B. Miller, "Device requirements for optical interconnects to silicon chips," *Proc. IEEE*, vol. 97, no. 7, pp. 1166–1185, 2009, doi: 10.1109/jproc.2009.2014298.

[72] S. Jain *et al.*, "Thermally Stable Optical Filtering Using Silicon-Based Comb-Like Asymmetric Grating for Sensing Applications," *IEEE Sens. J.*, vol. 20, no. 7, pp. 3529–3535, Apr. 2020, doi: 10.1109/JSEN.2019.2960604.

[73] Sulabh, L. Singh, S. Jain, and M. Kumar, "Optical Slot Waveguide With Grating-Loaded Cladding of Silicon and Titanium Dioxide for Label-Free Bio-Sensing," *IEEE Sens. J.*, vol. 19, no. 15, pp. 6126–6133, Aug. 2019, doi: 10.1109/JSEN.2019.2910278.

[74] L. Singh, S. Jain, and M. Kumar, "Electrically writable silicon nanophotonic resistive memory with inherent stochasticity," *Opt. Lett.*, vol. 44, no. 16, p. 4020, Aug. 2019, doi: 10.1364/OL.44.004020.

[75] R. A. Soref and B. R. Bennett, "Electrooptical effects in silicon," *IEEE J. Quant. Electron.*, vol. 23, no. 1, pp. 123–129, 1987, doi: 10.1109/jqe.1987.1073206.

[76] M. Casalino *et al.*, "Cu/p-Si Schottky barrier-based near infrared photodetector integrated with a silicon-on-insulator waveguide," *Appl. Phys. Lett.*, vol. 96, no. 24, Jun. 2010, doi: 10.1063/1.3455339.

[77] S. Zhu, G. Q. Lo, and D. L. Kwong, "Low-cost and high-speed

SOI waveguide-based silicide Schottky-barrier MSM photodetectors for broadband optical communications,” *IEEE Photonics Technol. Lett.*, vol. 20, no. 16, pp. 1396–1398, Aug. 2008, doi: 10.1109/LPT.2008.927876.

[78] “INVESTIGATION OF SEMICONDUCTOR SCHOTTKY BARRIERS FOR OPTICAL DETECTION AND CATHODIC EMISSION.” https://www.researchgate.net/publication/235194332_INVESTIGATION_OF_SEMICONDUCTOR_SCHOTTKY_BARRIERS_FOR_OPTICAL_DETECTION_AND_CATHODIC_EMISSION (accessed Jan. 04, 2022).

[79] H. Elabd, W. K.- Review, and undefined 1982, “PtSi Infrared Schottky-Barrier Detectors With Optical Cavity,” *rsp-italy.it*, 1982, Accessed: Jan. 08, 2022. [Online]. Available: http://www.rsp-italy.it/Electronics/Magazines/RCA Review/_contents/RCA Review 1982-12.pdf#page=5.

[80] V. E. Vickers, “Model of Schottky Barrier Hot-Electron-Mode Photodetection,” *Appl. Opt.*, vol. 10, no. 9, p. 2190, Sep. 1971, doi: 10.1364/AO.10.002190.

[81] I. Goykhman, B. Desiatov, J. Shappir, … J. K. preprint arXiv, and undefined 2014, “Model for quantum efficiency of guided mode plasmonic enhanced silicon Schottky detectors,” *arxiv.org*, Accessed: Jan. 08, 2022. [Online]. Available: https://arxiv.org/abs/1401.2624.

[82] “M. L. Brongersma, N. J. Halas, and P. Nordlander,... - Google Scholar.” https://scholar.google.co.in/scholar?hl=en&as_sdt=0%2C5&q=M.+L.+Brongersma%2C+N.+J.+Halas%2C+and+P.+Nordlander%2C+“Plasmon-induced+hot+carrier+science+and+technology%2C”+Nature+Nanotechnol.%2C+vol.+10%2C+no.+1%2C+pp.+25–34%2C+2015.&btnG= (accessed Jan. 08, 2022).

[83] D. W. Peters, “An Infrared Detector Utilizing Internal Photoemission,” *Proc. IEEE,* vol. 55, no. 5, pp. 704–705, 1967,

doi: 10.1109/PROC.1967.5648.

[84] P. Berini, “Plasmon–polariton waves guided by thin lossy metal films of finite width: bound modes of symmetric structures,” *Phys. Rev. B,* vol. 61, pp. 10484–10503, 2000.

[85] A. Olivieri, A. Akbari, and P. Berini, “Surface plasmon waveguide Schottky detectors operating near breakdown,” *Phys. Status Solidi - Rapid Res. Lett.*, vol. 4, no. 10, pp. 283–285, Oct. 2010, doi: 10.1002/PSSR.201004245.

[86] “A. Sobhani et al., “Narrowband photodetection in... - Google Scholar.” https://scholar.google.co.in/scholar?hl=en&as_sdt=0%2C5&q=A.+Sobhani+et+al.%2C+“Narrowband+photodetection+in+the+near-infrared+with+a+plasmon-induced+hot+electron+device%2C”+Nature+Commun.%2C+vol.+4%2C+no.+1%2C+2013%2C+Art.+no.+1643&btnG= (accessed Jan. 08, 2022).

[87] “M. W. Knight, H. Sobhani, P. Nordlander, and N.... - Google Scholar.” https://scholar.google.co.in/scholar?hl=en&as_sdt=0%2C5&q=+M.+W.+Knight%2C+H.+Sobhani%2C+P.+Nordlander%2C+and+N.+J.+Halas%2C+“Photodetection+with+active+optical+antennas%2C”+Science%2C+vol.+332%2C+no.+6030%2C+pp.+702–704%2C+2011.&btnG= (accessed Jan. 08, 2022).

[88] A. Akbari and P. Berini, “Schottky contact surface-plasmon detector integrated with an asymmetric metal stripe waveguide,” *Appl. Phys. Lett.*, vol. 95, no. 2, 2009, doi: 10.1063/1.3171937.

[89] F. Bonaccorso, Z. Sun, T. Hasan, and A. C. Ferrari, “Graphene photonics and optoelectronics,” *Nat. Photon.*, vol. 4, no. 9, pp. 611–622, Sep. 2010, doi: 10.1038/nphoton.2010.186.

[90] “A. C. Ferrari et al., “Science and technology roadmap... - Google Scholar.” https://scholar.google.co.in/scholar?hl=en&as_sdt=0%2C5&q=A.+C.+Ferrari+et+al.%2C+“Science+and+technology+roadmap+for+graphene%2C+related+two-

dimensional+crystals%2C+and+hybrid+systems%2C"+Nanoscale%2C+vol.+7%2C+no.+11%2C+pp.+4598–4810%2C+2015&btnG= (accessed Jan. 08, 2022).

[91] A. N. Grigorenko, M. Polini, and K. S. Novoselov, "Graphene plasmonics," *Nat. Photonics 2012 611*, vol. 6, no. 11, pp. 749–758, Nov. 2012, doi: 10.1038/nphoton.2012.262.

[92] F. H. L. Koppens, D. E. Chang, and F. J. García De Abajo, "Graphene plasmonics: A platform for strong light-matter interactions," *Nano Lett.*, vol. 11, no. 8, pp. 3370–3377, Aug. 2011, doi: 10.1021/NL201771H.

[93] Z. S. T. H. A. F. F Bonaccorso, "Graphene photonics and optoelectronics," *Nat. Photon.*, vol. 4, pp. 611–622, 2010.

[94] F. H. L. Koppens, T. Mueller, P. Avouris, A. C. Ferrari, M. S. Vitiello, and M. Polini, "Photodetectors based on graphene, other two-dimensional materials and hybrid systems," *Nat. Nanotechnol.*, vol. 9, no. 10, pp. 780–793, Jan. 2014, doi: 10.1038/NNANO.2014.215.

[95] "I. Goykhman, B. Desiatov, J. Shappir, J. B. Khurgin,... - Google Scholar." https://scholar.google.com/scholar?hl=en&as_sdt=0%2C5&q=+I.+Goykhman%2C+B.+Desiatov%2C+J.+Shappir%2C+J.+B.+Khurgin%2C+and+U.+Levy%2C+"Model+for+quantum+efficiency+of+guided+mode+plasmonic+enhanced+silicon+Schot%02tky+detectors%2C"+2014%2C+arXiv%3A1401.26&btnG= (accessed Jan. 08, 2022).

[96] U. Levy, M. Grajower, P. G.-A. Photonics, and undefined 2017, "Plasmonic silicon Schottky photodetectors: The physics behind graphene enhanced internal photoemission," *aip.scitation.org*, Accessed: Jan. 08, 2022. [Online]. Available: https://aip.scitation.org/doi/abs/10.1063/1.4973537.

[97] "S. L. Shinde, S. Ishii, and T. Nagao, "Sub-band... - Google Scholar." https://scholar.google.com/scholar?hl=en&as_sdt=0%2C5&q=+S.+L.+Shinde%2C+S.+Ishii%2C+and+T.+Nagao%2C+"Sub-

band+gap+photodetection+from+the+titanium+nitride%2Fgermanium+heterostructure%2C"+ACS+Appl.+Mater.+Interfaces%2C+vol.+11%2C+no.+24%2C+pp.+21965–21972%2C+2019.&btnG= (accessed Jan. 08, 2022).

[98] "H. Tampo et al., "Band profiles of ZnMgO/ZnO heterostr... - Google Scholar." https://scholar.google.com/scholar?hl=en&as_sdt=0%2C5&q=+H.+Tampo+et+al.%2C+"Band+profiles+of+ZnMgO%2FZnO+heterostructures+confirmed+by+Kelvin+probe+force+microscopy%2C"+Appl.+Phys.+Lett.%2C+vol.+94%2C+no.+24%2C+2009%2C+Art.+no.+242107.&btnG= (accessed Jan. 08, 2022).

[99] "H. Tampo et al., "Two-dimensional electron gas... - Google Scholar." https://scholar.google.com/scholar?hl=en&as_sdt=0%2C5&q=H.+Tampo+et+al.%2C+"Two-dimensional+electron+gas+in+Zn+polar+Zn+Mg+O%2F+ZnO+heterostructures+grown+by+radical+source+molecular+beam+epitaxy%2C"+Appl.+Phys.+Lett.%2C+vol.+89%2C+no.+13%2C+2006%2C+Art.+no.+132113&btnG= (accessed Jan. 08, 2022).

[100] "P. Kumar, M. A. Khan, G. Siddharth, S. Kumar, R.... - Google Scholar." https://scholar.google.com/scholar?hl=en&as_sdt=0%2C5&q=+P.+Kumar%2C+M.+A.+Khan%2C+G.+Siddharth%2C+S.+Kumar%2C+R.+Singh+and+S.+Mukherjee%2C+"Electron+scattering+analysis+in+2DEG+in+sputtering-grown+MgZnO%2FZnO+heterostructure%2C"+J.+Phys.+D%3A+Appl.+Phys.%2C+vol.+53%2C+no.+12%2C+2020%2C+Art.+no.+125108.&btnG= (accessed Jan. 08, 2022).

[101] M. A. Khan, J. M. Van Hove, J. N. Kuznia, and D. T. Olson, "High electron mobility GaN/AlxGa1-xN heterostructures grown by low-pressure metalorganic chemical vapor deposition," *Appl. Phys. Lett.*, vol. 58, no. 21, pp. 2408–2410, 1991, doi: 10.1063/1.104886.

[102] V. Kaushik, S. Rajput, and M. Kumar, “Broadband optical modulation in a zinc-oxide-based heterojunction via optical lifting,” *Opt. Lett.*, vol. 45, no. 2, p. 363, Jan. 2020, doi: 10.1364/OL.379257.

[103] U. Levy, M. Grajower, P. A. D. Gonçalves, N. A. Mortensen, and J. B. Khurgin, “Plasmonic silicon Schottky photodetectors: The physics behind graphene enhanced internal photoemission,” *APL Photonics*, vol. 2, no. 2, Feb. 2017, doi: 10.1063/1.4973537.

[104] D. A. B. Miller *et al.*, “Electric field dependence of optical absorption near the bandgap of quantum well structures,” *Phys. Rev. B*, vol. 32, no. 2, pp. 1043–1060, 1985, doi: 10.1103/physrevb.32.1043.

[105] D. M.-C. E. and Photons and undefined 1995, “Quantum well optical switching devices,” *Springer*, 1995, doi: 10.1007/978-1-4615-1963-8_22.

[106] Ü. Özgür *et al.*, “A comprehensive review of ZnO materials and devices,” *J. Appl. Phys.*, vol. 98, no. 4, pp. 1–103, Aug. 2005, doi: 10.1063/1.1992666.

[107] K. Alfaramawi, “Electric field dependence of the electron mobility in bulk wurtzite ZnO,” *Bull. Mater. Sci.*, vol. 37, no. 7, pp. 1603–1606, Dec. 2014, doi: 10.1007/S12034-014-0720-Z.

[108] S. H. Park and D. Ahn, “Internal field engineering in CdZnO/MgZnO quantum well structures,” *Appl. Phys. Lett.*, vol. 94, no. 8, 2009, doi: 10.1063/1.3090490.

[109] A. Nakamura *et al.*, “Full-color electroluminescence from ZnO-based heterojunction diodes,” *Appl. Phys. Lett.*, vol. 90, no. 9, 2007, doi: 10.1063/1.2709913.

[110] H. A. Atwater and A. Polman, “Plasmonics for improved photovoltaic devices,” *Nat. Mater.*, vol. 9, no. 3, pp. 205–213, Mar. 2010, doi: 10.1038/nmat2629.

[111] V. J. Sorger, R. F. Oulton, J. Yao, G. Bartal, and X. Zhang, “Plasmonic fabry-pérot nanocavity,” *Nano Lett.*, vol. 9, no. 10, pp. 3489–3493, Oct. 2009, doi: 10.1021/NL901682N.

[112] S. Rajput, V. Kaushik, P. Babu, P. Tiwari, A. K. Srivastava, and

M. Kumar, “Optical modulation via coupling of distributed semiconductor heterojunctions in a Si-ITO-Based Subwavelength Grating,” *Phys. Rev. Appl.*, vol. 15, no. 5, May 2021, doi: 10.1103/PHYSREVAPPLIED.15.054029.

[113] V. J. Sorger, N. D. Lanzillotti-Kimura, R. M. Ma, and X. Zhang, “Ultra-compact silicon nanophotonic modulator with broadband response,” *Nanophotonics*, vol. 1, no. 1, pp. 17–22, Jul. 2012, doi: 10.1515/NANOPH-2012-0009.

[114] Z. Ying *et al.*, “Electronic-photonic arithmetic logic unit for high-speed computing,” *Nat. Commun.*, vol. 11, no. 1, Dec. 2020, doi: 10.1038/S41467-020-16057-3.

[115] P. Cheben, R. Halir, J. H. Schmid, H. A. Atwater, and D. R. Smith, “Subwavelength integrated photonics,” *Nature*, vol. 560, no. 7720, pp. 565–572, Aug. 2018, doi: 10.1038/S41586-018-0421-7.

[116] S. Rajput, V. Kaushik, L. Singh, S. Srivastava, and M. Kumar, “Optical modulator based on a silicon-ITO grating embedded rib structure with a tunable group delay,” *Opt. Lett.*, vol. 46, no. 14, p. 3468, Jul. 2021, doi: 10.1364/OL.433458.

[117] T. Sarwar, S. Cheekati, K. Chung, and P. C. Ku, “On-chip optical spectrometer based on GaN wavelength-selective nanostructural absorbers,” *Appl. Phys. Lett.*, vol. 116, no. 8, Feb. 2020, doi: 10.1063/1.5143114.

[118] “(PDF) A high-resolution spectrometer based on a compact planar two dimensional photonic crystal cavity array.” https://www.researchgate.net/publication/233412571_A_high-resolution_spectrometer_based_on_a_compact_planar_two_dimensional_photonic_crystal_cavity_array (accessed Jan. 04, 2022).

[119] X. Gan, N. Pervez, I. Kymissis, F. Hatami, and D. Englund, “A high-resolution spectrometer based on a compact planar two dimensional photonic crystal cavity array,” *Appl. Phys. Lett.*, vol. 100, no. 23, Jun. 2012, doi: 10.1063/1.4724177.

[120] S. Zhu, G. Lo, D. K.-I. P. T. Letters, and undefined 2008, “Low-

cost and high-speed SOI waveguide-based silicide Schottky-barrier MSM photodetectors for broadband optical communications," *ieeexplore.ieee.org*, Accessed: Jan. 07, 2022. [Online]. Available: https://ieeexplore.ieee.org/abstract/document/4579338/.

[121] R. M. Ma, R. F. Oulton, V. J. Sorger, G. Bartal, and X. Zhang, "Room-temperature sub-diffraction-limited plasmon laser by total internal reflection," *Nat. Mater.*, vol. 10, no. 2, pp. 110–113, 2011, doi: 10.1038/NMAT2919.

[122] J. Lin *et al.*, "Polarization-controlled tunable directional coupling of surface plasmon polaritons," *Science (80-.).*, vol. 340, no. 6130, pp. 331–334, Apr. 2013, doi: 10.1126/SCIENCE.1233746.

[123] M. Liu *et al.*, "A graphene-based broadband optical modulator," *Nat. 2011 4747349*, vol. 474, no. 7349, pp. 64–67, May 2011, doi: 10.1038/nature10067.

[124] X. Ma *et al.*, "Engineering photonic environments for two-dimensional materials," *Nanophotonics*, vol. 10, no. 3, pp. 1031–1058, Jan. 2021, doi: 10.1515/NANOPH-2020-0524.

[125] H. Dalir, Y. Xia, Y. Wang, and X. Zhang, "Athermal Broadband Graphene Optical Modulator with 35 GHz Speed," *ACS Photonics*, vol. 3, no. 9, pp. 1564–1568, Sep. 2016, doi: 10.1021/ACSPHOTONICS.6B00398.

[126] R. Maiti *et al.*, "A semi-empirical integrated microring cavity approach for 2D material optical index identification at 1.55 μm," *Nanophotonics*, vol. 8, no. 3, pp. 435–441, Mar. 2019, doi: 10.1515/NANOPH-2018-0197.

[127] Y. Xue *et al.*, "Atomic-scale ion transistor with ultrahigh diffusivity," *Science (80-.).*, vol. 372, no. 6541, pp. 501–503, Apr. 2021, doi: 10.1126/SCIENCE.ABB5144.

[128] V. Kaushik, S. Rajput, S. Shrivastava, S. Jain, L. Singh, and M. Kumar, "Efficient Sub-Bandgap Photodetection via Two-Dimensional Electron Gas in ZnO Based Heterojunction," *J. Light. Technol.*, vol. 38, no. 21, pp. 6031–6037, Nov. 2020, doi: 10.1109/JLT.2020.3003371.

[129] F. Capasso, "BAND-GAP ENGINEERING: FROM PHYSICS AND MATERIALS TO NEW SEMICONDUCTOR DEVICES.," *Science (80-.).*, vol. 235, no. 4785, pp. 172–176, 1987, doi: 10.1126/SCIENCE.235.4785.172.

[130] Y. W. Huang *et al.*, "Gate-Tunable Conducting Oxide Metasurfaces," *Nano Lett.*, vol. 16, no. 9, pp. 5319–5325, Sep. 2016, doi: 10.1021/ACS.NANOLETT.6B00555.

[131] H. Tampo *et al.*, "Band profiles of ZnMgO/ZnO heterostructures confirmed by Kelvin probe force microscopy," *Appl. Phys. Lett.*, vol. 94, no. 24, 2009, doi: 10.1063/1.3157149.

[132] S. Choi and I. Aharonovich, "Zinc Oxide Nanophotonics," *Nanophotonics*, vol. 4, no. 1, pp. 437–458, 2015, doi: 10.1515/NANOPH-2015-0023.

[133] J. Bao, M. A. Zimmler, F. Capasso, X. Wang, and Z. F. Ren, "Broadband ZnO single-nanowire light-emitting diode," *Nano Lett.*, vol. 6, no. 8, pp. 1719–1722, Aug. 2006, doi: 10.1021/NL061080T.

[134] R. Cheng, C. L. Zou, X. Guo, S. Wang, X. Han, and H. X. Tang, "Broadband on-chip single-photon spectrometer," *Nat. Commun.*, vol. 10, no. 1, Dec. 2019, doi: 10.1038/S41467-019-12149-X.

[135] A. Li and Y. Fainman, "On-chip spectrometers using stratified waveguide filters," *Nat. Commun.*, vol. 12, no. 1, Dec. 2021, doi: 10.1038/S41467-021-23001-6.

[136] S. J. Savage *et al.*, "Scalable modulator for frequency shift keying in free space optical communications," *Opt. Express*, vol. 21, no. 3, p. 3342, Feb. 2013, doi: 10.1364/OE.21.003342.

[137] R. H. Hadfield, "Single-photon detectors for optical quantum information applications," *Nat. Photonics*, vol. 3, no. 12, pp. 696–705, Dec. 2009, doi: 10.1038/NPHOTON.2009.230.

[138] M. Long, P. Wang, H. Fang, and W. Hu, "Progress, Challenges, and Opportunities for 2D Material Based Photodetectors," *Adv. Funct. Mater.*, vol. 29, no. 19, May 2019, doi: 10.1002/ADFM.201803807.

[139] C. Gong, E. M. Kim, Y. Wang, G. Lee, and X. Zhang, "Multiferroicity in atomic van der Waals heterostructures," *Nat. Commun.*, vol. 10, no. 1, Dec. 2019, doi: 10.1038/S41467-019-10693-0.

[140] L. Zheng, L. Zhongzhu, and S. Guozhen, "Photodetectors based on two dimensional materials," *J. Semicond.*, vol. 37, no. 9, Sep. 2016, doi: 10.1088/1674-4926/37/9/091001.

[141] S. Lan *et al.*, "Observation of strong excitonic magneto-chiral anisotropy in twisted bilayer van der Waals crystals," *Nat. Commun.*, vol. 12, no. 1, Dec. 2021, doi: 10.1038/S41467-021-22412-9.

[142] J. Bao and M. G. Bawendi, "A colloidal quantum dot spectrometer," *Nature*, vol. 523, no. 7558, pp. 67–70, Jul. 2015, doi: 10.1038/NATURE14576.

[143] P. Guyot-Sionnest, M. M. Ackerman, and X. Tang, "Colloidal quantum dots for infrared detection beyond silicon," *J. Chem. Phys.*, vol. 151, no. 6, Aug. 2019, doi: 10.1063/1.5115501.

[144] C. M. Natarajan, M. G. Tanner, and R. H. Hadfield, "Superconducting nanowire single-photon detectors: Physics and applications," *Supercond. Sci. Technol.*, vol. 25, no. 6, Jun. 2012, doi: 10.1088/0953-2048/25/6/063001.

[145] G. N. Gol'tsman *et al.*, "Picosecond superconducting single-photon optical detector," *Appl. Phys. Lett.*, vol. 79, no. 6, pp. 705–707, Aug. 2001, doi: 10.1063/1.1388868.

[146] V. J. Sorger and R. Maiti, "Roadmap for gain-bandwidth-product enhanced photodetectors: opinion," *Opt. Mater. Express*, vol. 10, no. 9, p. 2192, Sep. 2020, doi: 10.1364/OME.400423.

[147] P. K. Jain, "Plasmon-in-a-Box: On the Physical Nature of Few-Carrier Plasmon Resonances.," *J. Phys. Chem. Lett.*, vol. 5, no. 18, pp. 3112–9, Sep. 2014, doi: 10.1021/jz501456t.

[148] A. B. Djuriić, A. M. C. Ng, and X. Y. Chen, "ZnO nanostructures for optoelectronics: Material properties and device applications," *Prog. Quantum Electron.*, vol. 34, no. 4, pp. 191–259, 2010, doi: 10.1016/j.pquantelec.2010.04.001.

[149] B. Tandon, G. S. Shanker, and A. Nag, “Multifunctional Sn- and Fe-codoped In2O3 colloidal nanocrystals: Plasmonics and magnetism,” *J. Phys. Chem. Lett.*, vol. 5, no. 13, pp. 2306–2311, Jul. 2014, doi: 10.1021/JZ500949G.

[150] A. Khorsand Zak, R. Razali, W. H. Abd Majid, and M. Darroudi, “Synthesis and characterization of a narrow size distribution of zinc oxide nanoparticles,” *Int. J. Nanomedicine*, vol. 6, no. 1, pp. 1399–1403, 2011, doi: 10.2147/IJN.S19693.

[151] I. K. Aliyu, N. Saheb, S. F. Hassan, and N. Al-Aqeeli, “Microstructure and properties of spark plasma sintered aluminum containing 1 wt.% SiC nanoparticles,” *Metals (Basel).*, vol. 5, no. 1, pp. 70–83, Jan. 2015, doi: 10.3390/MET5010070.